Heriot-Watt University

Local Travelling Wave Solutions and Self-Similar Solutions for a Green Roof Model

Abdulah Alzahrani

July 15, 2014

Submitted for the degree of
Doctor of Philosophy in Mathematics
on completion of research in the
Department of Mathematics,
School of Mathematical and Computer Sciences.

Abstract

In this thesis we study travelling wave solutions and self-similar solutions for a green roof model and for some simpler models which are derived from that model. We focus on two limiting cases near a dry region and near a saturated region.

We start by considering a convection model in the absence of diffusion and sink terms. We show that rarefaction waves and shock solutions exist for several cases.

Next, we consider a convection-diffusion model where both the convective and diffusive terms are present and we show that travelling wave solutions and self-similar solutions exist for some cases. Moreover, numerical simulations are used for the travelling wave and self-similar solutions and confirm the analytic predictions.

Finally, we consider the green roof model where all terms are present and we show that travelling wave solutions exist, whereas self-similar solutions are not found. We also show the travelling wave solutions exist for the two limiting cases.

Acknowledgements

I would like to thank my supervisor, Prof. Andrew Lacey, whose encouragement, kind guidance and support from the initial to the final level enabled me to develop an understanding of the subject. His extensive knowledge has played a crucial role in the development of this thesis. Without his help and advice, this thesis could not have been completed. He could not even realize how much I have learned from him. I am also extremely grateful to my second supervisor, Dr. Lubomir Banas, for his help with numerical simulations. I wish also to thank the other members of staff of the Department of Mathematics for their help and support.

I must express my gratitude to my wife Hamidah and my sons Yazan and Murad for their love, support and patience. My sincere thanks are due to my parents, brothers and sisters for continued support and encouragement me during my studies.

Finally, I would like to thank the Department of Mathematics at King Abdulaziz University and Saudi Cultural Bureau in London for their funding support.

List of Figures

Contents

Chapter 1

Introduction

A green roof is a roof of a building that is covered with vegetation and a growing medium on top of a waterproof membrane. The main advantages of the green roof are assistance in the management of storm water by reducing the amount of runoff, absorbing rain water, pollution control, providing insulation, helping to lower air temperatures, reduction in energy usage, in addition to being aesthetically pleasing [1, 18]. It has also been shown recycling of carbon dioxide to be environmentally friendly. Green roofs are of two types, intensive roofs and extensive roofs [22, 23]. The first type has a thick layer of soil and needs more maintenance while the second one has a light layer and requires little maintenance. Due to the low maintenance requirements, an extensive roof is more common and less expensive than an intensive roof.

Green roofs have been increasing in popularity in the world because they create additional green spaces that bring some nature and also attract wildlife including butterflies, honeybees and other insects. Green roofs are seen in a number of European Countries such as Germany, Switzerland, the Netherlands, Italy, Sweden and the UK. They are also becoming popular in the United States, Australia and Canada but they are not as common as in Europe [53]. As the green roof industry grows, research to determine the construction and design of green roofs is needed.

Green roofs are affected by various weather factors such as wind-loading and rainfall. It is important to understand the transport of water through the structure of green roof to have healthy plants and safe loads. If the saturation levels inside the structure of roof are too high this will cut off the air supply

to the plants while if the saturation levels are too low the plants will die from lack of water. The degree of saturation for a typical green roof is less than 80% and it is important to be maintained at all times [18].

The dynamics of water flow through the soil layer in an unsaturated region was modelled by Hewitt and others [18] in the form of a nonlinear convection-diffusion sink equation. This was the starting point of the present research. The model is based on Richard's equation [37] which we will come to below. The aim is to model the variation of the degree of saturation through the depth of the soil layer, and to see how it changes due to spells of rain, and under the influence of moisture uptake by plant roots.

Richard's equation, which describes groundwater flow through unsaturated porous media, was derived in 1931 [37]. Two terms in Richard's equation present soil retention functions. There are many expressions for soil retention models in literature and practice. Three typical soil retention functions used are known as Brooks-Corey [44], Mualem-Van Genuchten [49] and Storm-Fujita (see [44]). The first one is applicable for small degree of liquid saturation while the third one is applicable for large degree of liquid saturation. The second one is used for the whole range of the water content and was used for the green roof model [18]. The structure of the solution depends on these retention functions.

Studying travelling wave solutions of nonlinear convection-diffusion sink equations has become an essential part of mathematical analysis because the analysis of travelling wave provides a means of finding explicit solutions as well as characterizing the long-term behaviour in numerous situations. Travelling wave solutions are known for Richard's equation. In particular, front solutions for some typical soil retention functions are found in [7]. Caputo and Stepanyants (see [7]) have studied only one case for travelling wave solutions for Richard's equation where the saturation goes between 0 and 1. This case is a front travelling wave solution, i.e where the solution has constant values at plus and minus infinity. In this work we also consider travelling wave solutions which are fronts, with the saturation approaching different limits well ahead and well behind the fronts. Several different cases for the green roof model (without sink term) are considered, according to whether the limiting saturations might be zero, one or in between. We consider a travelling wave which links a fully saturated region to a fully dry region and also a

travelling wave links a fully dry region to a fully saturated region. In addition, we investigate two limiting cases and then we find explicit forms in both cases. There has been much work in the study of travelling wave solutions for convection-diffusion equations and convection-diffusion reaction equations (for example, see [16, 31, 46]). Also, self-similar solutions are discussed in [7] for Richard's equation. This paper studied an infiltration problem (convection-diffusion model) and an imbibition problem (nonlinear diffusion model) based on the simple soil retention functions that are given by Brooks-Corey and Storm-Fujita. It considered only the front solutions. In this thesis we consider self-similar solutions to the green roof model for a convection-diffusion model and also for a nonlinear diffusion model with the forms of soil retention functions that are given by Mualem-Van Genuchten. We also investigate self-similar solutions for the two limiting cases in both problems (diffusion model and convection-diffusion model).

In this thesis we aim to study the travelling wave solutions for the green roof model of [18] and for some simplified equations which are derived from the green roof model. We study travelling wave solutions, particularly locally (near a dry region and near a saturated region) for all these models. We also investigate self-similar solutions for all the models, and in particular, we look at the limiting cases that we mentioned above. Numerical simulations are obtained for both travelling wave and self-similar solutions which confirm the analytic predictions. In additional, we use a finite difference method to solve the green roof model (without sink term) numerically. We observe that a shock-like structure solution is found when δ is small for different initial value problems, namely those with regions of high saturation overlying regions of low saturation.

Following [18], we consider a one-dimensional model for a flat roof of thickness L. We write $S(z,t)$ = saturation at a time t, and height z, $0 \leq z \leq L$; $0 \leq S \leq 1$. Here $S = 0$ means the roof is dry while $S = 1$ means it is saturated. We can consider (at least) two cases for the structure of a green roof:
(i) the entire roof, $0 < z < L$ unsaturated.
(ii) there are a saturated zone, $0 < z < h(t)$, and a saturated region, $h(z) < z < L$, see the diagram below in Figure 1.1.

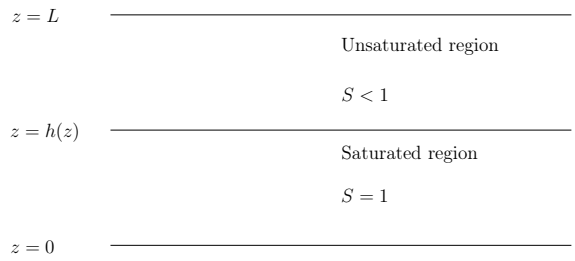

Figure 1.1: Green roof regions.

To provide motivation for the model which was derived in [18], we begin briefly with some basic equations for the water movement in an unsaturated region. Following [39, 49], the basic equation for conservation of water in the soil in three dimensions is given by

$$\phi \frac{\partial S}{\partial \hat{t}} + \nabla . \mathbf{u} = -F_w, \tag{1.1}$$

where ϕ is the porosity of the soil, S is the water saturation in the soil and F_w is the rate of water uptake by plant roots per unit volume of soil. Also, $\mathbf{u}$ is the volume flux of water which is given by Darcy's law:

$$\mathbf{u} = -\frac{k}{\mu}[\nabla p - \rho g \hat{\mathbf{k}}], \tag{1.2}$$

where k is the soil permeability, μ is the viscosity of water, p is the water pressure in the soil, ρ is the density of water, g is the gravitational acceleration and $\hat{\mathbf{k}}$ is the unit vector downwards. The soil permeability function, expressed in terms of relative water saturation, that is used for the whole range of saturation in [18], is given by (see [49])

$$\begin{aligned} k &= k_s K(S) \\ &= k_s S^{1/2} \left[1 - (1 - S^{1/m})^m\right]^2, \quad 0 < m < 1, \end{aligned}$$

where k_s is the water permeability in fully saturated soil. The water pressure, p, in the soil is also linked to the relative water saturation by the suction

characteristic (see [49]).

$$p_a - p = p_c f(S) \quad \text{where} \quad f(S) = \left(S^{-\frac{1}{m}} - 1\right)^{1-m} \tag{1.3}$$

where p_a is atmospheric pressure, and p_c is a characteristic suction pressure. The parameter m is experimentally determined for different soils [49]. The water conservation equation (1.1) combined with Darcy's law (1.2) results in a general known equation, called Richard's equation, for water flow in soil. This equation gives relative water saturation as follows:

$$\phi \frac{\partial S}{\partial \hat{t}} = \nabla.[D_0 D(S) \nabla S - K_s K(S) \hat{\mathbf{k}}] - F_w, \tag{1.4}$$

where the diffusive term $D_0 D(S) = (k/\mu)|\partial p/\partial S|$, and

$$D_0 = \frac{p_c k_s}{\mu} \left(\frac{1-m}{m}\right), \tag{1.5}$$

$$D(S) = S^{1/2-1/m}[(1 - S^{1/m})^{-m} + (1 - S^{1/m})^m - 2], \tag{1.6}$$

and the K_s represents the saturated hydraulic conductivity given by

$$K_s = \frac{\rho g k_s}{\mu}. \tag{1.7}$$

The limiting cases might be better covered by other forms of the soil retention functions that are given by Brooks-Corey and Storm-Fujita (see [44]). With the nondimensionalisation that was given in [18],

$$\tilde{z} = Lz, \; p_r = |P|\tilde{p}_r, \; t = \frac{L}{K_0}\tilde{t}, \; p = p_a + p_c\tilde{p}, \; F_w = 2\pi a k_r l_d |P| R, \tag{1.8}$$

where L is the thickness of single soil layer, P is the root pressure at the soil surface, k_r is the radial conductivity of water, a is the root radius and l_d is the root length density. Parameter values were given in [18, 39]. These values are $L = 10^{-1}$ m, $|P| = 10^6$ Nm^{-2}, $K_0 = 10^{-1}$m s^{-1}, $2\pi a k_r = 7.85 \times 10^{-16}$m^2 s^{-1}Pa^{-1}, $l_d = 5 \times 10^3$m^{-2}, $p_c = 10^4$Nm^{-2}, $p_a = 0$ and $D_0 = 10^{-6}$m^2 s^{-1}. After dropping the tildes, for convenience, the scalar equation (1.4) in one

dimension now becomes

$$\phi\frac{\partial S}{\partial t} = \frac{\partial}{\partial z}\left(\delta D\left(S\right)\frac{\partial S}{\partial z} + K\left(S\right)\right) - R(S), \tag{1.9}$$

where $R(S) = \eta\left(\theta - \epsilon f\left(S\right) - \hat{p}_r\right)$, and the values of the nondimensional parameters are

$$\begin{aligned} &\delta = \frac{D_0}{LK_0} \approx 10^{-4},\ \eta = \frac{2\pi a k_r l_d |P| L}{K_0} \approx 4\times 10^{-6},\ \theta = \frac{p_a}{|P|} \approx 10^{-1}, \\ &\epsilon = \frac{p_c}{|P|} \approx 10^{-2} \text{ and } \tilde{p}_r = \theta - 1. \end{aligned} \tag{1.10}$$

ϕ is the constant porosity of the soil taken here to be 0.25. $K(S)$ and $D(S)$ are the dimensionless water diffusivity and hydraulic conductivity respectively.

The second-order term on the right hand side of (1.9) indicates a diffusive effect, the first-order term represents convection due to gravity, while the last term, of size η, corresponds to a sink due to water uptake by plant roots. For future reference, we call equation (1.9) the Green Roof Model or GRM.
The dimensionless water flux in the z direction (upwards) is

$$q = -\left(\delta D\left(S\right)\frac{\partial S}{\partial z} + K\left(S\right)\right).$$

The functions $D(S)$ and $K(S)$ are given by

$$\begin{aligned} K(S) =& S^{1/2}\left[1-\left(1-S^{1/m}\right)^m\right]^2, \\ D(S) =& \frac{\left[1-\left(1-S^{1/m}\right)^m\right]^2}{S^{1/m-1/2}\left(1-S^{1/m}\right)^m}. \end{aligned} \tag{1.11}$$

The parameter m pertains to the expanded-clay soil used in the green roofs studied in [18] and lies in the range $0 < m < 1$. It is not known in [18] but was taken to be $m = 1/2$ for the analysis and simulations. The water diffusivity $D(S)$ and hydraulic conductivity $K(S)$ are increasing functions of the moisture content and approach zero as $S \to 0$. $D(S) \to \infty$ as $S \to 1$, and we have $K(S) = 1$ at $S = 1$. The forms of $D(S)$ and $K(S)$ are shown in Figure 1.2.

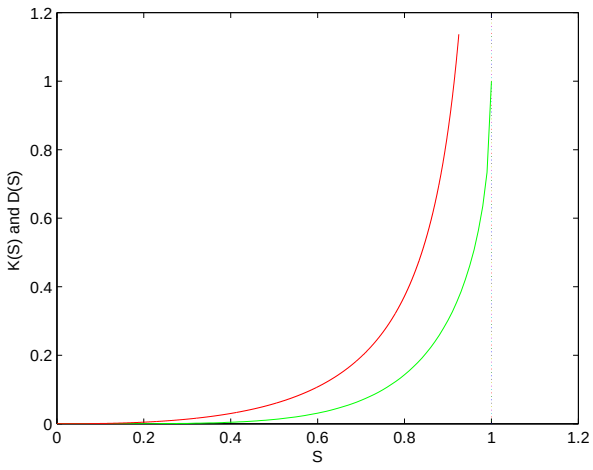

Figure 1.2: The functions $D(S)$ (red) and $K(S)$ (green) with $m = 1/2$.

By local solutions we mean a solution where S is small (close to 0) or close to 1. The local behaviour where S is small (where the soil is fully dry) and where S becoming close to 1 (where the soil is fully saturated) allows us to find a solution in a closed form. Figure 1.3 shows the graph of the local solutions near a dry region and near a saturated region.

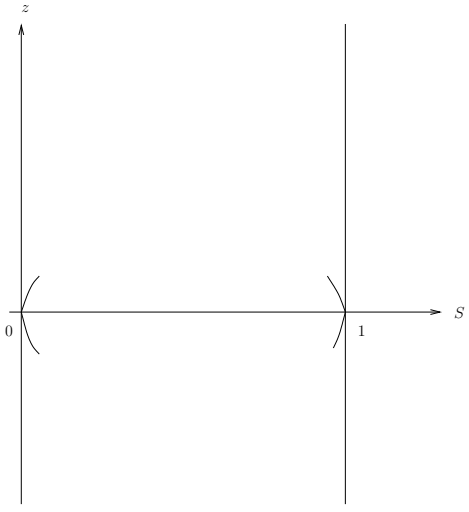

Figure 1.3: Local solutions near a dry region and near a saturated region.

To determine the local behaviour of the solution near a dry and near a saturated region, we need to approximate the water diffusivity $D(S)$ and hydraulic conductivity $K(S)$ for S small and for $1-S$ small. In addition, the approximate sink term is important when we study the the full green roof model locally. Taylor series are used to find approximate forms of $D(S)$ and $K(S)$ functions when $S \to 0$ and also when $S \to 1$. These approximations give us simple forms for these two functions which can be written as power series. They will be useful when we look at travelling wave solutions and self-similar solutions locally in this thesis.

1.1 Approximate Forms of $D(S)$, $K(S)$ and $R(S)$ Terms with Low Saturation

Taking $m = 1/2$ in (1.11) and applying the Taylor series for small S in the term in $(1-S^2)^{1/2}$, we can write

$$\begin{aligned} D(S) &= \frac{\left[1-(1-S^2)^{1/2}\right]^2}{S^{3/2}\left(1-S^2\right)^{1/2}} \sim \frac{\left(\frac{1}{2}S^2\right)^2}{S^{3/2}} \\ &\sim \frac{1}{4}S^{5/2} \quad \text{as} \quad S \to 0^+ \end{aligned} \tag{1.12}$$

and

$$\begin{aligned} K(S) &= S^{1/2}\left[1-(1-S^2)^{1/2}\right]^2 \sim S^{1/2}\left(\frac{1}{2}S^2\right)^2 \\ &\sim \frac{1}{4}S^{9/2} \quad \text{as} \quad S \to 0^+. \end{aligned} \tag{1.13}$$

Clearly, from (1.12) and (1.13) we see that $D(S) \to 0$ and $K(S) \to 0$ as $S \to 0$. When S is small the last term in (1.9) becomes

$$R(S) = \eta\left(1-\epsilon(S^{-2}-1)^{1/2}\right) \quad (\text{since } \theta - \hat{p}_r = 1) \tag{1.14}$$

$$\sim \eta\left(1-\frac{\epsilon}{S}+...\right) \sim \eta\left(\frac{S-\epsilon}{S}\right)$$

$$\sim \eta\left(\frac{S-s_-}{S}\right) \quad \text{for} \quad s_- = \epsilon. \tag{1.15}$$

Here $R(S) = 0$ for $S = S_- = \epsilon/\sqrt{1+\epsilon^2} \sim s_- = \epsilon$ for $\epsilon \ll 1$ and then

$$R(S) \sim \kappa(S - s_-), \tag{1.16}$$

in a neighbourhood of s_- where $\kappa = \eta/\epsilon$ is a positive constant. The approximate form, (1.16), behaves linearly as $S \to s_-$. For $S > s_-$, the plants roots take up the water from soil because $R(S) > 0$. No water enters or leaves the plants roots if $S = s_-$ since $R(S) = 0$. To see the approximate form of $R(S)$ where $S < s_-$, i.e $S \to 0$, from (1.15) we obtain

$$R(S) \sim -\frac{\eta s_-}{S} \text{ as } S \to 0^+. \tag{1.17}$$

Since $R(S) < 0$, the plants roots provide water to soil. This behaviour could be physically unacceptable. When $S = 0$, $R(S)$ becomes large and negative whereas we might expect the roots to neither take up or let out water.

1.2 Approximate Forms of $D(S)$, $K(S)$ and $R(S)$ Terms with High Saturation

We now take $S = 1 - \sigma$ (near saturation), where $\sigma \to 0$, and apply the Taylor series for small σ. From (1.11) with $m = 1/2$, we have

$$\begin{aligned} D(1-\sigma) &\sim \frac{\left[1-(1-(1-\sigma)^2)^{1/2}\right]^2}{(1-\sigma)^{3/2}\left(1-(1-\sigma)^2\right)^{1/2}} \sim \frac{\left[1-(1-(1-2\sigma))^{1/2}\right]^2}{(1-\frac{3}{2}\sigma)\left(1-(1-2\sigma)\right)^{1/2}} \\ &\sim \frac{\left(1-(2\sigma)^{1/2}\right)^2}{(2\sigma)^{1/2}} \sim \frac{1}{(2\sigma)^{1/2}} \quad \text{as} \quad \sigma \to 0^+ \end{aligned} \tag{1.18}$$

and

$$\begin{aligned} K(1-\sigma) &= (1-\sigma)^{1/2}\left[1-(1-(1-\sigma)^2)^{1/2}\right]^2 \sim \left[1-(1-(1-2\sigma))^{1/2}\right]^2 \\ &\sim \left(1-(2\sigma)^{1/2}\right)^2 \\ &\sim 1 - 2^{3/2}\sigma^{1/2} \qquad (1.19) \\ &\sim 1. \qquad (1.20) \end{aligned}$$

We see that from (1.18) and (1.19), $D(S) \to \infty$ and $K(S)$ approaches a positive constant as $S \to 1$.
The second term in (1.14), $\epsilon(S^{-2}-1)^{1/2}$, vanishes as S close to 1, and then the $R(S)$ term approches a constant value as

$$R(S) \quad \sim \quad \eta \quad \text{as} \qquad S \to 1. \tag{1.21}$$

For the saturated region, when the soil saturation S is identically one ($S \equiv 1$) for $z \in [0, h]$, a model for this region was given in [18] which was based on equations (1.1) and (1.2) without (1.3). This model was given by the form

$$\frac{\partial}{\partial z}\left(1 + \frac{1}{\gamma}\frac{\partial p}{\partial z}\right) - \eta\left(\theta - \epsilon\hat{p} - \hat{p}_r\right) = 0, \tag{1.22}$$

got, in the one-dimensional case, simply by substituting (1.2) into (1.1), with S set identically equal to 1 and S_t to 0. In (1.22) $\gamma = \dfrac{\rho g L}{p_c} \approx 10^{-1}$.
The sink term in (1.22) can generally be neglected because the η term is small [18]. Then the flow can be driven by an imposed pressure gradient and in such a saturated region the flux should be given by

$$q = -\left(1 + \frac{1}{\gamma}\frac{\partial p}{\partial z}\right), \tag{1.23}$$

where $p = A(\dot{s}t - z)$ and $\dot{s}$ is the velocity of the interface between the partially and fully saturated regions. Then $\dfrac{\partial p}{\partial z} = -A =$ constant and the flux now is

$$q = -1 + A/\gamma \quad \text{and} \quad \frac{\partial q}{\partial z} = 0. \tag{1.24}$$

We will use (1.24) later in Chapter 2 when we study shock cases where a saturated region is present.

1.3 Outline of the Thesis

The thesis is organized as follows. In Chapter 2, we start by using the method of characteristics with step-function initial data for a convection model (the

diffusive term is absent) which is derived from the green roof equation (1.9). Then we show that rarefaction waves and shock solutions exist for several cases. We also study self-similar solutions and we focus on the local behaviour for a nearly dry and a nearly saturated region. Numerical solutions are presented for this convection model by using the conservative upwind method in Subsection 2.4.1. The numerical results are compared with the approximate analytic solutions.

In Chapter 3, we consider the problem (1.9) without the sink term but where both the convective and diffusive terms are present. We investigate travelling wave solutions and self-similar solutions for this model for several cases. Travelling wave solutions for the convection-diffusion model are found for the same cases that are discussed for the convection model in Chapter 2. In the last part of Chapter 3, Subsection 3.6.1, we use a finite difference method to solve the nonlinear convection-diffusion model numerically. We observe that as $\delta \to 0$, the solutions become sharper and approach the discontinuous solutions with shocks. For small enough δ, solutions to the nonlinear convection-diffusion model look nearly identical to the solutions of convection model which were discussed in Chapter 2.

In Chapter 4, we study travelling wave solutions of the full model (1.9) where all the terms are present. Again we focus on local behaviour near a dry region and near a saturated region. We show that travelling wave solutions exist for the full green roof model and also for the two limiting cases. Self-similar solutions are not found for the full model even for the two local cases (S small and S close to 1). Self-similar solutions do exist for the diffusion-sink model (convection term dropped) for the limiting case of a nearly saturated region. Also, it is noted that we can proceed as in Chapter 2 to use the method of characteristics to solve problems corresponding to the different cases of Chapter 2, getting similar results. Finally, we finish with conclusions and suggest some possible topics for future work in Chapter 5.

1.4 Background Literature

The problem of modelling water and nutrient uptake by plant roots has previously been studied extensively. For example, [39] and [14] develop some mathematical models based on water uptake by plant roots. [49] and [39] get

some experimental results for hydraulic conductivity of unsaturated soil and the water uptake by roots for different values of rainfall.

Many of our results are like those found for Burger's equation which is one of the simplest examples of a nonlinear partial differential equation. It is well-known as an example for studying a conservation law. The inviscid Burger's equation [33, 54] is

$$\frac{\partial u}{\partial t} + \frac{\partial}{\partial x}\left(\frac{1}{2}u^2\right) = 0. \tag{1.25}$$

This equation appears in studies of gas dynamics and other models. In general, it serves as a prototype for nonlinear hyperbolic equations and conservation laws. The corresponding parabolic equation with the same conservation law is the viscous Burger's equation,

$$\frac{\partial u}{\partial t} + \frac{\partial}{\partial x}\left(\frac{1}{2}u^2\right) = \nu u_{xx}, \tag{1.26}$$

where $\nu > 0$ is a constant. The second order derivative in (1.26) is multiplied by a small coefficient, ν, called the viscosity coefficient. This is the simplest equation that includes the nonlinear and viscous effects of fluid dynamics. Equation (1.25) is the vanishing viscosity ($\nu \to 0$) limit of equation (1.26). The solutions of the two equations (1.26) and (1.25) should be close in some sense as the viscosity coefficient tends to zero.
Two different limiting equations are obtained from the green roof model (a convection equation and a convection-diffusion equation). We consider an approach similar to that used for the Burger's equation and which is motivated by physical considerations. For particular initial data, we obtain the existence of solutions for the convection equation as limits of solutions of the convection-diffusion equation as the viscosity coefficient tends to zero.

The method of characteristics with step-function initial data is used for studying the inviscid Burger's equation (1.25) (see, for example, [29, 46]). Shocks and rarefaction waves are found for (1.25). Some numerical results for viscous Burger's equation are given in [33]. In addition, shocks and rarefaction waves are known for the simple traffic flow model [30] and gas dynamics. In a similar way, in Chapter 2, we consider a convection equation that is derived from the green roof model and we show that rarefaction waves and shocks exist for several cases. These different cases for the convection model are considered

according to whether the limiting saturations might be near zero (almost dry region), near one (almost saturated region) or in between (partially saturated region). The travelling wave or wavefront solution is studied for (1.26), and then the shock structure solution is found [3]. The shock solution is physically unacceptable because the solution is supposed to represent a physical quantity and must therefore assume a unique value at each point. For more detailed discussion on Burger's equation see [40, 54]. Shock waves are also discussed in the book [46]. Part of this book in [46] deals with discontinuous solutions for general system of conservation laws. The speed of the discontinuity (shock speed) is given by the Rankine-Hugoniot condition. It represents the jump condition for conservation equations. In Chapter 2, we will derive the Rankine-Hugoniot condition for the convection model which allows us to describe physical situations between two different regions. Similarity solutions of a nonlinear diffusion model and convection-diffusion model exist in [7]. The similarity solutions are also discussed in [4].

There is a small parameter δ multiplying the highest derivative term in (1.9) and in various ordinary differential equations which are obtained for the self-similar solutions of (1.9). The ordinary differential equations are singular perturbation problems as discussed in [11, 15, 20, 32] and are considered in places in this work. The use of perturbation methods allows for significant progress to be made in trying to understand the solution's properties. We are able to obtain a solution in analytical form or reduce the equation to something simpler. The solution of the perturbed problem will often behave analytically quite differently from the solution of the original problem. A singular perturbation problem is a problem containing a small parameter that cannot be approximated by setting the parameter value to zero. This is in contrast to regular perturbation problems for which an approximation can be obtained by taking the small parameter to zero.

Chapter 2

Model without Diffusion or Sink Term

2.1 Introduction

In this chapter, we consider a convection model which is derived from the green roof equation (1.9). We use the method of characteristics with piecewise constant initial condition to find analytic solutions of this simpler model. We show that rarefaction waves and shock solutions exist. We find that rarefaction waves exist for four possible cases and shock solutions exist for four possible cases as well. Numerical results are presented for all these cases. Self-similar solutions are investigated. In particular, local behaviour near a dry region (where S is small) and near a saturated region (where S is close to 1) are discussed in Subsections 2.3.1 and 2.3.2 respectively. The self-similar solutions for S small and S close to 1 have simple closed forms. These self-similar solutions agree well with cases of rarefaction wave solutions in Subsection 2.2.2. In the last part of Chapter 2, Section 2.4, we use a conservative upwind method to solve the nonlinear convection model numerically.

To begin, we consider equation (1.9) without sink term because the η term is small ($\eta \ll 1$). The value of η in [18] was 4×10^{-6}. We can consider therefore the model in absence of the last term and then (1.9) becomes

$$\phi \frac{\partial S}{\partial t} = \frac{\partial}{\partial z}\left(\delta D\left(S\right)\frac{\partial S}{\partial z} + K\left(S\right)\right), \tag{2.1}$$

which is a nonlinear convection-diffusion model. As $\delta \ll 1$, the diffusive term is also small and (away from a boundary or internal layers) can also be neglected. Equation (2.1) then can be considered without the diffusive term and reduces to

$$\phi \frac{\partial S}{\partial t} = \frac{\partial}{\partial z} \left(K \left(S \right) \right), \tag{2.2}$$

where the first-order term on the right hand side of (2.2) represents the influence of gravity, this being now much more important than diffusion. Equation (2.2) is a nonlinear convection model and can be written as

$$\frac{\partial S}{\partial t} + c(S) \frac{\partial S}{\partial z} = 0 \quad \text{where} \quad c(S) = \frac{1}{\phi} \frac{d}{dS}(-K(S)), \tag{2.3}$$

is the wave velocity which depends on the saturation. The form of $c(S)$ is shown in Figure 2.1. Note that it is negative and decreasing with $c(0) = 0$ and $c(S) \to -\infty$ as $S \to 1^-$. We use equations (2.2) and (2.3) to investigate the nature of shockwaves in the next section.

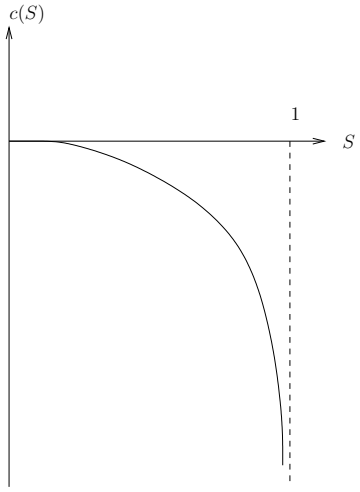

Figure 2.1: Wave velocity as in equation (2.3).

2.2 Step-Function Initial Data

Consider (2.2) with piecewise constant initial data

$$S(z,0) = \begin{cases} S_l & z < z_0 \\ S_r & z > z_0, \end{cases} \tag{2.4}$$

with $0 \leq S_l \leq 1$, $0 \leq S_r \leq 1$ both constant. Then the form of solution depends on the relation between S_l and S_r. In order to determine the behaviour of the solution which is based on the initial condition (2.4), we have two main cases to consider [27,28]. Firstly, we consider the case where $S_r < S_l$, and secondly, we consider the case where $S_l < S_r$.

2.2.1 Method of Characteristics

Consider now equation (2.3) with general initial data. For small time, a solution can be constructed by using the method of characteristics. Using this method, we obtain

$$z(t, S_0) \quad = \quad z_0 + c(S_0)t, \qquad S(z,0) = S_0, \tag{2.5}$$

where z_0 is an arbitrary point on the z axis and S_0 is the initial value of S which comes from the initial data. Here $c(S_0)$ is the characteristic speed. Note that the characteristics are straight lines along which the saturation S remains constant. This would change if we reintroduced the sink term $R(S)$ in the convection model (2.2). We discuss this case later in Chapter 4.

2.2.2 Appearance of Rarefaction Waves

In this section, we consider the first case where $S_r < S_l$ with piecewise constant initial data as in Figure 2.2.

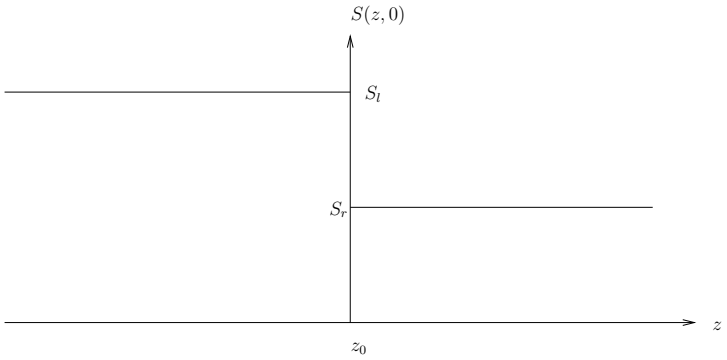

Figure 2.2: Initial data leading to rarefaction waves with $0 \leq S_r < S_l \leq 1$.

Since the characteristic speed of $c(S_l) < c(S_r)$, we find that these two sets of characteristics never cross as time advances. However, there is a region where the characteristic solutions are not apparent and in this region we know that

$$\frac{z - z_0}{t} = c(S) \quad \text{for} \quad S_r < S < S_l. \tag{2.6}$$

Then it is straightforward to solve this expression to determine S for any value of z and t and hence we can write

$$S = c^{-1}\left(\frac{z - z_0}{t}\right) \quad \text{with} \quad S_r < S < S_l, \tag{2.7}$$

and we have a rarefaction wave.

In this case, $S_r < S_l$, we find types of rarefaction wave for four possible cases corresponding to different values of S_r and S_l. All of these cases have physical meaning which we come to below. The corresponding characteristic lines for these four cases are sketched in Figures 2.3, 2.5, 2.7 and 2.9.

We use the method of characteristics to solve equation (2.6) numerically by plotting z against S for fixed $t > 0$ and for some different values of S_r and S_l with $S_r < S < S_l$. We have $S = S_l$ for $z \leq z_0 + c(S_l)t$ and $S = S_r$ for $z \geq z_0 + c(S_r)t$. These numerical results are presented for all possible cases of S_r and S_l and are shown in Figures 2.4, 2.6, 2.8 and 2.10.

Case 1: Partially saturated region above a partially saturated region

Consider equation (2.3) with initial condition

$$S(z,0) = \begin{cases} S_r & z > z_0 \\ S_l & z < z_0, \end{cases} \tag{2.8}$$

with $0 < S_r < S_l < 1$ where S_r, S_l both represent partially saturated regions.

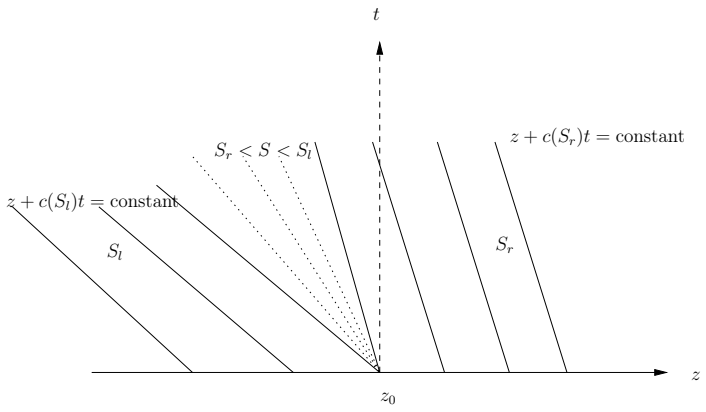

Figure 2.3: Characteristic diagram for equation (2.3) with condition (2.8). Here $0 < S_r < S_l < 1$. The characteristics emanating from $z \geq z_0$ on the z axis have velocity $c(S_r)$ and on them the solution has a constant value S_r, whereas the characteristics emanating from $z < z_0$ have velocity $c(S_l)$ and on them the solution has a constant value S_l. The dotted lines represent an expansion fan where $S_r < S < S_l$.

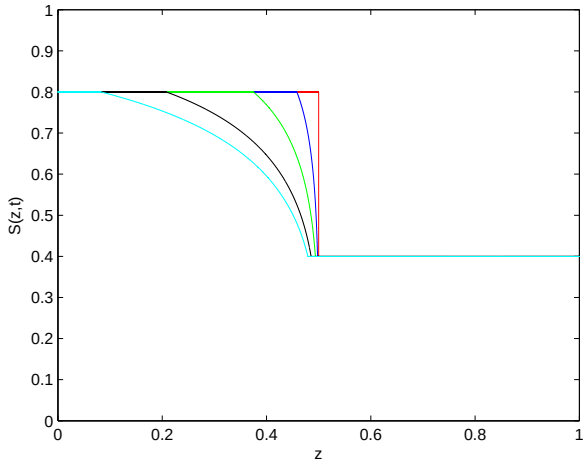

Figure 2.4: The solution of (2.2) with (2.8) at different times $t = 0$ (red), 0.01 (blue), 0.03 (green), 0.07 (black) and 0.1 (cyan) by using the method of characteristics. Here $S_l = 0.8,\ S_r = 0.4$, $\phi = \dfrac{1}{4}$ and $z_0 = \dfrac{1}{2}$.

In this standard case we have for $t \geq 0$ two partially saturated regions where saturation is constant, one with $S = S_r$ and the other $S = S_l$, with $S_l > S_r$. The saturation of S_l region shrinks gradually while the $S = S_r$ region expands. The saturation between these two regions is given by (2.7).

Case 2: Dry region above a partially saturated region

Consider equation (2.3) with initial condition

$$S(z,0) = \begin{cases} 0 & z > z_0 \\ S_l & z < z_0, \end{cases} \tag{2.9}$$

with $0 = S_r < S_l < 1$ where $S_r = 0$ gives a dry region and $0 < S_l < 1$ gives a partially saturated region.

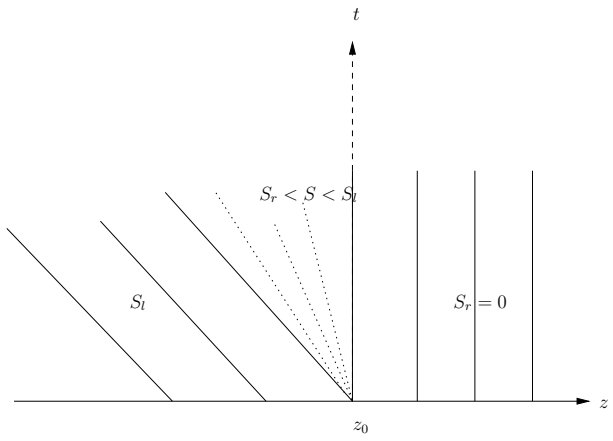

Figure 2.5: Characteristic diagram for equation (2.3) with condition (2.9). Here $0 = S_r < S_l < 1$. The characteristics emanating from $z \geq z_0$ on the z axis have velocity zero and the characteristics are vertical lines corresponding to $S_r = 0$, whereas the characteristics emanating from $z < z_0$ have finite negative velocity $c(S_l)$ and here the solution has a constant value S_l. The dotted lines represent an expansion fan where $0 < S < S_l$.

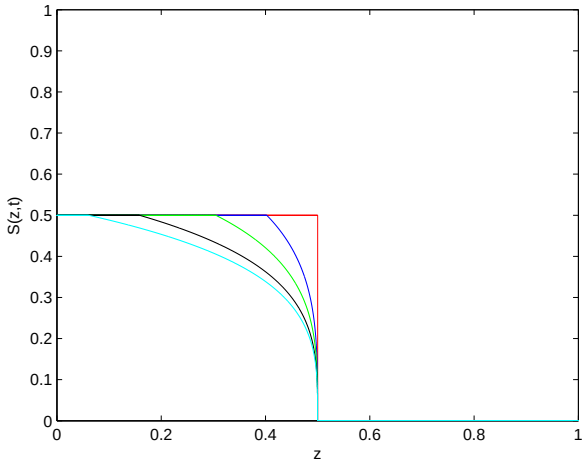

Figure 2.6: The solution of (2.2) with (2.9) at different times $t = 0$ (red), 0.2 (blue), 0.4 (green), 0.7 (black) and 0.9 (cyan) by using the method of characteristics. Here $S_l = 0.5$, $S_r = 0$, $\phi = \frac{1}{4}$ and $z_0 = \frac{1}{2}$. Note that since the characteristics are stationary at $z = z_0$, we see that there is no expansion of the dry region.

In this case for $z \geq z_0$ we have a dry region, so that $S = S_r = 0$, which is fixed in space. The boundary of the dry region remains at $z = z_0$. Below the dry region, the moisture drains and there are two further zones. In the lower one, which moves downwards, S is again constant $S = S_l$. Between this zone and the dry region, we have the expansion fan where the saturation is again given by (2.7).

Case 3: Partially saturated region above a saturated region

Consider equation (2.3) with initial condition

$$S(z,0) = \begin{cases} S_r & z > z_0 \\ 1 & z < z_0, \end{cases} \tag{2.10}$$

with $0 < S_r < S_l = 1$ where $0 < S_r < 1$ represents a partially saturated region and $S_l = 1$ represents a saturated region.

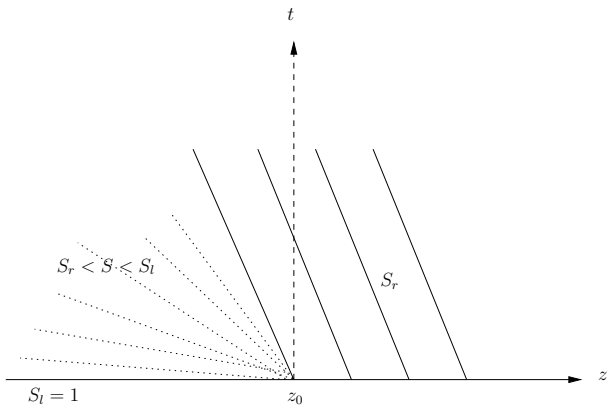

Figure 2.7: Characteristic diagram for equation (2.3) with condition (2.10). Here $0 < S_r < S_l = 1$. The characteristics emanating from $z \geq z_0$ on the z axis have finite negative velocity $c(S_r)$ and make the solution have a constant value S_r, whereas the characteristics emanating from $z < z_0$ have infinite velocity corresponding to $S_l = 1$. The dotted lines represent an expansion fan where $S_r < S < 1$.

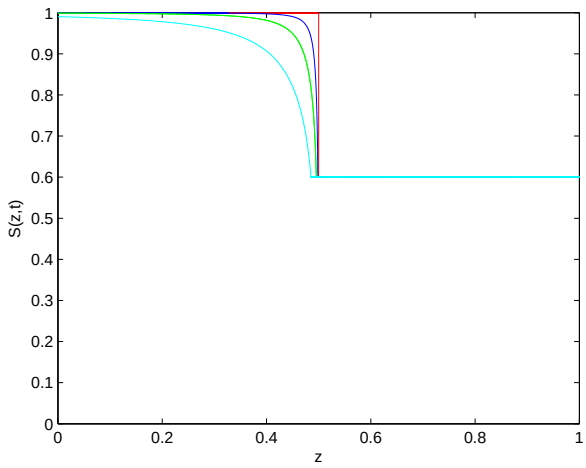

Figure 2.8: The solution of (2.2) with (2.10) at different times $t = 0$ (red), 0.001 (blue), 0.003 (green) and 0.01 (cyan) by using the method of characteristics. Here $S_l = 1$, $S_r = 0.6$, $\phi = \frac{1}{4}$ and $z_0 = \frac{1}{2}$. Characteristics from $z = z_0$ reach all of $z < z_0$ (e.g bottom boundary for our finite interval) immediately: $S < 1$ if $t > 0$.

Here we have a partially saturated region where the saturation remains constant $S = S_r$. This region expands downwards. All the space below it, for $t > 0$, is occupied by the expansion fan, extending from $z = -c(S_r)t$ (where $S = S_r$) to $z = -\infty$, where $S_l = 1$. The saturation of the upper region, S_r, expands gradually while it disappears in the bottom region.
We discuss this limiting case later for the convection-diffusion model in Chapter 3 in Section 3.3. There, we shall see that travelling waves, like the shock solutions in Subsection 2.2.3, are also possible.

Case 4: Dry region above a saturated region

Consider equation (2.3) with initial condition

$$S(z,0) = \begin{cases} 0 & z > z_0 \\ 1 & z < z_0, \end{cases} \tag{2.11}$$

with $0 = S_r < S_l = 1$ where $S_r = 0$ gives a dry region and $S_l = 1$ gives a saturated region.

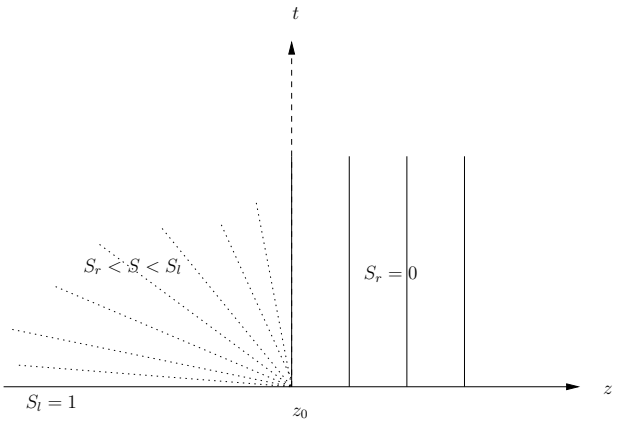

Figure 2.9: Characteristic diagram for equation (2.3) with condition (2.11). Here $0 = S_r < S_l = 1$. The characteristics emanating from $z \geq z_0$ on the z axis have velocity zero and the characteristics are vertical lines, whereas the characteristics emanating from $z < z_0$ have infinite velocity. The dotted lines represent an expansion fan where $0 < S < 1$.

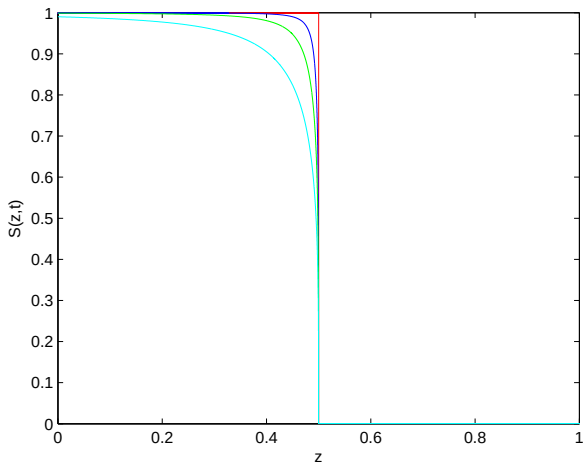

Figure 2.10: The solution of (2.2) with (2.11) at different times $t = 0$ (red), 0.001 (blue), 0.003 (green) and 0.01 (cyan) by using the method of characteristics. Here $S_l = 1$, $S_r = 0$, $\phi = \frac{1}{4}$ and $z_0 = \frac{1}{2}$. There is no expansion, at $z = z_0$, of the boundary of the dry region.

In this case we have again only 2 regions in the half plane ($z < z_0$, $z > z_0$). For $z > z_0$ we have a dry region which is fixed in space and the boundary of this region remains at $z = z_0$. The moisture drains below the dry region and all the space below it, for $t > 0$, is covered by the expansion fan linking $z = z_0$ to $z = -\infty$, where $S_l = 1$: for $t > 0$, $0 < S < 1$ for all $z < z_0$.
As with the previous case, we shall see in Section 3.3 that it is possible to get quite different, shock-like behaviour, when we consider a similar problem with diffusion in Section 3.3.

2.2.3 Appearance of Shocks

In this section we look at piecewise constant initial data but now with $S_r > S_l$ (see Figure 2.11).

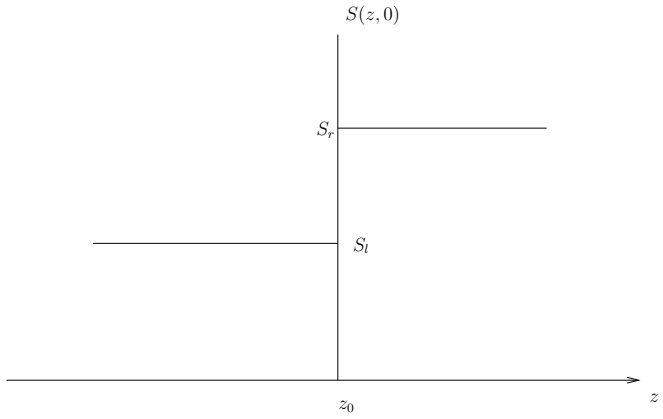

Figure 2.11: Initial data leading to shock waves with $0 \leq S_l < S_r \leq 1$.

Since the characteristic speed of $c(S_l) > c(S_r)$ we find that the characteristic lines cross as time advances and subsequently there will be a shock.

The shock speed satisfies the Rankine-Hugoniot condition [34] and it can be written as

$$\dot{s} = -\frac{1}{\phi}\left(\frac{[K(S)]_l^r}{[S]_l^r}\right), \tag{2.12}$$

where $[K(S)]_l^r = K(S_l) - K(S_r)$ and similarly $[S]_l^r = S_l - S_r$. Equation (2.12) is also called the jump condition. Since S_r and S_l are constants here, the shock front will take the form of straight line in the $z-t$ plane. In this case, $S_r > S_l$, we find that the shock solutions exist for four possible cases corresponding to different values of S_r and S_l. The last two cases, a saturated region above a partially saturated region and a saturated region above a dry region, are unusual since the characteristic lines for saturated region become parallel to the z axis. They are also found to exhibit non-unique shock speed. They are also studied for the convection-diffusion model in Chapter 3 (see Section 3.3), where the same non-uniqueness is found. The corresponding characteristic lines for these four cases are sketched in Figures 2.12, 2.13, 2.14 and 2.16.

Case 1: Partially saturated region above a partially saturated region

Consider equation (2.3) with initial condition as before in case 1 in Subsection 2.2.2,

$$S(z,0) = \begin{cases} S_r & z > z_0 \\ S_l & z < z_0, \end{cases} \tag{2.13}$$

but now with $0 < S_l < S_r < 1$ so that S_l, S_r both give partially saturated regions.

This is a standard case where the solution has a shock wave travelling with speed given by (2.12). The shock speed in equation (2.12) is negative and hence the shock propagates to the left.

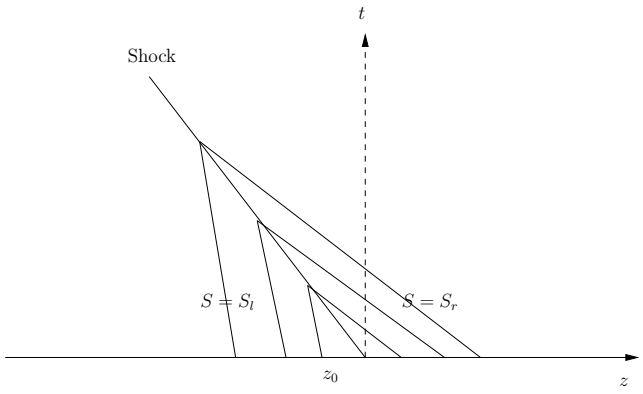

Figure 2.12: Characteristic diagram for equation (2.3) with condition (2.13) where $0 < S_l < S_r < 1$. Note that the characteristics in each of the regions, in which S stays constant, go into the shock.

Case 2: Partially saturated region above a dry region

Consider equation (2.3) with initial condition

$$S(z,0) = \begin{cases} S_r & z > z_0 \\ S_l & z < z_0, \end{cases} \tag{2.14}$$

with $0 = S_l < S_r < 1$ where $S_l = 0$ gives a dry region and $0 < S_r < 1$ gives a partially saturated region.

Then the solution is a shock wave travelling with speed

$$\dot{s} = -\frac{1}{\phi}\left(\frac{K(S_r)}{S_r}\right), \tag{2.15}$$

which was derived from (2.12), but has a simpler expression than for the previous case due to the saturation and flux both vanishing in the dry region. Note that (2.15) gives velocity of the flow: the water above the moving interface $z = z_0 + \dot{s}t$ simply moves uniformly downwards with constant speed.

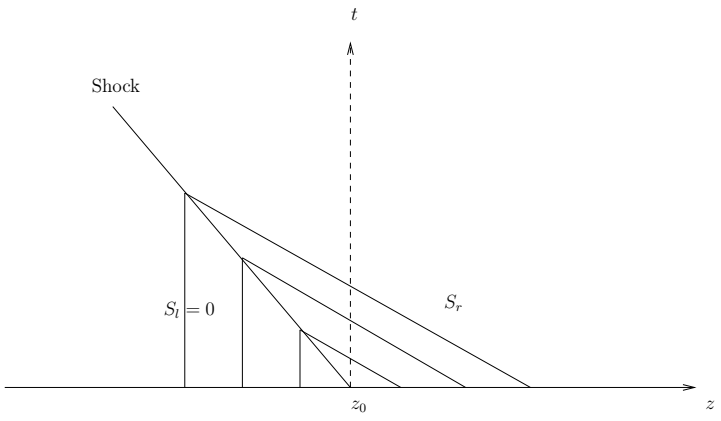

Figure 2.13: Characteristic diagram for equation (2.3) with condition (2.14) where $0 = S_l < S_r < 1$. Note that the characteristics in each of the regions, where S is constant, go into the shock.

Case 3: A saturated region above a partially saturated region

Consider equation (2.3) with initial condition

$$S(z,0) = \begin{cases} S_r & z > z_0 \\ S_l & z < z_0, \end{cases} \tag{2.16}$$

with $0 < S_l < S_r = 1$ where $0 < S_l < 1$ represents a partially saturated region and $S_r = 1$ represents a saturated region. The shock speed according to (2.12)

is given by

$$\dot{s} = -\frac{1}{\phi}\left(\frac{K(S_l)-1}{S_l-1}\right). \tag{2.17}$$

This is got by taking a limit of $S_r \to 1^-$ in Case 1. The characteristic diagram in such a case might be envisaged as in Figure 2.14, with the characteristics in the right-hand part of the diagram being nearly parallel to the z axis.

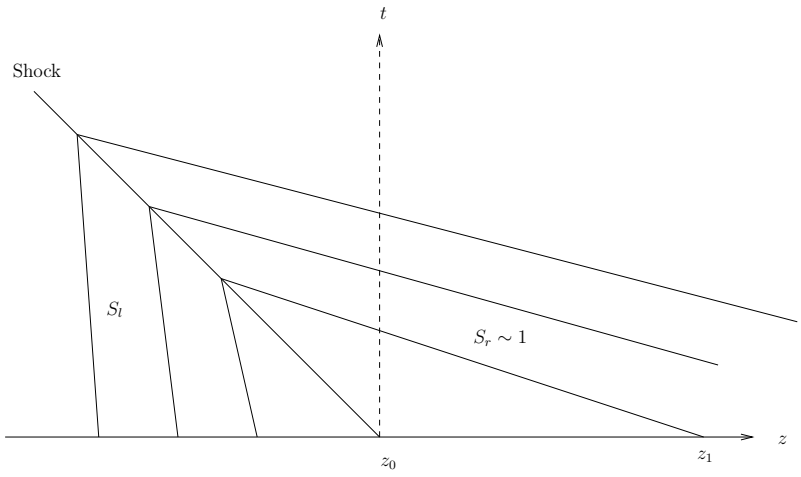

Figure 2.14: Characteristic diagram for equation (2.3) with condition (2.16) where $0 < S_l < S_r$ nearly 1. Note that characteristics in each of the regions where S is constant go into the shock. The characteristics on the right in the limiting case of $S_r = 1$ will be parallel to the z axis and come from $z = \infty$, see Figure 2.15.

Equation (2.5) can alternatively be written by

$$\frac{1}{c(S)}z \;=\; -t_0 + t, \tag{2.18}$$

where $t_0 = -z_1/c(S)$. We see that from (2.18), as $S = S_r \to 1$, we have $\dfrac{1}{c(S)}z \to 0$ and then each characteristic can be written as

$$t = t_0. \tag{2.19}$$

This allow the characteristic lines to be horizontal. The characteristic lines for this case are shown in Figure 2.15.

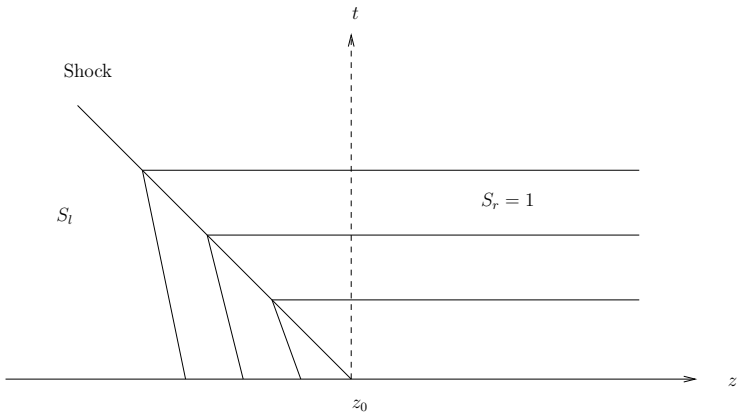

Figure 2.15: Characteristic diagram for equation (2.3) with (2.16) where $0 < S_l < S_r = 1$. Note that characteristics in each of the regions, where S is constant, go into the shock. The characteristics on the right are now parallel to the z axis and are given by $t =$ constant, see (2.19).

However, as we have a saturated region in $z > s(t)$ in this case, the flow in the region should be given by Darcy's law (1.23). The shock speed can then be given, using (1.24) in (2.12), by

$$\dot{s} = -\frac{1}{\phi}\left(\frac{K(S_l) + \frac{1}{\gamma}A - 1}{S_l - 1}\right), \tag{2.20}$$

for A an imposed negative pressure gradient. Equation (2.20) is identical to (2.17) when $A = 0$, i.e when the pressure is zero in the saturated region $(z > s(t))$.

Case 4: A saturated region above a dry region

Consider equation (2.3) with initial condition

$$S(z,0) = \begin{cases} S_r & z > z_0 \\ S_l & z < z_0, \end{cases} \tag{2.21}$$

with $0 = S_l < S_r = 1$ where $S_l = 0$ represents a dry region and $S_r = 1$ represents a saturated region. Again the characteristics go into the shock which has a simple shock speed, given by (2.12), which now reduces to

$$\dot{s} = -1/\phi. \tag{2.22}$$

The characteristic lines for this case are shown in Figure 2.16. The characteristics in the dry region, where $z < s(t)$, are vertical lines corresponding to $S_l = 0$ whereas the characteristics in the saturated region, where $z > s(t)$, being nearly parallel to the z axis.

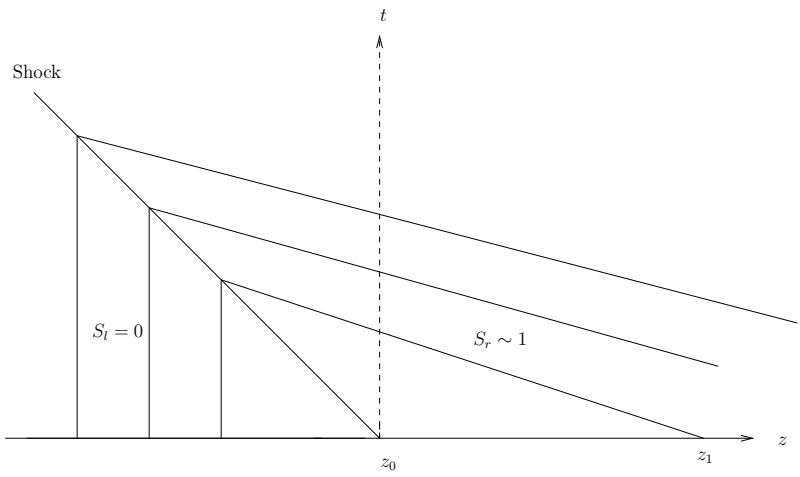

Figure 2.16: Characteristic diagram for equation (2.3) with condition (2.21) where $0 = S_l < S_r$ nearly 1. Note that characteristics in each of the regions where S is constant go into the shock. The characteristics on the right in the limiting case of $S_r = 1$ will be parallel to the z axis and come from $z = \infty$, see Figure 2.17.

As before, in Case 3, the shock speed might more generally be given by

$$\dot{s} = -\frac{1}{\phi}\left(1 - \frac{1}{\gamma}A\right), \tag{2.23}$$

if there is a forcing pressure gradient imposed in the saturated region. Equa-

tions (2.23) and (2.22) are same when $A = 0$. Avoiding negative pressure above the shock, we again have $A \leq 0$ so $\dot{s} \geq -\frac{1}{\phi}$.
With a similar argument as in Case 3, the characteristic diagram can also be shown in horizontal lines for the saturated region ($z > s(t)$). The corresponding characteristic lines for this case is sketched in Figure 2.17.

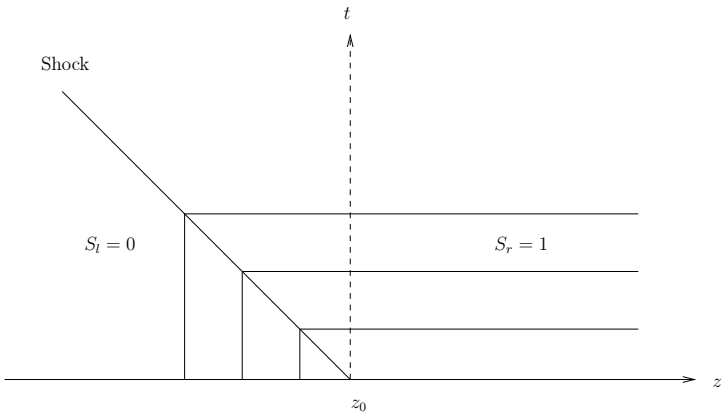

Figure 2.17: Characteristic diagram for equation (2.3) with condition (2.21) where $0 = S_l < S_r = 1$. Note that characteristics in each of the regions where S is constant go into the shock. The characteristics on the right are now parallel to the z axis.

In all the rarefaction waves and shock cases, the moisture moves downwards (to the left in our analytical and numerical solutions), corresponding to the influence of gravity. The shock speed that was derived from Rankine-Hugoniot condition is negative in each case. When we take A, an imposed pressure gradient in a saturated region, to be large and positive in (2.20) or (2.23) the shock speed can become now positive and then the moisture moves upwards. We come back to this in Section 3.3, but note now that this suction might not be very realistic in practice.

2.3 Self-Similar Solutions for the Convection Model

Introduction

Self-similar solutions give a powerful tool for solving partial differential equations. They allow us to reduce the number of independent variables in the partial differential equation through the use of new variables. By using self-similar solution we can transform the partial differential equation to an ordinary differential equation which may be easier to solve. They can be particularly useful when we are interested in determining local limiting behaviour, say for, short time and/or small space.

To begin, consider self-similar solutions to equation (2.2) in the form

$$S(t,z) = t^{\alpha}\Phi(\xi), \quad \text{where} \quad \xi = (z - z_0)t^{\beta} \text{ is the similarity variable,} \tag{2.24}$$

and α and β are some unknown powers. With these new variables equation (2.2) takes the form

$$\phi\left(\alpha\Phi + \beta\xi\frac{d\Phi}{d\xi}\right) = t^{\beta-\alpha+1}\frac{d}{d\xi}\left(K\left(t^{\alpha}\Phi\right)\right). \tag{2.25}$$

To eliminate t in equation (2.25), we need $\alpha = 0$, so $S \equiv \Phi$ then $\beta = -1$, and equation (2.25) becomes

$$\frac{d\Phi}{d\xi}\left(\phi\xi + K'(\Phi)\right) = 0, \tag{2.26}$$

where $K'(\Phi) = dK(\Phi)/d\Phi$. Solutions of (2.26) can be given by

$$\Phi = \text{constant}, \tag{2.27}$$

or by

$$K'(\Phi) = -\phi\xi. \tag{2.28}$$

Solutions satisfying (2.27) everywhere are trivial, $S =$ constant, on the other hand, solutions satisfying (2.28) are shown in Figure 2.18.

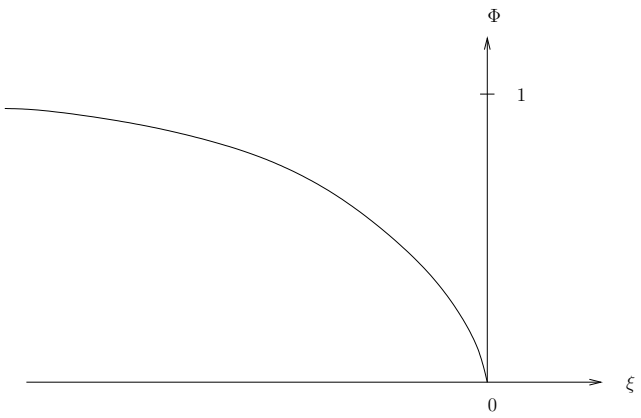

Figure 2.18: The form of the non-trivial solutions of (2.28).

The latter solution, given by (2.28), would only satisfy initial data $S = 1$ at $t = 0$ (corresponding to $\xi \to -\infty$) and boundary data $S = 0$ on $z = 0$ (i.e $\Phi = 0$ on $\xi = 0$). To get a non-constant solution satisfying other initial and boundary data, we can patch together up to three solutions of these forms. Taking initial condition $S = \Phi_l$ for $z < 0$ and boundary data $S = \Phi_r$ on $z = 0$ (for $t > 0$) with $0 < \Phi_r < \Phi_l < 1$, we then want boundary data for Φ: $\Phi = \Phi_l$ as $\xi \to -\infty$ and $\Phi = \Phi_r$ at $\xi = 0$. We therefore have

$$\Phi = \Phi_l = \text{constant} \quad \text{for} \quad \xi \leq \xi_l \text{ and } \Phi = \Phi_r = \text{constant} \quad \text{for} \quad \xi \geq \xi_r, \quad (2.29)$$

as shown in Figure 2.19.

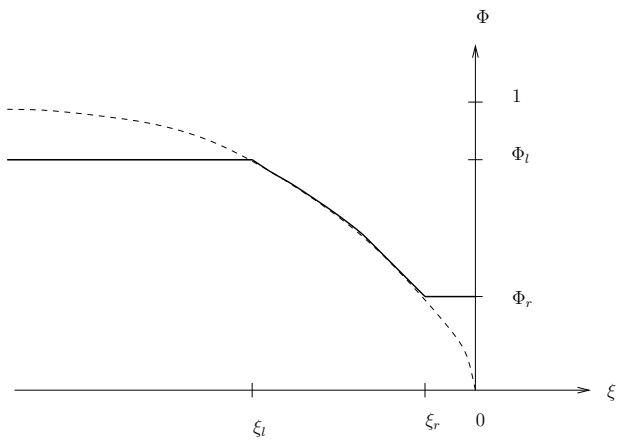

Figure 2.19: The form of the non-trivial and trivial solutions together.

For non-trivial solutions ($\frac{d\Phi}{d\xi} \not\equiv 0$) of (2.26), we find that the similarity solutions $S(t,z)$ can be written in the implicit form

$$\begin{aligned} \xi &= -\frac{1}{\phi}K'(\Phi) \quad \text{for} \quad \xi_l < \xi < \xi_r, \\ &= c(S), \quad \text{as in} \quad (2.3) \\ &= \frac{z-z_0}{t} \quad \text{from} \quad (2.24) \quad \text{with} \quad \beta = -1. \end{aligned} \tag{2.30}$$

From (2.29) and (2.30), we see that this similarity solution is simply the rarefaction wave, (2.6), we constructed earlier, by noting that $S = c^{-1}(\xi)$, $S_l = c^{-1}(\xi_l)$ and $S_r = c^{-1}(\xi_r)$. Note that to avoid discontinuities, such as shocks, we need $\xi = -\frac{1}{\phi}\frac{d}{d\Phi}K(\Phi)$ for $\xi = \xi_l$, $\Phi = \Phi_l$ and for $\xi = \xi_r$, $\Phi = \Phi_r$.

We can find local asymptotic behaviour for equation (2.2) for low saturation (where the soil region is nearly dry) and for high saturation (where it is nearly saturated). This will allow us to consider two main cases.

2.3.1 Case 1: Low Saturation

We consider again self-similar solutions to equation (2.2) (near $z = z_0$) as in form

$$S(t,z) = t^{\alpha}\Phi(\xi), \quad \text{where} \quad \xi = (z-z_0)t^{\beta}. \tag{2.31}$$

Using these expressions with the approximate form of $K(S)$ as in (1.13) taking S to be small, equation (2.25) becomes

$$\phi\left(\alpha\Phi + \beta\xi\frac{d\Phi}{d\xi}\right) = \frac{9}{8}t^{\beta+(7/2)\alpha+1}\left(\Phi^{7/2}\frac{d\Phi}{d\xi}\right). \tag{2.32}$$

For no explicit time dependence of equation (2.32) it is required that

$$\beta + \frac{7}{2}\alpha + 1 = 0. \tag{2.33}$$

We now look at various cases, for different sizes of α, the first of which is motivated by having constant boundary data. The other cases are fixed by their mathematical properties. Let us start first with two special cases when α or β is zero.

Case 1(i): α=0

Assuming the boundary condition takes the form

$$S = S_0 \quad \text{on} \quad z = z_0, \tag{2.34}$$

with $0 < S_0 \ll 1$, by using equation (2.34) in (2.31), we obtain

$$t^{\alpha}\Phi(0) = S_0, \tag{2.35}$$

and from (2.35) we again find that $\alpha = 0$ and $\Phi(0) = S_0 > 0$. Then from (2.33) $\beta = -1$. Hence equation (2.32) reduces

$$\frac{d\Phi}{d\xi}\left(\phi\xi + \frac{9}{8}\Phi^{7/2}\right) = 0. \tag{2.36}$$

Again, following a similar argument as in the standard case, we can patch the trivial and non-trivial solutions together. For a non-trivial solution of (2.36), we obtain

$$\Phi^{7/2} = -\frac{8}{9}\phi\xi. \tag{2.37}$$

Equation (2.37) is valid only for $\xi_l < \xi < \xi_r \leq 0$ (since $\Phi = S \geq 0$). If we keep to the boundary condition, (2.34), we have the stronger inequality $\xi_r < 0$

since $S_0 > 0$. Then solving (2.37) for Φ and replacing Φ by S we have

$$S = \left(-\frac{8}{9}\phi\xi\right)^{2/7} \quad \text{for} \quad \xi_l < \xi < \xi_r \leq 0. \tag{2.38}$$

The solution S of (2.38) can be written in term of z and t and hence we have

$$S(z,t) = \left(-\phi\frac{8}{9}\frac{(z-z_0)}{t}\right)^{2/7} \quad \text{for} \quad \xi_l < \xi < \xi_r \leq 0. \tag{2.39}$$

For $|z - z_0|$ small or t large, we have that from (2.39) S becomes close to 0 which gives a region which is nearly dry.
With a similar argument to that in the standard case, we see that the solution (2.39) agrees with the limiting version of the expansion fan solution in (2.7) by taking that $S_r = (-(8/9)\phi\xi_r)^{2/7}$ and $S_l = (-(8/9)\phi\xi_l)^{2/7}$ where $0 \leq S_r < S_l \ll 1$.

Case 1(ii): $\alpha = -\frac{2}{7}$

Taking $\alpha = -\frac{2}{7}$ gives $\beta = 0$ (see (2.33)) and then equation (2.32) reduces to

$$\frac{d\Phi}{d\xi} = -\frac{16\phi}{63}\Phi^{-5/2}. \tag{2.40}$$

Integrating (2.40) we obtain

$$\Phi^{7/2} = -c_0\xi + c_1, \tag{2.41}$$

where $c_0 = 8\phi/9$ and c_1 is an arbitrary constant. Without loss of generality, we take $c_1 = 0$ then equation (2.41) gives a solution valid only for $\xi < 0$. Then solving (2.41) for Φ, we get

$$\Phi = \left(-c_0\xi\right)^{2/7}. \tag{2.42}$$

Substituting this into equation (2.31) and noting that $\xi = z - z_0$ we are left with

$$S(t,z) = t^{-2/7}\left(-c_0(z-z_0)\right)^{2/7}, \tag{2.43}$$

or

$$S(t,z) \;=\; \left(-c_0\frac{(z-z_0)}{t}\right)^{2/7}. \tag{2.44}$$

Equation (2.44) represents the same non-trivial solution that was in (2.39), (remember that $c_0 = 8\phi/9$). From (2.44), we see that the solution gradually decays to 0 as $t \to \infty$ which gives a drying region as time advances.

Case 1(iii): $\alpha > 0$

For any $\alpha > 0$ in (2.33), we find that $\beta < 0$. Using this, equation (2.32) can then be written as

$$\frac{d\Phi}{d\xi} = \frac{\alpha\phi\Phi}{(9/8)\Phi^{7/2} - \beta\phi\xi}, \tag{2.45}$$

which has only one equilibrium point, $\Phi = 0$. The nullcline of (2.45) is

$$\xi = \frac{9}{8\beta\phi}\Phi^{7/2}, \tag{2.46}$$

where $\xi < 0$ since $\beta < 0$.
We now study the behaviour of the solutions of (2.45) for all ξ. We first study the solutions of (2.45) where $\xi \to \infty$ and $\Phi > 0$. We set

$$G(\Phi,\xi) = \frac{\alpha\phi\Phi}{(9/8)\Phi^{7/2} - \beta\phi\xi}. \tag{2.47}$$

Clearly, $\frac{d\Phi}{d\xi} = G(\Phi,\xi) \geq 0$ for $\xi > 0$, so that we have

$$\Phi \geq \Phi_0, \tag{2.48}$$

where $\Phi = \Phi_0$ at $\xi = 0$. Assuming that Φ is bounded, so that $\Phi \to \Phi_1^-$ as $\xi \to \infty$, for some $\Phi_1 > \Phi_0$, then $\Phi_0 < \Phi < \Phi_1$ for $\xi > 0$ and

$$G(\Phi,\xi) \geq \frac{\alpha\phi\Phi_0}{(9/8)\Phi_1^{7/2} - \beta\phi\xi}. \tag{2.49}$$

Integrating (2.49), we obtain

$$\begin{aligned}\Phi &\geq \Phi_0 + \int_0^{\xi} \frac{\alpha\phi\Phi_0}{(9/8)\Phi_1^{7/2} - \beta\phi\xi} d\xi \\ &= \Phi_0 - (\alpha\Phi_0/\beta)\ln((9/8)\Phi_1^{7/2} - \beta\phi\xi). \end{aligned} \tag{2.50}$$

The right hand side of (2.50) increases to infinity as $\xi \to \infty$, so the solution Φ in fact becomes unbounded.

To look at the solution behaviour when $\xi \to 0$, we look for a solution in the form

$$\Phi = a\xi^{2/7}, \tag{2.51}$$

where $a > 0$, because we have a similar form in the previous two cases, see equations (2.42) and (2.38). Then $\frac{d\Phi}{d\xi} = \frac{2}{7}a\xi^{-5/7}$. Using these expressions with $\beta = -(7/2)\alpha - 1$ (see (2.33)) in (2.45) we obtain

$$\frac{2}{7}a\xi^{-5/7} = \frac{a\phi\alpha\xi^{2/7}}{(9/8)a^{7/2}|\xi| + (1 + (7/2)\alpha)\phi\xi}. \tag{2.52}$$

We can write

$$\frac{2}{7}a\xi^{-5/7} = \begin{cases} \dfrac{a\phi\alpha}{(9/8)a^{7/2} + (1 + (7/2)\alpha)\phi}\xi^{-5/7} & \xi > 0 \\ \dfrac{a\phi\alpha}{(-9/8)a^{7/2} + (1 + (7/2)\alpha)\phi}\xi^{-5/7} & \xi < 0, \end{cases}$$

For $\xi > 0$, we have

$$(9/8)a^{7/2} + (1 + (7/2)\alpha)\phi = (7/2)\alpha\phi, \tag{2.53}$$

and this gives $(9/8)a^{7/2} = -\phi$, from which it is impossible to determine a value of a.

For $\xi < 0$, we have

$$-(9/8)a^{7/2} + (1 + (7/2)\alpha)\phi = (7/2)\alpha\phi, \tag{2.54}$$

then solving for a, we find $a = ((8/9)\phi)^{2/7}$. Using this value of a, we obtain a solution in the form

$$\Phi = \left(\frac{8}{9}\phi\right)^{2/7} \xi^{2/7}. \tag{2.55}$$

Note that this is valid only for $\xi < 0$. We now have exactly the same non-trivial solution as in (2.44) and (2.39) by replacing ξ by $(z - z_0)t^\beta$.
Finally, we look for local behaviour for ξ and Φ small with $\Phi \ll |\xi^{2/7}|$. We see from (2.45) the first term in denominator is small and not important compared with second term. Then, equation (2.45) reduces

$$\frac{d\Phi}{d\xi} = -\frac{\alpha}{\beta}\frac{\Phi}{\xi}, \quad \text{where} \quad \beta < 0 \tag{2.56}$$

and then solving for Φ, we obtain

$$\Phi = A\xi^{-(\alpha/\beta)}, \tag{2.57}$$

where A is a constant of integration. From the relation between α and β in (2.33), equation (2.57) gives

$$\Phi = A\xi^{(2/7)/(1+2/(7\alpha))}. \tag{2.58}$$

The power of ξ in (2.58) satisfies $(2/7)/(1 + 2/(7\alpha)) < 2/7$ for any $\alpha > 0$. Thus, $|A\xi^{(2/7)/(1+(2/7)\alpha)}| \gg |\xi^{2/7}|$ for $\xi \to 0$.
Alternatively, seeking local behaviour of Φ small with ξ small such that $\Phi \gg |\xi^{2/7}|$, we now neglect the second term in the denominator in the right-hand side of (2.45) to get

$$\frac{d\Phi}{d\xi} \sim \frac{8\alpha\phi}{9\Phi^{5/2}}. \tag{2.59}$$

Integration gets us back to the form (2.51), so that this assumed local behaviour, of $\Phi \gg \xi^{2/7}$, is also violated. We deduce that the only way Φ approaches 0 is according to (2.55). Also, note that from (2.59) blow-up does not occur in the left half plane.
It is also clear that any solution in $\xi < 0$ lying under the nullcline ($0 < (9/8)\Phi^{7/2} < (-\beta)\phi(-\xi)$), is decreasing but remains above $\Phi > 0$ and so must tend to $\Phi = 0$ as $\xi \to 0^-$.
Likewise, for $\xi > 0$, a solution above the nullcline is increasing but can not blow up at finite ξ (Φ large gives $d\Phi/d\xi \sim (8/9)\alpha\phi\Phi^{-5/2}$). These solutions must cross the positive Φ axis at $\xi = 0$.

With the above information in hand for $\alpha > 0$ and $\beta < 0$, the phase plane of equation (2.45) for ξ against Φ can be constructed, see Figure 2.20. Note that in order to create a phase plane, equation (2.45) can be converted to a system of two ordinary differential equations by taking Φ and ξ to be functions of a dummy independent variable.

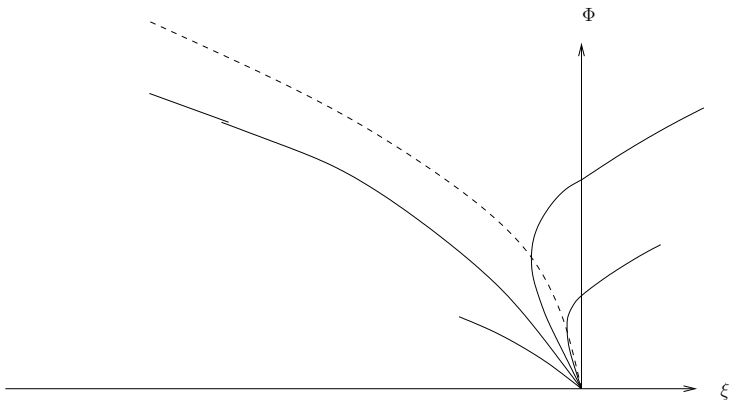

Figure 2.20: Phase plane for (2.45) with $\alpha > 0$ and $\beta < 0$. The dashed line represents the nullcline of (2.45).

For fixed $z < z_0$, we have that $\xi = (z - z_0)t^\beta \to 0^-$ as $t \to \infty$ (since $\beta < 0$), then substituting (2.55) into (2.31), we obtain

$$\begin{aligned} S(t,z) &= t^\alpha \left((8/9)\phi\right)^{2/7} \xi^{2/7} \\ &= t^\alpha \left((8/9)\phi\right)^{2/7} \left((z-z_0)t^\beta\right)^{2/7} \qquad \text{from (2.31)} \\ &= \frac{\left((8/9)\phi(z-z_0)\right)^{2/7}}{t^{2/7}} \qquad (\beta = -(7/2)\alpha - 1) \\ &\to 0 \quad \text{when } |z - z_0| \to 0 \text{ or } t \to \infty. \end{aligned} \tag{2.60}$$

Equation (2.60) gives a region which is nearly dry.
Note that along the trajectories that cross the Φ axis in the above figure, Φ must tend to some $\Phi_0 > 0$ as $\xi \to 0^-$. However, given that $\beta < 0$, this requires that $t \to \infty$ and then (2.31) leads to $S \to \infty$ rather than $S \to 0$, since $\alpha > 0$.

Case 1(iv): $\alpha < -\frac{2}{7}$

From (2.33) we see that for any $\alpha < -\frac{2}{7}$, $\beta > 0$. For $\xi < 0$, we see from (2.45) that $\frac{d\Phi}{d\xi} < 0$ and then it is also clear that no blow-up is possible in this region. Following a similar argument to Case 1(iii), as $\xi \to 0^-$ some solutions decrease and behave as (2.55). Also, there are solutions which cross the Φ axis and they continue decreasing until they hit the nullcline $\Phi = (8\phi\beta\xi/9)^{2/7}$. Solutions below the nullcline increase towards it. The phase plane is shown in Figure 2.21. Note that in this case, (2.58), $\Phi = A\xi^{(2/7)/(1+2/(7\alpha))}$, has a power $(2/7)/(1+2/(7\alpha))$ which is greater than $2/7$ permitting solutions tending to $\Phi = 0$ as $\xi \to 0$ with $\Phi \ll |\xi^{2/7}|$, for both $\xi \to 0^-$ and $\xi \to 0^+$.

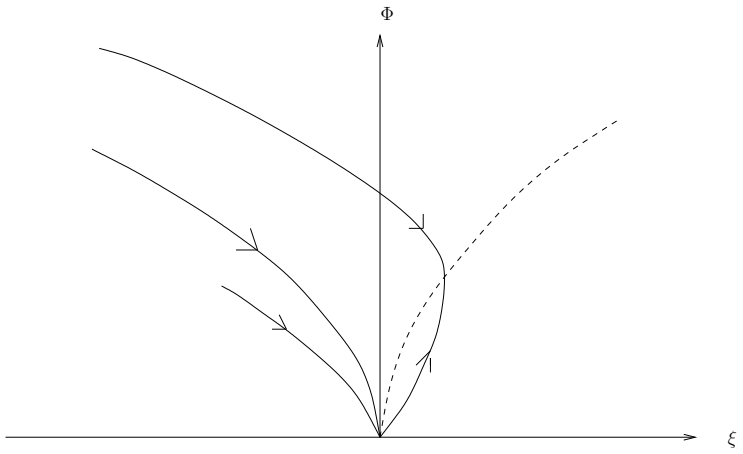

Figure 2.21: Phase plane for (2.45) with $\alpha < -\frac{2}{7}$ and $\beta > 0$. The dashed line represents the nullcline of (2.45).

For fixed $z < z_0$, we have that $\xi = (z - z_0)t^\beta \to 0^-$ as $t \to 0$ or $|z - z_0| \to 0$

(since $\beta > 0$), then substituting (2.58) into (2.31), we obtain

$$\begin{aligned} S(t,z) &= t^{\alpha} A \xi^{(2/7)/(1+2/(7\alpha))} \\ &= A t^{\alpha} \left((z-z_0)t^{\beta}\right)^{(2/7)/(1+2/(7\alpha))} \quad \text{from (2.31)} \\ &= A(z-z_0)^{(2/7)/(1+2/(7\alpha))} \quad (\beta = -(7/2)\alpha - 1) \\ &\to 0 \quad \text{only for } z \to z_0. \end{aligned}$$

This gives a nearly dry region at short distances from z_0. Also, along a trajectory which crosses the Φ axis in Figure 2.21, Φ must tend to some $\Phi_0 > 0$ as $\xi \to 0^-$, and again we have from (2.31) that $S \to \infty$ as $t \to 0$.
The special solution behaves as for the other cases.

Case 1(v): $-\frac{2}{7} < \alpha < 0$

For any $-\frac{2}{7} < \alpha < 0$ (2.33) gives $\beta < 0$. For $\xi < 0$ and $\Phi \gg \xi^{2/7}$, we see from (2.45) that $\frac{d\Phi}{d\xi} < 0$ and so such solutions decrease and cross the positive Φ axis at $\xi = 0$. They continue decreasing for $\xi > 0$. Such solutions above the nullcline decrease towards it while solutions below the nullcline increase towards it. As in the previous two cases, there is an exact solution, see (2.55), which tends to 0 as $\xi \to 0^-$. The power in (2.58) is now negative, ruling out the possibility of having $\Phi \ll |\xi^{2/7}|$. The phase plane is shown in Figure 2.22.

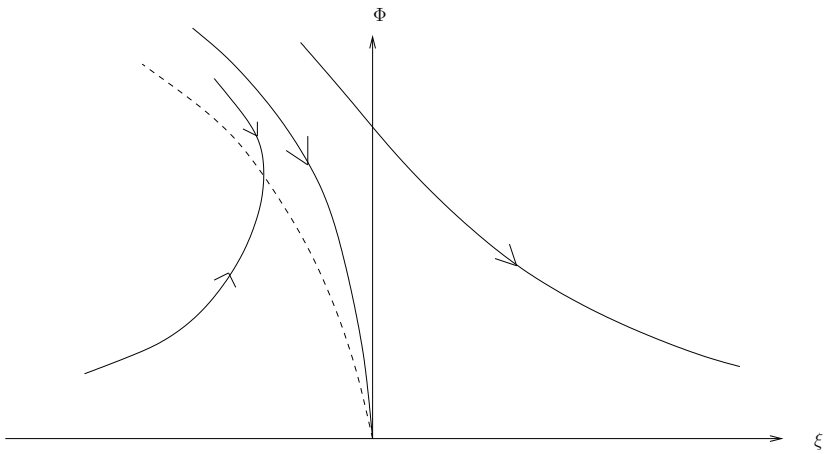

Figure 2.22: Phase plane for (2.45) with $-\frac{2}{7} < \alpha < 0$ and $\beta < 0$. The dashed line represents the nullcline of (2.45).

In Figure 2.22, the trajectory above the nullcine that goes to zero as $\xi \to 0^-$ corresponds to solution given by (2.55). Again substituting (2.55) into (2.31), see (2.60), gives a nearly dry region for large time or short space.
A trajectory that crosses Φ axis at $\Phi_0 > 0$ when $\xi = 0$ given by

$$S = t^\alpha \Phi(\xi) \sim t^\alpha \Phi_0 \to 0 \quad \text{as } t \to \infty, \tag{2.61}$$

which gives a nearly dry region (but, uninterestingly, an almost spatially uniform solution).
Solutions for $\xi \to \infty$ have $\Phi \to 0$, so $\Phi' \sim (-\alpha/\beta)\Phi/\xi$ (from (2.45)), giving $\Phi \sim A_0 \xi^{-\alpha/\beta}$ with $A_0 =$ constant. Then $S \sim t^\alpha (A_0((z - z_0)t^\beta)^{-\alpha/\beta}) \sim A_0(z - z_0)^{\alpha/(1+7\alpha/2)}$ on using (2.33), valid for $(z - z_0)$ large.

2.3.2 Case 2: High Saturation

We now consider local self-similar solutions to equation (2.2) when S is close to 1 (near saturation) in a rather different form:

$$S(t, z) = 1 - t^\alpha \Phi(\xi), \quad \xi = (z - z_0)t^\beta. \tag{2.62}$$

Substituting these expressions into (2.2), we obtain

$$-\phi\left(\alpha\Phi+\beta\xi\frac{d\Phi}{d\xi}\right)=t^{\beta-\alpha+1}\frac{d}{d\xi}\left(K\left(1-t^{\alpha}\Phi\right)\right). \tag{2.63}$$

Using the approximate form of $K(S)$ for S close to 1 as in (1.19), this gives

$$\phi\left(\alpha\Phi+\beta\xi\frac{d\Phi}{d\xi}\right)=\sqrt{2}t^{\beta-\frac{\alpha}{2}+1}\Phi^{-1/2}\frac{d\Phi}{d\xi}. \tag{2.64}$$

Equation (2.64) is independent of t if

$$\beta-\frac{\alpha}{2}+1=0. \tag{2.65}$$

We proceed much as in Case 1, eliminating t in (2.64), and looking at various cases for different values of α and β. Let us start with the simple case when α=0.

Case 2(i): α=0

Assume the boundary condition satisfies

$$S=1-S_1\neq 1 \quad \text{on} \quad z=z_0, \tag{2.66}$$

substituting (2.66) into (2.62), we obtain

$$t^{\alpha}\Phi(0)=S_1, \quad \text{where} \quad \xi=0. \tag{2.67}$$

This again gives $\alpha=0$, $\Phi(0)=S_1$, $\beta=-1$ and so equation (2.64) becomes

$$\left(\phi\xi+\sqrt{2}\Phi^{-1/2}\right)\frac{d\Phi}{d\xi}=0. \tag{2.68}$$

Following a similar argument to that of the standard case, we can patch the trivial and non-trivial solutions together. Then for a non-trivial solution of (2.68), we have

$$\sqrt{\Phi}=\frac{\sqrt{2}}{-\phi\xi}, \tag{2.69}$$

which gives a solution valid only for $-\infty \leq \xi_l < \xi < \xi_r < 0$, (since $\Phi < \infty$), then solving (2.69) for Φ yields

$$\Phi = \frac{2}{(\phi\xi)^2} \quad \text{for} \quad -\infty \leq \xi_l < \xi < \xi_r < 0. \tag{2.70}$$

Plugging (2.70) into (2.62), we obtain

$$S = 1 - \frac{2}{(\phi\xi)^2} \quad \text{for} \quad -\infty \leq \xi_l < \xi < \xi_r < 0. \tag{2.71}$$

For fixed $z < z_0$, we have that $\xi = (z - z_0)t^\beta \to -\infty$ as $t \to 0$, (since $\beta = -1$). Then from (2.71), the solution approaches 1 as $\xi \to -\infty$, so that away from z_0 the region is very nearly saturated. The solution of equation (2.71) can be written in term of z and t as

$$S = 1 - \left(\frac{\sqrt{2}t}{\phi(z - z_0)}\right)^2 \quad \text{for} \quad -\infty \leq \xi_l < \xi < \xi_r < 0. \tag{2.72}$$

From the trivial solution of (2.68) and the solution of equation (2.72) we find that these solutions agree with limiting rarefaction wave solutions in (2.6) by taking that $S_l = 1 - \left(\phi/\sqrt{2}\xi_l\right)^{-2}$ and $S_r = 1 - \left(\phi/\sqrt{2}\xi_r\right)^{-2}$.

Case 2(ii): α=2

From (2.65), $\alpha = 2$ gives $\beta = 0$. Substituting these values into equation (2.64), we obtain

$$\frac{d\Phi}{d\xi} = \sqrt{2}\phi\Phi^{3/2}. \tag{2.73}$$

Integrating (2.73), we obtain

$$\frac{1}{\sqrt{\Phi}} = -c_0\xi + c_1, \tag{2.74}$$

where $c_0 = \phi/\sqrt{2}$ and c_1 is an arbitrary constant. Without loss of generality, take $c_1 = 0$ then equation (2.74) gives a solution valid only for $\xi < 0$. Solving (2.74) for Φ, we get

$$\Phi = \frac{1}{(-c_0\xi)^2}, \tag{2.75}$$

and plugging (2.75) into (2.62), we obtain

$$S = 1 - \frac{t^2}{(-c_0\xi)^2}, \tag{2.76}$$

where $\xi = z - z_0$. This is the same equation (2.72) since $c_0 = \phi/\sqrt{2}$.

Case 2(iii): $0 < \alpha < 2$

For any $0 < \alpha < 2$, (2.65) gives $-1 < \beta < 0$. Using this, equation (2.64) can then be written as

$$\frac{d\Phi}{d\xi} = \frac{\alpha\phi\Phi}{-\beta\phi\xi + \sqrt{2}\Phi^{-1/2}}. \tag{2.77}$$

This is a non-autonomous first order differential equation and cannot be solved in closed form. However, we can use a phase plane to analyze how the solution $\Phi(\xi)$ of (2.77) will behave as ξ varies depending on an initial condition $\Phi(\xi_0) = \Phi_0$. It is clear that this system has only one equilibrium point which is $\Phi = 0$. The nullcline of (2.77) is the solution of $-\beta\phi\xi + \sqrt{2}\Phi^{-1/2} = 0$, namely

$$\xi = \frac{\sqrt{2}}{\beta\phi\sqrt{\Phi}}, \tag{2.78}$$

where $\xi < 0$ since $-1 < \beta < 0$.
Suppose that we want to study the behaviour of the solution Φ of equation (2.77) for $\xi \to \infty$. We start by setting

$$F(\Phi, \xi) = \frac{\alpha\phi\Phi}{-\beta\phi\xi + \sqrt{2}\Phi^{-1/2}}. \tag{2.79}$$

Since F is clearly an increasing function in Φ and $\frac{d\Phi}{d\xi} \geq 0$ for $\xi > 0$, we have

$$\frac{d\Phi}{d\xi} \geq \frac{\alpha\phi\Phi_0}{-\beta\phi\xi + \sqrt{2}\Phi_0^{-1/2}}, \tag{2.80}$$

where $\Phi = \Phi_0$ at $\xi = 0$. We can then integrate,

$$\begin{aligned}\Phi &\geq \Phi_0 + \int_0^{\xi} \frac{\alpha\phi\Phi_0}{-\beta\phi\xi + \sqrt{2}\Phi_0^{-1/2}} d\xi \\ &= \Phi_0 - (\alpha\Phi_0/\beta)\ln(-\beta\phi\xi + \sqrt{2}\Phi_0^{-1/2}). \end{aligned} \tag{2.81}$$

We see that the solution Φ becomes unbounded, since the right hand side of (2.81) increases as $\xi \to \infty$. Note that β is negative here.
For $\Phi \gg \xi^{-2}$, we see that the second term in the denominator in equation (2.77) can be neglected. Then (2.77) reduces to

$$\frac{d\Phi}{d\xi} \sim \frac{\alpha\Phi}{-\beta\xi}. \tag{2.82}$$

This can be integrated to give, approximately,

$$\Phi = A_0\xi^{-(\alpha/\beta)}, \tag{2.83}$$

where A_0 is a constant of integration. Using the value of $\beta = (\alpha/2) - 1$, see (2.65), in (2.83) we obtain

$$\Phi = A_0\xi^{1/((1/\alpha)-1/2)}, \tag{2.84}$$

and clearly, $1/((1/\alpha)-1/2) > -2$ for any α in the range $0 < \alpha < 2$. This gives $|A_0\xi^{1/((1/\alpha)-1/2)}| \gg |\xi^{-2}|$ as $\xi \to \pm\infty$. Note that the same argument indicates that solutions do not blow-up except possibly at $\xi = 0$.
To study the solution behaviour of (2.77) when $\xi \to 0^-$, we assume that the solution takes the form $\Phi = a\xi^{-2}$ where $a > 0$, since we have a similar form in the previous two cases, see equations (2.75) and (2.70). Using this expression in (2.77), in a similar way to Case 1(iii), we obtain the value of a which is $a = 2/\phi^2$, then we have

$$\Phi = \frac{2}{(\phi\xi)^2}. \tag{2.85}$$

This is the same solution as for Case 2(i) and Case 2(ii). Clearly, from (2.85) we see that

$$\Phi \to \infty \quad \text{as} \quad \xi \to 0^-. \tag{2.86}$$

With the above information in hand, the phase plane of equation (2.77) for

ξ against Φ can be constructed. It is given in Figure 2.23.

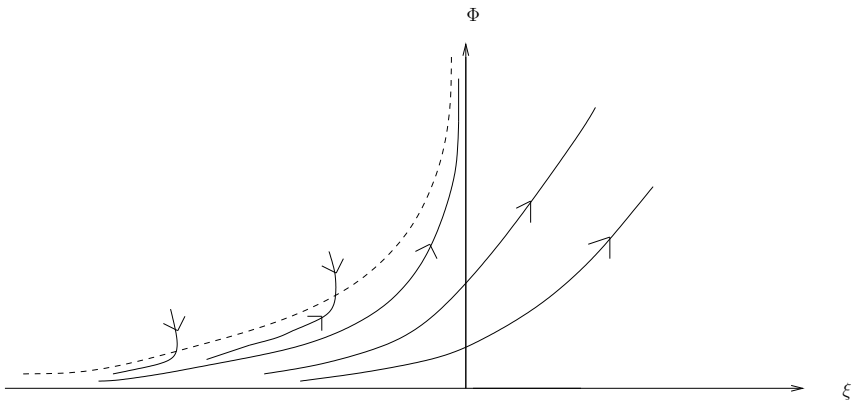

Figure 2.23: Phase plane for (2.77) with $0 < \alpha < 2$ and $-1 < \beta < 0$. The dashed line represents the nullcline of (2.77).

For fixed $z < z_0$, and taking $t \to 0$ we have that $\xi = (z - z_0)t^\beta \to -\infty$. Then substituting equation (2.85) into the basic form of the similarity solution of the high saturation, see (2.62), we obtain

$$\begin{aligned} S(t,z) &= 1 - \frac{2t^\alpha}{(\phi\xi)^2} = 1 - \frac{2t^\alpha}{(\phi(z-z_0)t^\beta)^2} \quad \text{from (2.62)} \\ &= 1 - \frac{2t^\alpha t^{-2\beta}}{\phi^2(z-z_0)^2} = 1 - \frac{2t^\alpha t^{-\alpha+2}}{\phi^2(z-z_0)^2} \qquad (\beta = (\alpha/2) - 1) \\ &= 1 - \frac{2t^2}{\phi^2(z-z_0)^2}. \end{aligned} \tag{2.87}$$

For t small or $z - z_0$ large, (2.87) gives a nearly saturated region. In Figure 2.23, there are some trajectories which cross Φ axis and then Φ must tend to some $\Phi_0 > 0$ as $\xi \to 0^-$. For such solutions, restricting our attention to a limited range of z (recall that $\beta = 0$ in this case),

$$S = 1 - t^\alpha \Phi(\xi) \sim 1 \quad \text{as } t \to 0. \tag{2.88}$$

Case 2(iv): $\alpha > 2$

For $\alpha > 2$, then we have $\beta > 0$ from (2.65). For $\xi < 0$, we see that from equation (2.77) $\frac{d\Phi}{d\xi} > 0$ and clearly blow-up does not occur in the left half plane. Following a similar argument to Case 2(iii), $\Phi \to 0^+$ as $\xi \to -\infty$. There is a limiting solution which blows up as in (2.85) when $\xi \to 0^-$. Bigger solutions blow-up in same way while smaller solutions cross the Φ axis. The solutions which cross the axis continue increasing until they hit the nullcline $\Phi = 2/(\beta\phi\xi)^2$. The solutions above the nullcline decrease towards it. The form of the solution of equation (2.77) with $\alpha > 2$ and $\beta > 0$ can be analyzed by using the phase plane. It is shown in Figure 2.24.

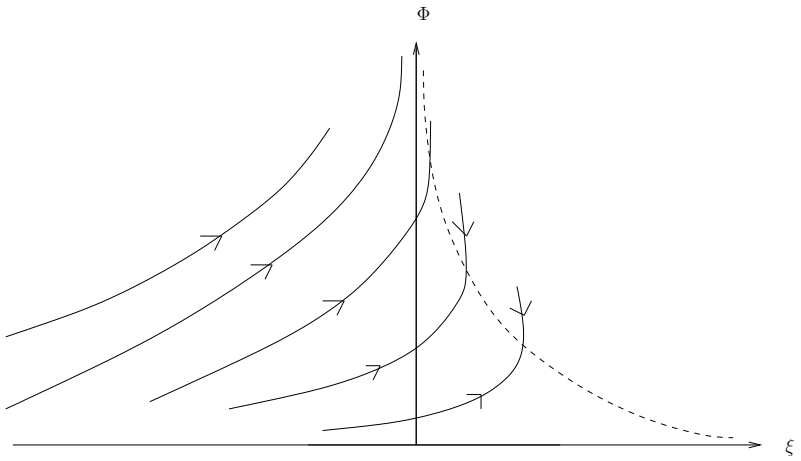

Figure 2.24: Phase plane for (2.77) with $\alpha > 2$ and $\beta > 0$. The dashed line represents the nullcline solution of (2.77).

The solutions crossing the positive Φ axis at $\xi = 0$ correspond to $S = 1 - t^\alpha\Phi(\xi) \sim 1$ as $t \to 0$, again giving a nearly saturated region with approximately uniform saturation. Also, the solution given by (2.85) gives again a nearly saturated region for $t \to 0$ or $(z - z_0) \to -\infty$ as shown in (2.87). In this case the solutions valid in $\xi \leq 0$ with $\Phi(0)$ finite have $\Phi \to 0$ as $\xi \to -\infty$ (see (2.84)). From this $S = 1 - t^\alpha\Phi((z - z_0)t^\beta) \sim 1 - A_0(z - z_0)^{-(\alpha/\beta)} = 1 - A_0(z - z_0)^{1/((1/\alpha)-1/2)}$, valid for $z - z_0$ large and negative.

Case 2(v): $\alpha < 0$

For any $\alpha < 0$, (2.65) gives $\beta < -1$. For $\xi > 0$ it is clear that the solution of (2.77) decays to 0 as $\xi \to \infty$. Solutions above the nullcline (which only exists for $\xi < 0$) increase, while solutions below the nullcline decrease, cross Φ axis and continue decreasing as $\xi \to \infty$. As $\xi \to 0^+$, blow-up of some solutions occurs (like solutions in $\xi < 0$ for the previous cases) according to equation (2.85). The phase plane of equation (2.77) with $\alpha < 0$ and $\beta < -1$ is shown in Figure 2.25.

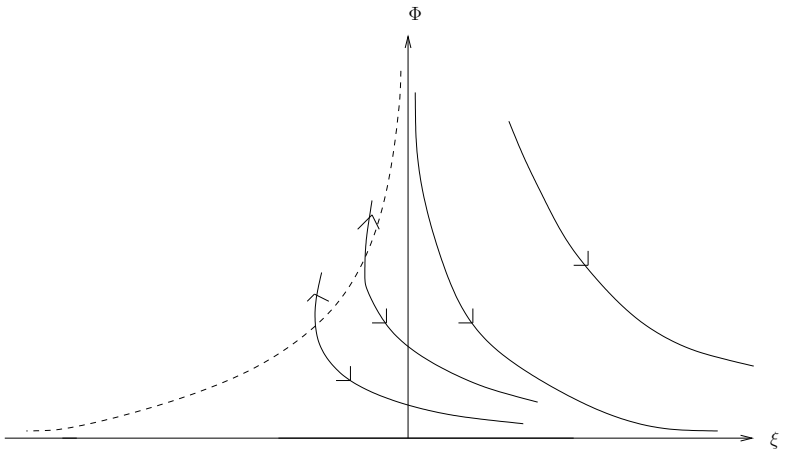

Figure 2.25: Phase plane for (2.77) with $\alpha < 0$ and $\beta < -1$. The dashed line represents the nullcline of (2.77).

For fixed $z > z_0$, $\xi = (z - z_0)t^\beta \to \infty$ as $t \to 0$, then we have from equations (2.85) and (2.62) $S \to 1$ as $t \to 0$ which gives a nearly saturated region. For those solutions cross the positive Φ axis at $\xi = 0$ we have $S = 1 - t^\alpha \Phi(\xi) \to 1$ as $t \to \infty$ which gives again a nearly saturated region.
Solutions of Φ valid for ξ large and positive give, like the previous case, steady saturation $S = 1 - A_0(z - z_0)^{1/((1/\alpha)-1/2)}$, now valid for $z - z_0$ large and positive.

2.3.3 Summary of Limiting Similarity Solutions

For both limiting cases, low and high saturation, whatever particular powers α and β were applied, with the exception of the last case looked at for high

saturation, Case 2(v), there was always an exact solution of the simplified equation. This corresponded to the limiting version of (2.25) and gave part of a rarefaction wave. Only the $\alpha = 0$ cases corresponded exactly to the rarefaction waves (applying in $z < z_0$, i.e in $\xi < 0$) as only the differential equations for these permitted the $S = \Phi =$ constant trivial solutions.

2.4 Numerical Results for Initial Value Problems

2.4.1 Conservative Upwind Method

We consider the conservative upwind method (one-sided approximations, [27]) to equation (2.2) by replacing the time and space derivatives by their first order finite difference approximations. This yields

$$\phi\frac{S_j^{n+1}-S_j^n}{\Delta t}=\left[\frac{K(S_{j+1}^n)-K(S_j^n)}{\Delta z}\right], \tag{2.89}$$

which can be rewritten as

$$S_j^{n+1}=S_j^n+\frac{\Delta t}{\phi\Delta z}\left[K(S_{j+1}^n)-K(S_j^n)\right]. \tag{2.90}$$

We can assume that $S_j^n \geq 0$ for all j, n, so that the upwind direction is always to the right. Since any shock travels to the left, the upwind method is appropriate for the initial value problem. This method uses two values (S_j^n and S_{j+1}^n) for the calculation of S_j^{n+1}.
Using the centred difference approximation to the z derivative of $\frac{\partial}{\partial z}\left(K(S)\right)$ at time t_n in equation (2.2) suffers from stability problems. A stable method may be obtained by evaluating the centred difference approximation to $\frac{\partial}{\partial z}\left(K(S)\right)$ at time t_{n+1} rather than at time t_n but it requires the use of an implicit scheme [27].

In order to have stability, we are required to apply the necessary condition known as the Courant-Friedrichs-Lewy condition. It is often referred to as the CFL and is

$$\left|c(S_j^n)\frac{\Delta t}{\phi\Delta z}\right|\leq 1 \tag{2.91}$$

where $c(S_j^n)$ represents the wave speed. If a small space step is used then a small time step is needed to keep the numerical simulation stable.

The conservative upwind method is used with step-function initial data for all the four cases of the rarefaction wave that are discussed in Subsection 2.2.2. The numerical results for all these cases are presented in Figures 2.26,

2.27, 2.28 and 2.29. The upwind method is also used for the four cases of the shock solutions in Subsection 2.2.3 which are shown in Figures 2.32, 2.33, 2.34 and 2.35. The results given by the two numerical methods, the upwind method and method of characteristics, are plotted together in Figures 2.30 and 2.31. We see that they give a good fit. We notice that in Figures 2.30 there is a very slight difference between these two methods near $S_r = 0.4$ and near $S_l = 0.8$. A similar observation applies for Figure 2.31. We still keep $m = \frac{1}{2}$, and, in each case, take $z_0 = \frac{1}{2}$.

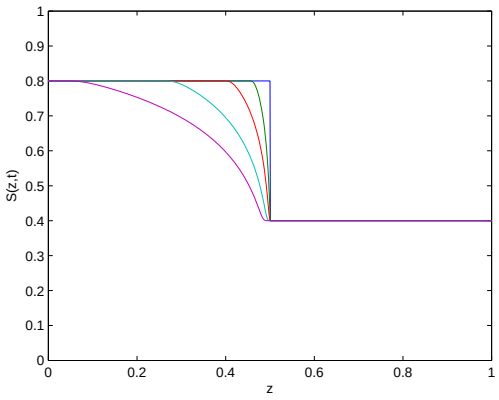

Figure 2.26: The numerical solution of (2.2) with (2.8) at times $t = 0$ (blue), $1/125$ (green), $1/50$ (red), $1/20$ (cyan) and 0.1 (pink), using the conservative upwind method. Here $S_l = 0.8$, $S_r = 0.4$ and $\phi = \frac{1}{4}$. The values of the parameters used for the simulation with the upwind method are $\Delta t = 1/5000$ and $\Delta z = 1/1000$. The solution gives good agreement with that shown in Figure 2.4 (Case 1, Subsection 2.2.2).

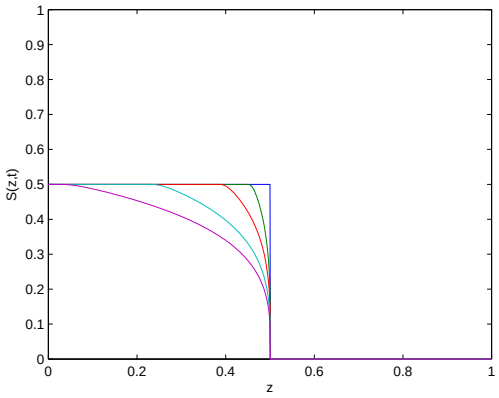

Figure 2.27: The numerical solution of (2.2) with (2.9) at times $t = 0$ (blue), 0.08 (green), 0.2 (red), 0.5 (cyan) and 0.9 (pink), using the conservative upwind method. Here $S_l = 0.5$, $S_r = 0$ and $\phi = \frac{1}{4}$. The values of the parameters used for the simulation with the upwind method are $\Delta t = 1/1000$ and $\Delta z = 1/1000$. The solution gives good agreement with that shown in Figure 2.6 (Case 2, Subsection 2.2.2).

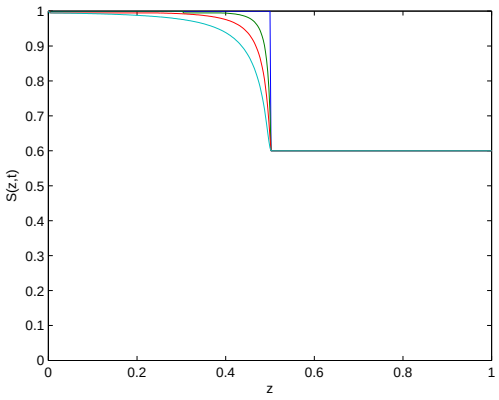

Figure 2.28: The numerical solution of (2.2) with (2.10) at times $t = 0$ (blue), $1/750$ (green), $1/300$ (red) and $1/150$ (cyan), using the conservative upwind method. Here $S_l = 1$, $S_r = 0.6$ and $\phi = \frac{1}{4}$. The values of the parameters used for the simulation with the upwind method are $\Delta t = 1/60000$ and $\Delta z = 1/400$. The results give good agreement with those shown in Figure 2.8 (Case 3, Subsection 2.2.2).

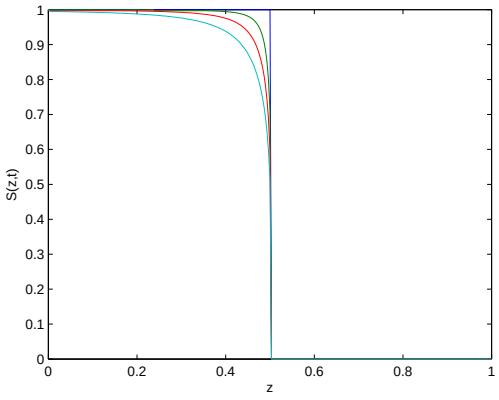

Figure 2.29: The numerical solution of (2.2) with (2.11) at times $t = 0$ (blue), $1/750$ (green), $1/300$ (red) and $1/150$ (cyan), using the conservative upwind method. Here $S_l = 1$, $S_r = 0$ and $\phi = \frac{1}{4}$. The values of the parameters used for the simulation with the upwind method are $\Delta t = 1/60000$ and $\Delta z = 1/300$. The results give good agreement with those shown in Figure 2.10 (Case 4, Subsection 2.2.2).

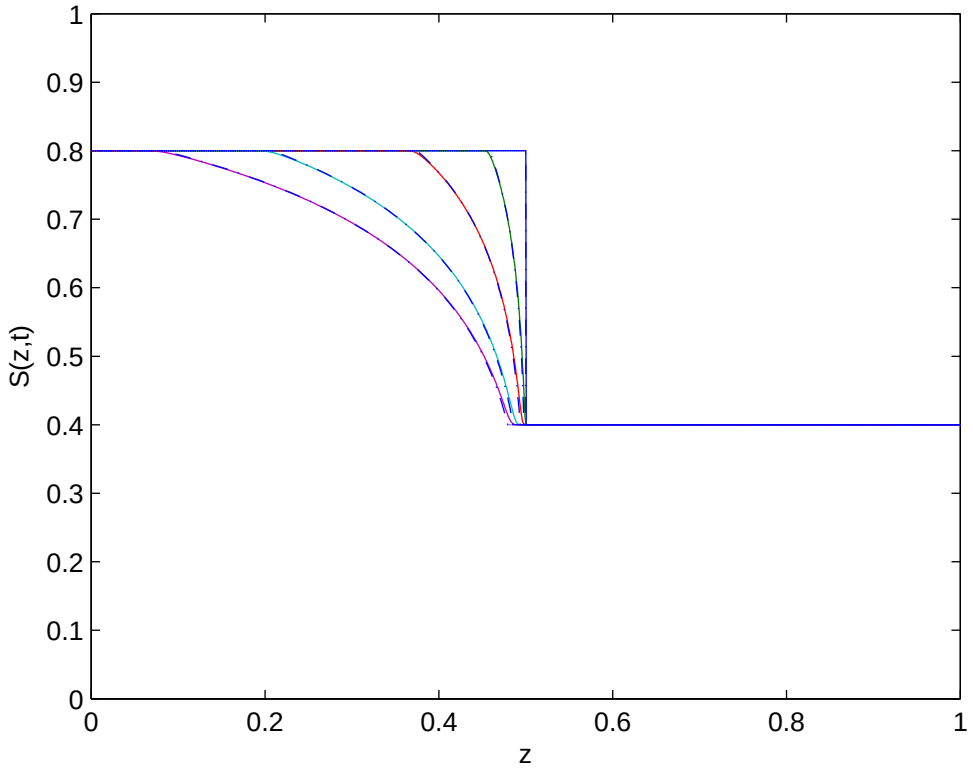

Figure 2.30: The numerical solution of (2.2) with (2.8) at times $t = 0$ (blue), 0.01 (green), 0.03 (red), 0.07 (cyan) and 0.1 (pink), using the conservative upwind method (solid curves) and the method of characteristics (dash-dotted lines). Here $S_l = 0.8$, $S_r = 0.4$ and $\phi = \frac{1}{4}$. The values of the parameters used for the simulation with the upwind method are $\Delta t = 1/10000$ and $\Delta z = 1/1800$.

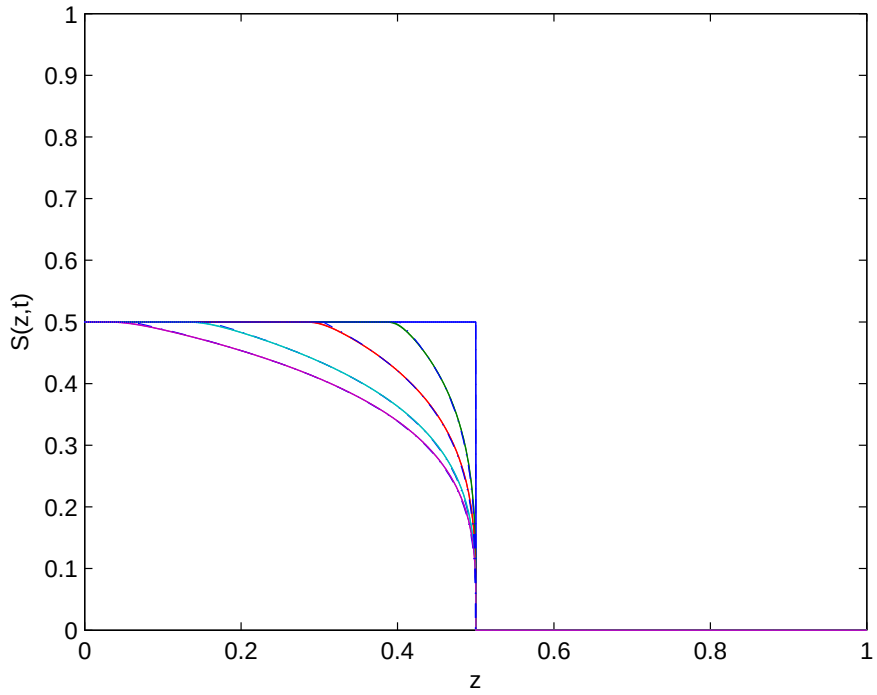

Figure 2.31: The numerical solution of (2.2) with (2.9) at times $t = 0$ (blue), 0.2 (green), 0.4 (red), 0.7 (cyan) and 0.9 (pink), using the conservative upwind method (solid curves) and the method of characteristics (dash-dotted lines). Here $S_l = 0.5$, $S_r = 0$ and $\phi = \dfrac{1}{4}$. The values of the parameters used for the simulation with the upwind method are $\Delta t = 1/10000$ and $\Delta z = 1/1800$.

The numerical results that are presented in Figures 2.26-2.29, which are obtained for all the four cases of the rarefaction wave that are discussed in Subsection 2.2.2, show how the rarefaction wave develops with increasing time. Also, the numerical results that are presented in Figures 2.32-2.35, which are obtained for all the four cases of the shock solutions in Subsection 2.2.3, reproduce these shocks and their propagation with increasing time. All these numerical results, in each case, are compared with the approximate analytic solutions that are discussed in Subsection 2.2.2 and 2.2.3. They are seen to very similar to our exact analytic solutions. Figures 2.30 and 2.31 show very good qualitative agreement between the numerical results of upwind method and method of characteristics.

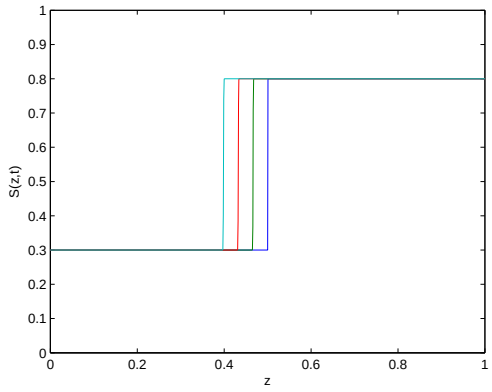

Figure 2.32: The numerical solution of (2.2) with (2.13) at times $t = 0$ (blue), 0.3 (green), 0.6 (red) and 0.9 (cyan), using the conservative upwind method. Here $S_l = 0.3$, $S_r = 0.8$ and $\phi = \frac{1}{4}$. The values of the parameters used for the simulation with the upwind method are $\Delta t = 1/10000$ and $\Delta z = 1/1000$. The wave velocity determined from the numerical simulation is $C_n \approx -1.14$ and agrees with the theoretical value given by $C_t = -1.135$. This discontinuous solution gives a good indication of the appearance of shocks which were discussed analytically, in Case 1, in Subsection 2.2.3.

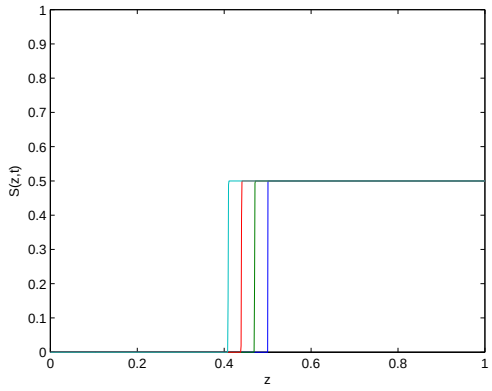

Figure 2.33: The numerical solution of (2.2) with (2.14) at times $t = 0$ (blue), 0.3 (green), 0.6 (red) and 0.9 (cyan), using the conservative upwind method. Here $S_l = 0$, $S_r = 0.5$ and $\phi = \frac{1}{4}$. The values of the parameters used for the simulation with the upwind method are $\Delta t = 1/10000$ and $\Delta z = 1/1000$. The wave velocity determined from the numerical simulation is $C_n \approx -0.11$ and agrees with the theoretical value given by $C_t = -0.101$. This discontinuous solution gives a good indication of the appearance of shocks which were discussed analytically, in Case 2, in Subsection 2.2.3.

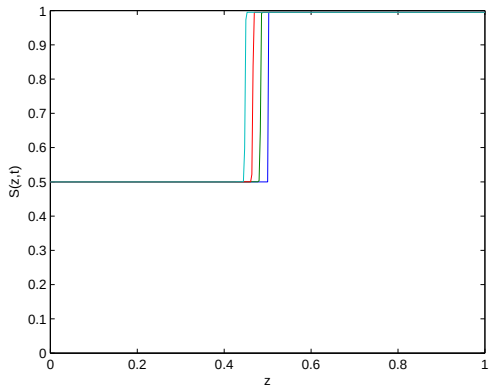

Figure 2.34: The numerical solution of (2.2) with (2.16) at times $t = 0$ (blue), $1/360$ (green), $1/180$ (red) and $1/120$ (cyan), using the conservative upwind method. Here $S_l = 0.5$, $S_r = 1$ and $\phi = \frac{1}{4}$. The values of the parameters used for the simulation with the upwind method are $\Delta t = 1/18000$ and $\Delta z = 1/360$. The wave velocity determined from the numerical simulation is $C_n \approx -7.84$ and agrees with the theoretical value given by $C_t = -7.8985$. This discontinuous solution gives a good indication of the appearance of shocks which were discussed analytically, in Case 3, in Subsection 2.2.3.

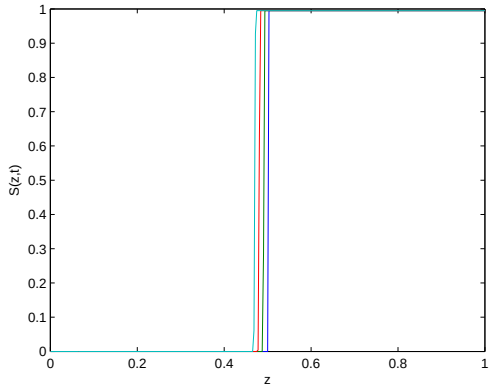

Figure 2.35: The numerical solution of (2.2) with (2.21) at times $t = 0$ (blue), $1/300$ (green), $1/150$ (red) and $1/100$ (cyan), using the conservative upwind method. Here $S_l = 0$, $S_r = 1$ and $\phi = \frac{1}{4}$. The wave velocity determined from the numerical simulation is $C_n \approx -4.02$ and agrees with the theoretical value given by $C_t = -4$. The values of the parameters used for the simulation with the upwind method are $\Delta t = 1/15000$ and $\Delta z = 1/310$. This discontinuous solution gives a good indication of the appearance of shocks which were discussed analytically, in Case 4, in Subsection 2.2.3.

We will finish this chapter with a few examples with equation (2.2) for different initial value problems to see how a shock forms and then develops over time. The solutions for the different examples are shown in Figures 2.36, 2.37 and 2.38. The initial condition for the solution shown in Figure 2.36 is $S(z,0) = 0.8\sin(\pi z)$ and the boundary condition at the top of the interval is $S(1,t) = 0$. Piecewise linear initial conditions are used in Figure 2.37, with the top boundary condition $S(1,t) = 0.8$, and in Figure 2.38 with the top boundary condition $S(1,t) = 0.5$, see Examples 2 and 3.

Example 1 Consider the convection model, (2.2), with initial condition

$$S(z,0) = S_* \sin(\pi z), \tag{2.92}$$

where $S_* = 0.8$ is the maximum saturation, see Figure 2.36 with the boundary condition $S(1,t) = 0$.

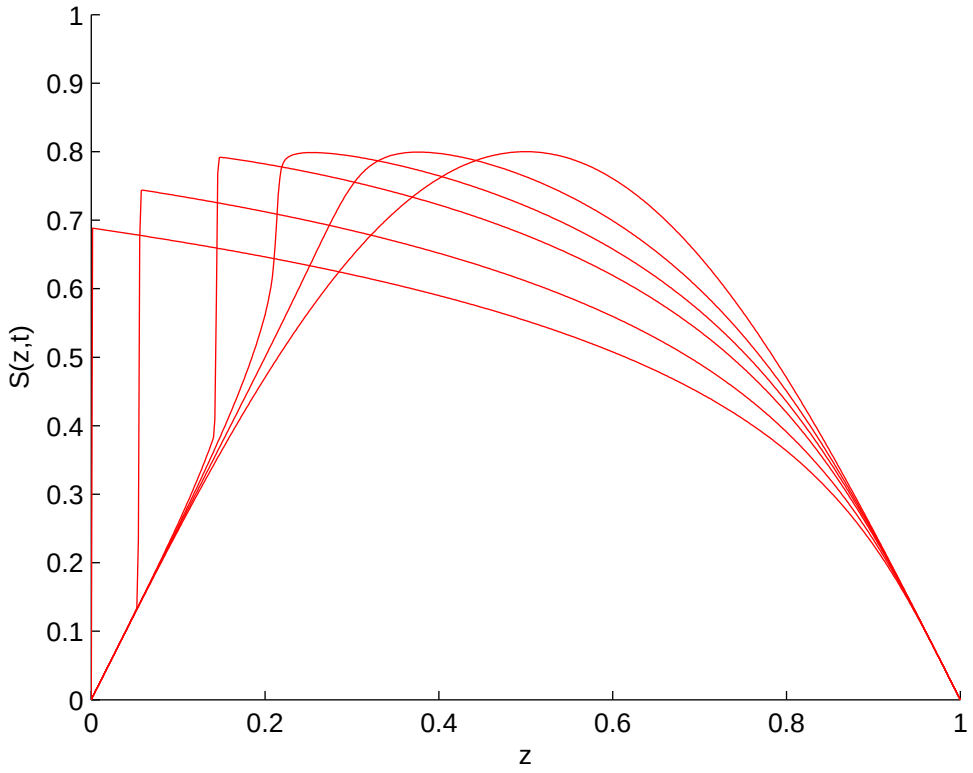

Figure 2.36: The numerical solutions to equation (2.2) with (2.92) at times $t = 0$, 0.03, 0.06, 0.1, 0.2 and 0.35 (where the shock reaches $z = 0$). Solution moves to the left corresponding to the negative speed. Here the solution gets steep as t increases and becomes a sharp, discontinuous solution, near $t = 0.1$ when a shock develops. The values of the parameters used for the simulation are $\Delta t = 1/10000$ and $\Delta z = 1/590$. Taking smaller Δt and Δz makes no visible difference to the solution.

Example 2 Consider the convection model, (2.2), with initial condition

$$S(z,0) = \begin{cases} 0.2 & z < 0.25 \\ 2.4z - 0.4 & 0.25 \leq z \leq 0.5 \\ 0.8 & z > 0.5, \end{cases} \tag{2.93}$$

see Figure 2.37, with the boundary condition $S(1,t) = 0.8$. The results are also shown in Figure 2.37.

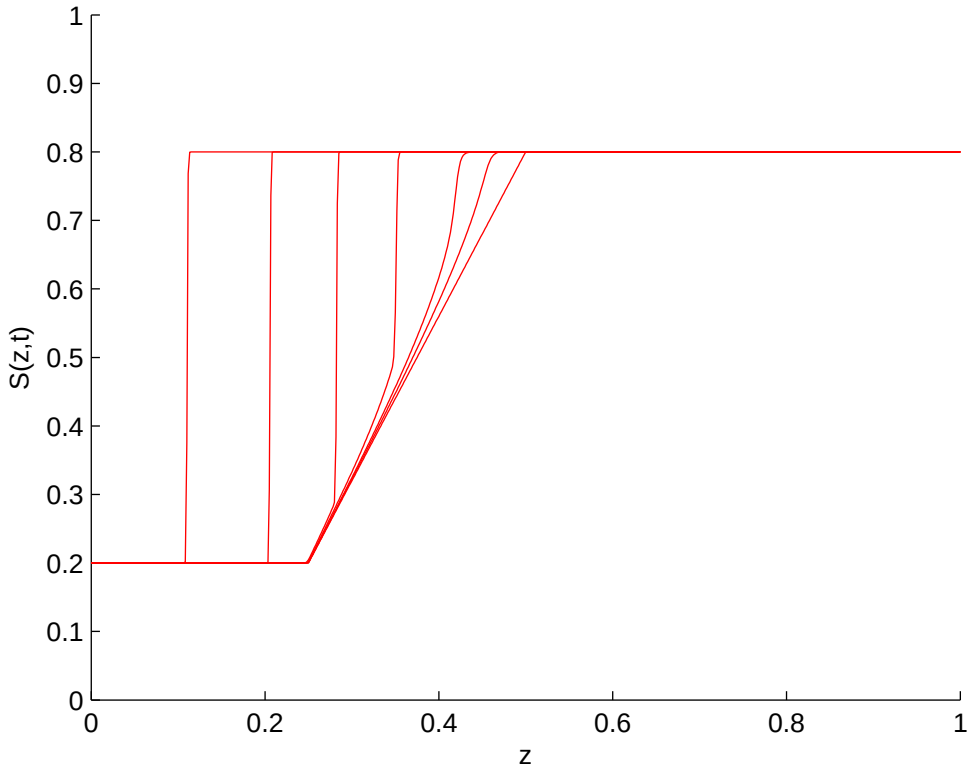

Figure 2.37: The numerical solutions to equations (2.2) with (2.93) at times $t = 0,\ 0.01,\ 0.02,\ 0.05,\ 0.1,\ 0.17$ and 0.27. Solution moves to the left corresponding to the negative speed. As t increases the solution becomes very steep and a shock forms. The values of the parameters used for the simulation are $\Delta t = 1/9000$ and $\Delta z = 1/600$.

.

Example 3 Consider the convection model, (2.2), with initial condition

$$S(z,0) = \begin{cases} 0 & z < 0.25 \\ 2z - 0.5 & 0.25 \leq z \leq 0.5 \\ 0.5 & z > 0.5, \end{cases} \tag{2.94}$$

see Figure 2.38, with the boundary condition $S(1,t) = 0.5$. The results are also shown in Figure 2.38.

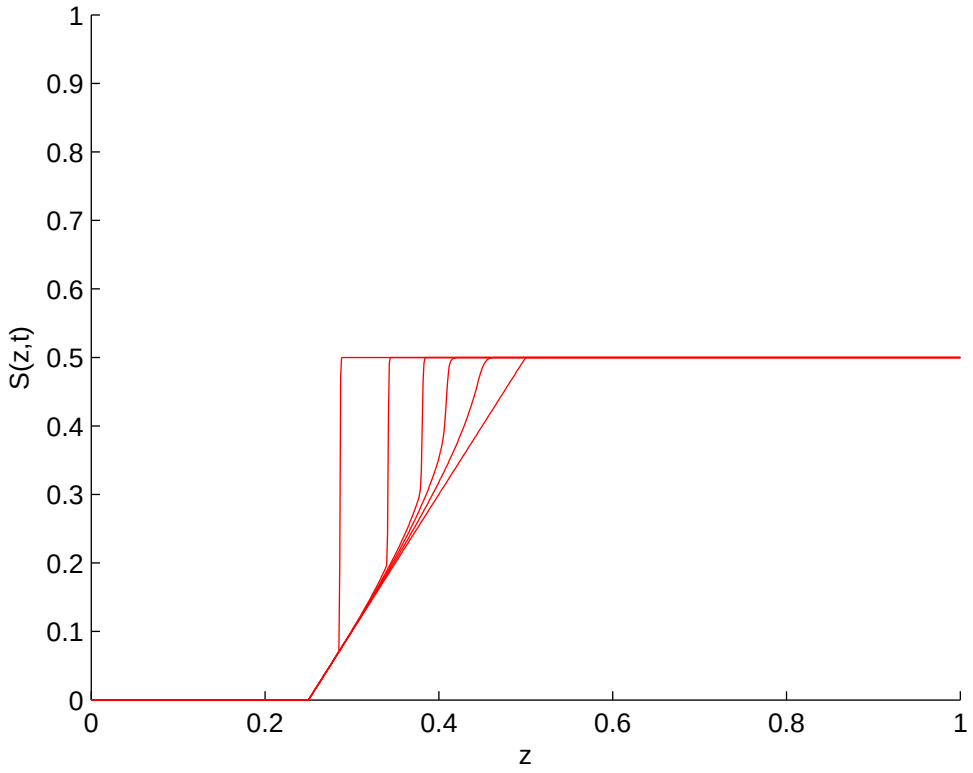

Figure 2.38: The numerical solutions to equation (2.2) with (2.94) at times $t = 0,\ 0.1,\ 0.2,\ 0.3,\ 0.5$ and 0.9. Solution moves to the left corresponding to the negative speed. As t increases the solution becomes very steep and a shock forms. The values of the parameters used for the simulation are $\Delta t = 1/10000$ and $\Delta z = 1/1000$.

The numerical results in Figures 2.36-2.38 show how a shock forms and develops over time. These initial conditions are different from the piecewise constant initial data used in Subsection 2.2.3. We start with continuous initial data and the solutions produce a shock. Due to the higher saturation and large saturation gradient a shock forms in Figure 2.37 faster than in Figure 2.38 and then it reaches $z = 0$ in a short time. The initial value problems that were used in Example 2 and Example 3, see equations (2.93) and (2.94), can be seen to give the same analytic solutions as the first and second cases in Subsection 2.2.3, after an initial transient while a zone of finite slope steepens, but they are, of course, more difficult to solve exactly than the piecewise constant initial data. The method of characteristics is only applied easily for the convection model with piecewise constant initial data. Using this method for solving a convection model with more general initial condition seems to be difficult, especially for shock solutions. The upwind method is popular for solving nonlinear hyperbolic equation because of its excellent shock capturing ability.
The numerical results that were obtained for the shock solutions give a good indications of how fast water gets through a soil layer. In all the numerical results shocks move to left (meaning down in the original problem) corresponding to a negative speed: shocks, along with characteristics, move in the direction of gravity. Rarefaction waves can give some indications of drying through water drainage.

In fact, there is an important connection between the equation (2.1) and equation (2.2). Equation (2.2) is the limit as $\delta \to 0$ of (2.1). This fact will be studied numerically with similar examples to these in Chapter 3 where the diffusion term is kept in and we will see how the solutions behave as $\delta \to 0$.

Chapter 3

Models with Diffusion but no Sink Term

3.1 Introduction

In this chapter, we first consider a nonlinear diffusion model (without the convection term) which describes the evolution of saturation without the influence of gravity. Travelling wave solutions (TWS) and self-similar solutions are investigated. In particular, local behaviour for a nearly dry region (S small) and for a nearly saturated region (S close to 1) is discussed. Local TWS for these two limiting cases are found in explicit forms. Next, we consider the model where both the convective and diffusive terms are present (convection-diffusion models). Travelling wave solutions and self-similar solutions are again discussed for various possible cases. In particular, local behaviour for a nearly dry region and for a nearly saturated region is looked at. We find that TWS exist for six possible cases. In only one case is there no TWS. Local TWS for the two limiting cases are also found in explicit forms. Perturbation methods are also used for some ordinary differential equations which are obtained for the self-similar solutions in the two limiting cases. Numerical results are presented for these perturbation methods. Numerical results are also presented for all cases of TWS. A finite difference method is used for solving the convection-diffusion model. We use the convection-diffusion model to study the combined effects of the diffusion term and nonlinear convection in the equation. For small enough δ, solutions of convection-diffusion model produce what is effectively a shock over time as its smoothing effect is lost giving discontinuous solutions.

3.2 Travelling Wave Solutions for the Diffusion Model Only

Equation (2.1) has two complicated terms that make it very difficulty to obtain a solution. Firstly, the right hand side contains the function $D(S)$ which depends on S in a highly nonlinear way and models diffusion. Secondly, the first-order term represents the influence of gravity on the process again in significantly nonlinear way. Equation (2.1) can be considered in the absence of the gravity term and then reduces to a porous-media type nonlinear diffusion equation

$$\phi\frac{\partial S}{\partial t} = \frac{\partial}{\partial z}\left(\delta D\left(S\right)\frac{\partial S}{\partial z}\right). \tag{3.1}$$

This simplified equation could be valid if the saturation is varying over a very short distance scale. To motivate the travelling wave solutions we consider (3.1) subject to the conditions

$$t = 0, \quad z > 0, \quad S = S_r, \tag{3.2}$$

and

$$t = 0, \quad z < 0, \quad S = S_l. \tag{3.3}$$

It was initial data like this that led to shocks, discontinuous travelling waves, in the previous chapter. More generally, we expect that a solution has to problem (3.1)-(3.3) to satisfy $S = S_r$ as $z \to \infty$ and $S = S_l$ as $z \to -\infty$ for $t > 0$, so it has a front-like profile. In particular, there is the possibility that the solution to (3.1)-(3.3) evolves to a travelling wave, in the form of a front, which would have the appearance of a smoothed version of the initial data (and the shock solution in the previous chapter).
Consider now a travelling wave solution for the nonlinear diffusion equation (3.1) of the form

$$S(z,t) = S(\zeta) \quad \text{with} \quad \zeta = z - ct, \tag{3.4}$$

where c is the wave velocity. The case where $c < 0$ can be reduced to $c > 0$ by a reflection that gives a solution in opposite direction. Taking thus $c > 0$ and substituting equation (3.4) into equation (3.1), we arrive at the ODE

$$\frac{d}{d\zeta}\left(\delta D(S)\frac{dS}{d\zeta}\right) + c\phi\frac{dS}{d\zeta} = 0. \tag{3.5}$$

Integrating once we get

$$\delta D(S)\frac{dS}{d\zeta} + c\phi S = B_0, \tag{3.6}$$

where B_0 is a constant of integration. Solving (3.6) for $\dfrac{dS}{d\zeta}$ we find that

$$\frac{dS}{d\zeta} = \frac{B_0 - c\phi S}{\delta D(S)}. \tag{3.7}$$

If the travelling wave is to act as a limiting solution for a problem with initial data (3.2) and (3.3) to give us a front we require conditions

$$S = S_r, \quad \zeta \to \infty \tag{3.8}$$

and

$$S = S_l, \quad \zeta \to -\infty \tag{3.9}$$

which imply

$$\frac{dS}{d\zeta} \to 0 \quad \text{for} \quad \zeta \to \pm\infty. \tag{3.10}$$

To satisfy (3.7) and (3.8), we must take $B_0 = c\phi S_r$, assuming that $S_r < 1$. If we had been looking for a steady solution, $c = 0$, (3.7) would now imply $\frac{dS}{d\zeta} \equiv 0$, so we would simply have a constant, uniform solution, $S \equiv S_r$. Hence, we now restrict our attention to $c > 0$.
To additionally satisfy (3.9), assuming that $S_l < 1$, also gives $B_0 = c\phi S_l$ so $S_r = S_l$, and once again we have a uniform steady state.

If we ignore condition (3.9) and look for a solution to (3.7) with $B_0 = c\phi S_r$ then we first note that for $c > 0$ if $S < S_r$ then $\frac{dS}{d\zeta} > 0$, while $\frac{dS}{d\zeta} < 0$ for $S > S_r$.
Looking at the first case, the solution to (3.7) can be obtained in implicit form,

$$\zeta = \delta \int_S \frac{D(S)}{B_0 - c\phi S} dS, \tag{3.11}$$

and must therefore reach, since $D(S)$ is well behaved for S small, $S = 0$ at a finite value of ζ, which we can take as $\zeta = 0$, so we may write

$$\zeta = \delta \int_0^S \frac{D(S)}{B_0 - c\phi S} dS. \tag{3.12}$$

The numerical solution to equation (3.12) is obtained by using an adaptive Simpson quadrature and the result is shown in Figure 3.1. We see that as $\zeta \to 0$ and $S \to 0$, $\frac{dS}{d\zeta} \to \infty$ since $D(S)\frac{dS}{d\zeta} = (B_0 - c\phi S)/\delta = c\phi(S_r - S)/\delta \to c\phi S_r/\delta$. If we consider the flux $q = -\delta D\,(S)\,\frac{\partial S}{\partial z}$, conditions (3.8) and (3.9) along with (3.7) for S_l and S_r both less than 1, demand that $q \to 0$ as $S \to S_r$ and $S \to S_l$. The solution shown in Figure 3.1, and any other case of $S_l < S_r < 1$, violates this giving lack of conservation of mass. For the solution of Figure 3.1 to make sense, we would need a moving sink at $\zeta = 0$, like the heat sink produced by phase change in Stefan problems.

We can, however, get a global travelling wave in the form of a front if we take $S_r < S_l = 1$. Now $B_0 = c\phi S_l$ from (3.9) but (3.8) does not give $B_0 = c\phi S_r = c\phi$ here, since $D(S) \to \infty$ as $S \to 1$. In such cases, flux $q \to 0$ as $S \to S_r$, as before, and $q \to -c\phi(1 - S_r)$ as $S \to 1$. This is permitted here, as any flux is possible in a saturated region.

.

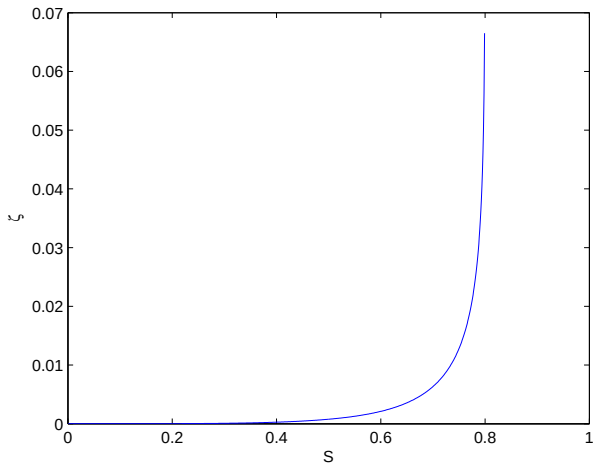

Figure 3.1: Travelling wave solution for equation (3.12), with $c = 1$, $B_0 = c\phi S_r$, $S_r = 0.8$, $S_l = 0$ at $\zeta = 0$ and $\delta = 10^{-4}$. Water is being lost at $S = 0$ where $\zeta = 0$ because the flux, $q = -c\phi S_r$, is negative.

Local travelling wave solutions of equation (3.1) can be obtained in explicit forms for S small and S close to 1.

3.2.1 Case 1: Low Saturation

In this case we look for a solution where S is small. By using the approximate form of $D(S)$ with S small, as in (1.12), we find that the left hand side of (3.6) is zero as $S \to 0$ and then the constant, B_0, on the right hand side must be zero.
Taking $S_r = 0$ at $\zeta = 0$ and substituting the approximate form of $D(S)$ with small S, as in (1.12), equation (3.11) becomes

$$\zeta = -\frac{\delta}{4}\int_0^S \frac{S^{5/2}}{c\phi S} dS,$$

where $0 < S \ll 1$. Then we obtain

$$\zeta = -\frac{\delta}{10c\phi} S^{5/2}. \tag{3.13}$$

Figure 3.2 shows the graph of equation (3.13) for several values of the wave velocity c. Then the local asymptotic behaviour of the solution can be written in explict form as

$$S(\zeta) \sim \left(-\frac{10c\phi}{\delta}\zeta\right)^{2/5}. \tag{3.14}$$

As $\zeta \to 0$, S becomes small. In other words, the region where ζ is small is nearly dry.

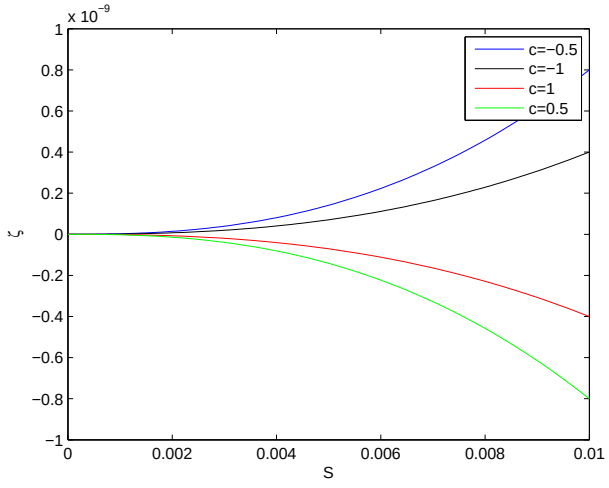

Figure 3.2: Local forms of a travelling wave solution for equation (3.13) for some values of c. Here $\delta = 10^{-4}$ and $\phi = 1/4$.

3.2.2 Case 2: High Saturation

We now look for a solution where S is close to 1. Taking $S_l = 1$ at $\zeta = 0$ and using the approximate form of $D(S)$ with S close to 1, as in (1.18), equation (3.11) becomes approximately,

$$\zeta = -\frac{\delta}{\sqrt{2}}\int_S^1 \frac{(1-S)^{-1/2}}{B_0 - c\phi}dS,$$

where $0 < 1 - S \ll 1$. Then

$$\zeta = -\frac{2\delta(1-S)^{1/2}}{\sqrt{2}(B_0 - c\phi)}. \tag{3.15}$$

Figure 3.3 shows the graph of (3.15) for ζ against S for some different values of c. Solving (3.15) for S we find that

$$S = 1 - \left(\frac{\sqrt{2}(B_0 - c\phi)}{2\delta}\zeta\right)^2. \tag{3.16}$$

We see from (3.16), for small ζ, S will be close to 1, which represents a region which is nearly saturated.

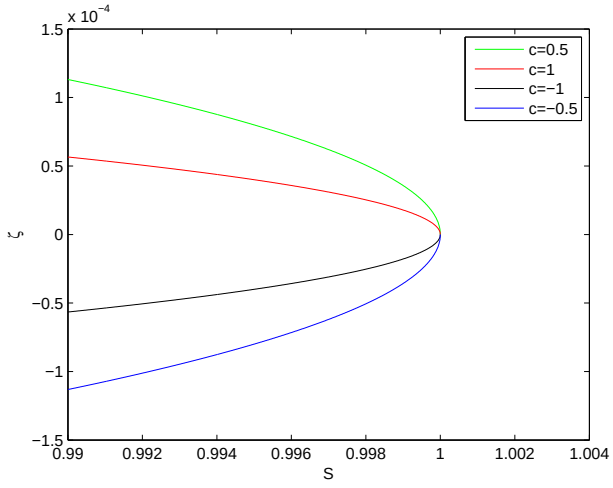

Figure 3.3: Travelling wave solution where $S \to 1$ for some values of c. Here $B_0 = 0$ and $\delta = 10^{-4}$.

3.3 Travelling Wave Solutions for the Convection-Diffusion Model

In this section, we study travelling wave solution to the nonlinear convection-diffusion equation (2.1). Consider now a travelling wave solution to (2.1) as in form (3.4), then equation (3.7) becomes

$$\frac{dS}{d\zeta} = \frac{B_0 - K(S) - c\phi S}{\delta D(S)}, \tag{3.17}$$

where B_0 is again the constant of integration and c is the wave velocity. The two constants c and B_0 depend on the convection function $K(S)$, they are independent of the diffusivity term $D(S)$. Since the solution depends on these two constants, there are several cases we have to consider. All of these have a physical sense which we come to below. As we mentioned in the introduction, we study these different cases according to whether the limiting saturations might be zero, one or in between. The travelling wave front, with the limiting saturations in (0,1), has the solution taking limiting values at plus and minus infinity, $S(\infty) = S_r$ and $S(-\infty) = S_l$, and $\frac{dS}{d\zeta} = 0$ at $\zeta = \pm\infty$. The other cases we look at have one or both of the limiting saturations either zero or one.
The analytical solution of (3.17) can be obtained in an implicit form as

$$\zeta = \int_S \frac{\delta D(S)}{B_0 - K(S) - c\phi S} dS. \tag{3.18}$$

We again use adaptive Simpson quadrature to obtain the numerical solutions of (3.18) for some of the cases.

Case 1: Dry region above a saturated region

Firstly, we look for a travelling wave which links a fully dry region to a fully saturated region. We take $\zeta = 0$ to be where the soil is fully dry. Now, equation (3.17) can also be written as

$$\delta D(S)\frac{dS}{d\zeta} + K(S) + c\phi S = B_0. \tag{3.19}$$

Using the approximate forms of the $D(S)$ and $K(S)$ with S small, as in (1.12) and (1.13), we find that the left hand side of (3.19) is zero in the region where

$S = 0$ and it immediately follows that constant B_0 in (3.19) vanishes. We then obtain

$$\zeta = -\int_0^S \frac{\delta D(S)}{K(S) + c\phi S} dS. \tag{3.20}$$

where $0 < S \leq 1$. From (3.20) we have $K(S) + c\phi S > 0$ for $c \geq 0$, to give $\zeta < 0$ (This is equivalent to using (3.17) and noting that S should be decreasing). Travelling waves exist from a dry region ($S = 0$) to a saturated region $S = 1$ with wave velocity $c \geq 0$.

Note that this case was discussed in Subsection 2.2.2, Case 4 for the convection model corresponding to piecewise initial data and we only found a rarefaction wave.

Equation (3.20) allows us to find local asymptotic behaviour near ζ=0 (where the soil is fully dry). By using the approximate forms of $D(S)$ and $K(S)$ with S small, equation (3.20) gives:

$$\zeta \sim -\delta \int_0^S \frac{\frac{1}{4}S^{5/2}}{\frac{1}{4}S^{9/2} + c\phi S} dS \tag{3.21}$$

$$\sim -\delta \int_0^S \frac{\frac{1}{4}S^{5/2}}{c\phi S} dS \quad \text{as} \quad S \to 0^+ \quad \text{assuming} \quad c \neq 0$$

$$\sim -\frac{\delta}{4c\phi} \int_0^S S^{3/2} dS \sim -\frac{\delta}{10c\phi} S^{5/2}. \tag{3.22}$$

The local asymptotic behaviour of the solution can be written in explicit form as

$$S(\zeta) \sim \left(-\frac{10c\phi}{\delta} \zeta \right)^{2/5}. \tag{3.23}$$

This local solution is the same as in (3.14) because the convection term goes to zero faster than the diffusion term when S is small and hence does not have a significant local effect in this case. Equation (3.23) gives again a nearly dry region where ζ is small. Note that when $c = 0$, we have from (3.21), $S = 1/\zeta$. We only consider here in detail cases when S is small, in particular, S reaches 0 at finite ζ, and we do not look at steady states, $c = 0$.

The local behaviour for S becoming close to 1 (where the soil is fully saturated) can also be obtained. We now take $\zeta = 0$ to be where the soil is fully saturated. Again since we have a dry region, we must take $B_0 = 0$ in

(3.19). Substituting the approximate forms of $D(S)$ and $K(S)$ with S close to 1, as in (1.18) and (1.20) respectively, into equation (3.19) we obtain

$$\zeta \sim \delta \int_S^1 \frac{(1-S)^{-1/2}}{\sqrt{2}(1+c\phi)} dS, \tag{3.24}$$

where $0 < 1 - S \ll 1$. Then

$$\zeta \sim \frac{2\delta(1-S)^{1/2}}{\sqrt{2}(1+c\phi)}. \tag{3.25}$$

Clearly, $\zeta > 0$ if $c > -1/\phi$ and $\zeta < 0$ if $c < -1/\phi$. Figures 3.4 and 3.5 show the graph of equation (3.24) for several values of the wave velocity c. The local asymptotic behaviour of the travelling wave solution when S close to 1 can be written in explicit form as

$$S(\zeta) \sim 1 - \left(\frac{1+c\phi}{\sqrt{2}\delta}\zeta\right)^2. \tag{3.26}$$

As $\zeta \to 0$ the last term of equation (3.26) becomes small in comparison to the other, S approaches 1 and the region saturates.

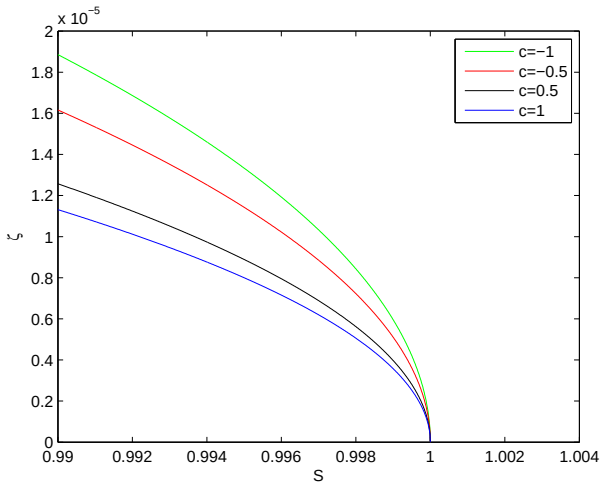

Figure 3.4: Travelling wave solution where $S \to 1$ for some values of c where $c > -1/\phi$ and $\delta = 10^{-4}$.

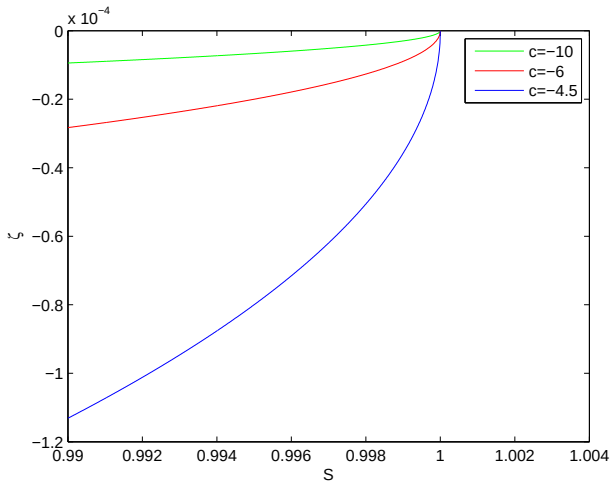

Figure 3.5: Travelling wave solution where $S \to 1$ for some values of c where $c < -1/\phi$ and $\delta = 10^{-4}$.

Case 2: A saturated region above a dry region

Secondly, we look for a travelling wave which links a fully saturated region to a fully dry region. We take $\zeta = 0$ to be where the soil is fully saturated. Since we have a dry region, using a similar argument as in Case 1, we must take $B_0 = 0$ in (3.17). We now look for a solution of (3.17) with $\frac{dS}{d\zeta} > 0$, as well as $B_0 = 0$. To satisfy this, we need $c \leq -1/\phi$ to give $K(S) + c\phi S < 0$ for $0 < S < 1$. It follows from (3.20) that the solution applies only for $\zeta > 0$. The form of solution in this case is given again in implicit form as shown in (3.20). According to the reduced model with piecewise initial data, this case was also discussed in Chapter 2, in Subsection 2.2.3, Case 4 which approaches a shock. The shock speed given by (2.22) agrees with wave velocity c for this a travelling wave solution.

Case 3: Partially saturated region above a dry region

In this case we again have a dry region, so that the limiting saturation below the wave is zero, $S_l = 0$. Since we have a partially saturated region, the limiting saturation above the wave, S_r, lies in the range $0 < S_r < 1$. A similar argument to before, as in Case 1, gives $B_0 = 0$ in equation (3.17) and we look

for a TWS between the two limiting saturations satisfying

$$\frac{dS}{d\zeta} = \frac{-(K(S)+c\phi S)}{\delta D(S)} \quad \text{with} \quad 0 < S < S_r. \tag{3.27}$$

Then it follows that

$$\frac{dS}{d\zeta} > 0 \quad \text{if} \quad K(S)+c\phi S < 0 \ \text{ for } \ 0 < S < S_r. \tag{3.28}$$

Then from equation (3.27) the analytical solution can be obtained in the implicit form:

$$\zeta = -\int_0^S \frac{\delta D(S)}{K(S)+c\phi S} dS \quad \text{with} \quad 0 < S < S_r. \tag{3.29}$$

From the numerator in equation (3.27), we can write

$$K(S)+c\phi S = 0 \quad \text{for} \quad S = S_r. \tag{3.30}$$

Figure 3.6 shows the graph of the function on the left-hand side of equation (3.30) for several values of the wave velocity c. From (3.30), it follows that there can only be a travelling wave of this type, i.e the wave velocity satisfies (3.30), if

$$c = -\frac{K(S_r)}{\phi S_r} \quad \text{for} \quad 0 < S_r < 1, \tag{3.31}$$

which gives the wave velocity c in the range $-1/\phi < c < 0$ as shown in Figure 3.7. We see that the right hand side of (3.27) is zero when $S = S_r$ and from (3.29) that ζ tends to plus infinity (because $K(S)+c\phi S < 0$ where $-1/\phi < c < 0$) as $S \to S_r$. Figure 3.8 shows TWS of (3.29) connecting $S_l = 0$ to S_r.

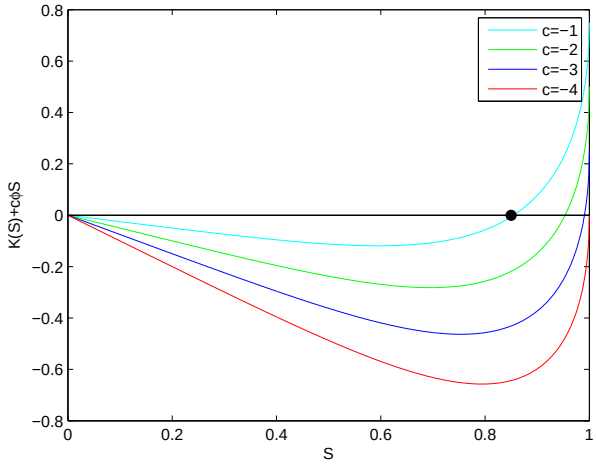

Figure 3.6: $F(S) = K(S) + c\phi S$ for some values of c. It is negative for $0 < S < S_r$, (3.28), with $F(0) = 0$ and $F(S_r) = 0$, where $-1/\phi < c < 0$ and $0 < S_r < 1$. Note that S_r for $c = -1$ is marked with the dot. The value of $c = 0$ in $F(S)$ gives $K(S)$ which is positive and increasing as shown in Figure 1.2 and clearly no TWS possible with this value.

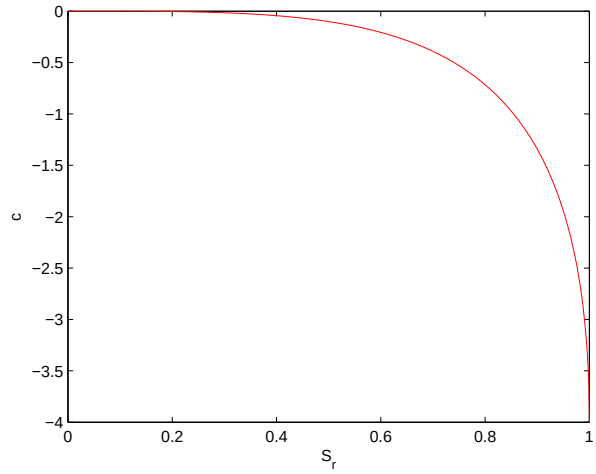

Figure 3.7: Wave velocity $c(S)$ which depends on S_r. It is negative, decreasing and lies in the range $-1/\phi < c < 0$ where $0 < S_r < 1$.

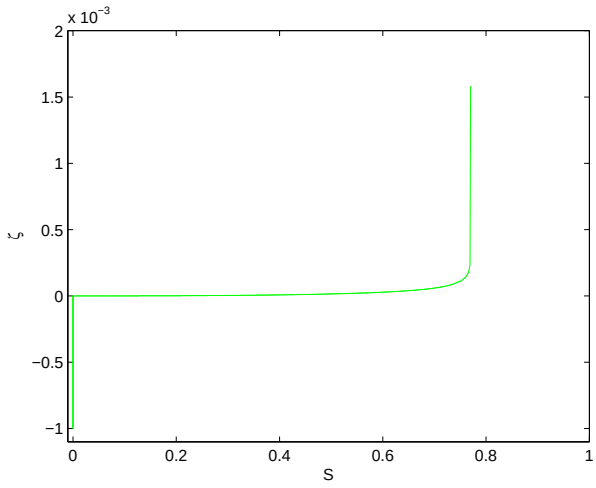

Figure 3.8: Travelling wave solution of (3.29) where $S_r = 0.77$ and $\delta = 10^{-4}$. Solutions of (3.29) apply only for $\zeta > 0$ otherwise $S = 0$ for $\zeta < 0$.

Case 4: Dry region above a partially saturated region

Assume now the limiting saturation above the wave is zero, $S_r = 0$, (dry region) while the limiting saturation below the wave (partially saturated region), S_l, lies in the range $0 < S_l < 1$. As before, we have

$$\frac{dS}{d\zeta} = \frac{-(K(S) + c\phi S)}{\delta D(S)} \quad \text{now with} \quad 0 < S < S_l. \tag{3.32}$$

We now need

$$\frac{dS}{d\zeta} < 0 \quad \text{so from (3.32)} \quad K(S) + c\phi S > 0 \quad \text{for} \quad 0 < S < S_l. \tag{3.33}$$

To satisfy $K(S) + c\phi S > 0$ in a right neighbourhood of 0 we have to take $c \geq 0$ (see Figure 3.9), and so

$$K(S) + c\phi S \neq 0 \quad \text{for any} \quad S = S_l \quad \text{with} \quad 0 < S_l < 1, \tag{3.34}$$

contradicting the condition at $\zeta \to -\infty$. So, there is no travelling wave solution in this case.

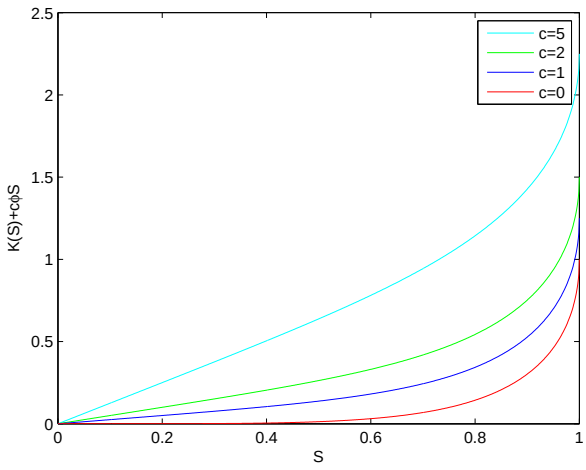

Figure 3.9: $K(S) + c\phi S$ for some non-negative values of c. It is positive and increasing.

Case 5: Partially saturated region above a partially saturated region

Since the both regions are partially saturated, we look for TWS of (3.17) between two limiting saturations as

$$\frac{dS}{d\zeta} = \frac{B_0 - K(S) - c\phi S}{\delta D(S)} > 0 \quad \text{with} \quad S_l < S < S_r, \tag{3.35}$$

where the right hand side of (3.35) must be zero when either $S = S_l$ or $S = S_r$, that is, S_l and S_r are equilibrium solutions of (3.35). Trying $S_r < S_l$, so $\frac{dS}{d\zeta} = 0$ for $S = S_l$ and S_r, and $\frac{dS}{d\zeta} < 0$ with $S_r < S < S_l$, then an argument like that in Case 4 shows that there is no travelling wave solution.
From equation (3.35) the analytical solution can be obtained in an implicit form:

$$\zeta = -\int_{S_*}^{S} \frac{\delta D(S)}{B_0 - K(S) - c\phi S} dS \quad \text{with} \quad S_l < S < S_r, \tag{3.36}$$

and where we arbitrarily take $\zeta = 0$ at $S_* = (S_l + S_r)/2$. From the numerator in equation (3.35), we can write

$$B_0 - K(S) - c\phi S = 0 \quad \text{for} \quad S = S_r \ \text{ and } \ S = S_l. \tag{3.37}$$

Then it follows that

$$K(S_l) - K(S_r) = c\phi S_r - c\phi S_l, \tag{3.38}$$

this gives the wave velocity in terms of S_l and S_r

$$c = -\frac{1}{\phi}\left(\frac{K(S_l) - K(S_r)}{S_l - S_r}\right). \tag{3.39}$$

The sign of c depends on the form of $K(S)$, see Figure 1.2. Since $K(S)$ is increasing, the wave velocity is always negative here. Equation (3.39) is identical to the jump condition as in equation (2.12). Figure 3.10 shows TWS of (3.36) connecting S_l to S_r. We also see that TWS tends to the step function (or shock) as $\delta \to 0$. The result is shown in Figure 3.11.

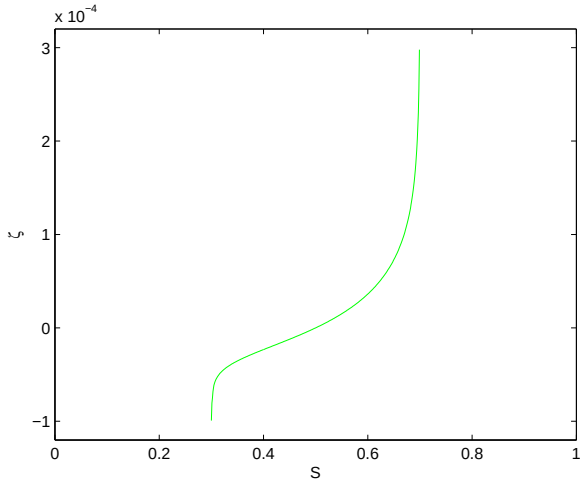

Figure 3.10: Travelling wave solution of (3.36) where $S_l = 0.3$, $S_r = 0.7$ and $\delta = 10^{-4}$.

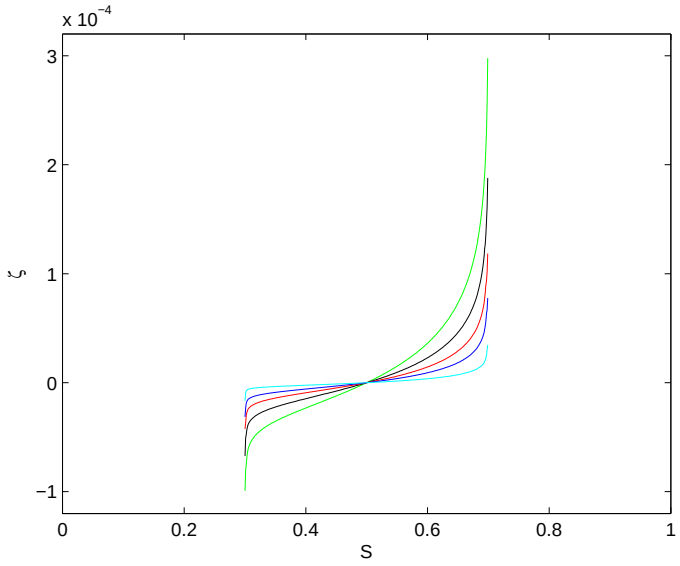

Figure 3.11: Travelling wave solution of (3.36) for different values of δ. Here $S_l = 0.3$, $S_r = 0.7$, $\delta = 10^{-4}$ (green), $\delta = 10^{-4.2}$ (black), $\delta = 10^{-4.4}$ (red), $\delta = 10^{-4.6}$ (blue) and $\delta = 10^{-5}$ (cyan).

Case 6: A saturated region above a partially saturated region

Consider now equation (3.17) with the limiting saturation above the wave, $S_r = 1$, while the limiting saturation below the wave, $0 < S_l < 1$, as

$$\frac{dS}{d\zeta} = \frac{B_0 - K(S) - c\phi S}{\delta D(S)} \quad \text{with} \quad S_l < S < S_r = 1, \tag{3.40}$$

and subject to condition

$$S = 1 \quad \text{at} \quad \zeta = 0. \tag{3.41}$$

From (3.40), we require

$$\frac{dS}{d\zeta} = \frac{B_0 - K(S) - c\phi S}{\delta D(S)} > 0 \quad \text{up to } S = 1, \tag{3.42}$$

and hence $B_0 \geq 1 + c\phi$ recalling that $K(1) = 1$. From the numerator in equation (3.40), we have

$$B_0 - K(S) - c\phi S = 0 \quad \text{for} \quad S = S_l, \tag{3.43}$$

then it follows that

$$B_0 = K(S_l) + c\phi S_l \geq 1 + c\phi, \tag{3.44}$$

and then

$$c \leq -\frac{1}{\phi}\left(\frac{K(S_l) - 1}{S_l - 1}\right). \tag{3.45}$$

Clearly, from (3.45) the wave velocity is always negative in this case for any $0 < S_l < 1$. Figure 3.12 shows a graph of $K(S) + c\phi S$ compared with B_0 where the inequality $B_0 \geq 1 + c\phi$ holds. A travelling wave solution connecting $S_l = 0.45$ to $S_r = 1$ with $c = -(1 - K(S_l))/(\phi(1 - S_l))$ is shown in Figure 3.13. From equation (3.42) the analytical solution can be obtained in an implicit form:

$$\zeta = -\delta \int_S^1 \frac{D(S)}{B_0 - K(S) - c\phi S} dS, \tag{3.46}$$

where $S_l < S < S_r = 1$ and $S_r = 1$ at $\zeta = 0$. With $B_0 > 1 + c\phi$, $c \leq -(1 - K(S_l))/(\phi(1 - S_l))$, it is clear from (3.46) that the solution applies only for $\zeta < 0$.

This case was also discussed in Chapter 2 for the convection model with piecewise initial data, in Subsection 2.2.3, Case 3 which approaches a shock. The shock speed given by (2.17) agrees with wave velocity c for this case of travelling wave.

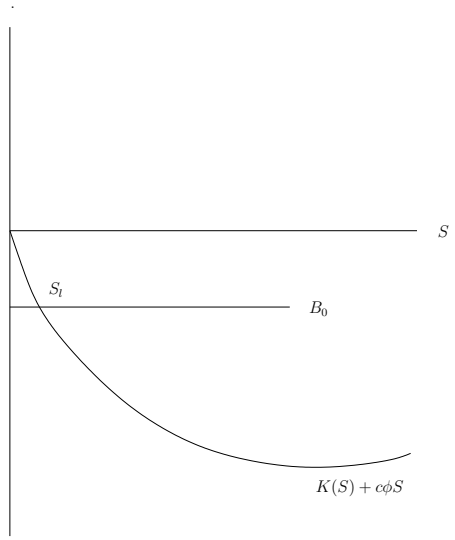

Figure 3.12: $K(S) + c\phi S$ is negative everywhere.

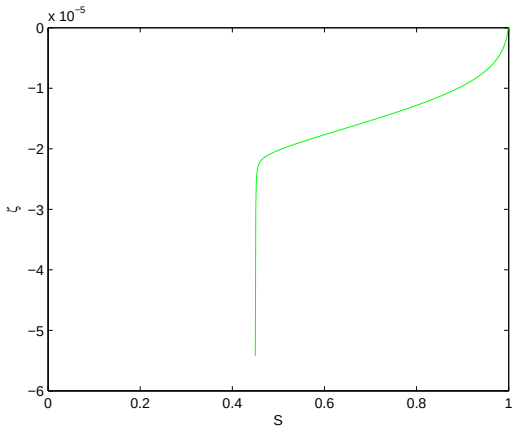

Figure 3.13: Travelling wave solution of (3.46) where $S_l = 0.45$ and $\delta = 10^{-4}$. Solutions of (3.46) apply only for $\zeta < 0$. $S \equiv 1$ for $\zeta \geq 0$.

Case 7: Partially saturated region above a saturated region

This is like Case 6, with equations (3.40) and (3.41), but now with

$$\frac{dS}{d\zeta} = \frac{B_0 - K(S) - c\phi S}{\delta D(S)} < 0 \quad \text{for} \quad 0 < S_r < S < S_l = 1, \tag{3.47}$$

which needs $B_0 \leq 1 + c\phi$. Like the previous case, we can write the analytic solution of (3.47) in an implicit form, see (3.46). Now with $B_0 < 1 + c\phi$ the solution applies for $\zeta > 0$, with $S = 1$ for $\zeta \leq 0$. Like the previous case, we can determine B_0 from the given S_r by

$$B_0 = K(S_r) + c\phi S_r \leq 1 + c\phi, \tag{3.48}$$

and then the wave velocity is

$$c \geq -\frac{1}{\phi}\left(\frac{1 - K(S_r)}{1 - S_r}\right). \tag{3.49}$$

From (3.49), the wave velocity might be positive, negative or zero for any $0 < S_r < 1$. All the possibilities of $K(S) + c\phi S$ compared with B_0, such that the inequality $B_0 \leq 1 + c\phi$ holds, are shown in Figure 3.14. Figure 3.15 shows a TWS of (3.46) connecting $S_r = 0.45$ to $S_l = 1$ with $c = -(1 - K(S_r))/(\phi(1 - S_r))$.

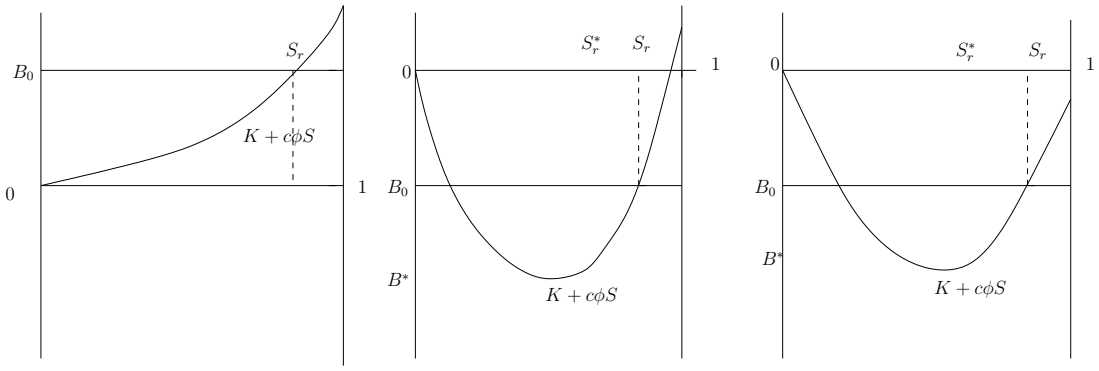

Figure 3.14: Case (i): (left) $1 + c\phi > 0$, where $c \geq 0$ and $0 < B_0 < 1 + c\phi$, $0 < S_r < 1$, case (ii): (middle) $1 + c\phi > 0$, where $c < 0$ and $0 > B^* \leq B_0 < 1 + c\phi > 0$, $S_r^* \leq S_r < 1$, $0 < S_r^* < 1$, case (iii): (right) $1 + c\phi \leq 0$ where $B^* \leq B_0 < 1 + c\phi < 0$, $B^* < 0$, and $S_r^* \leq S_r < 1$, $0 < S_r^* < 1$. Here B^* is the minimum value of $K(S) + c\phi S$ and S_r^* is the value of S giving this minimum.

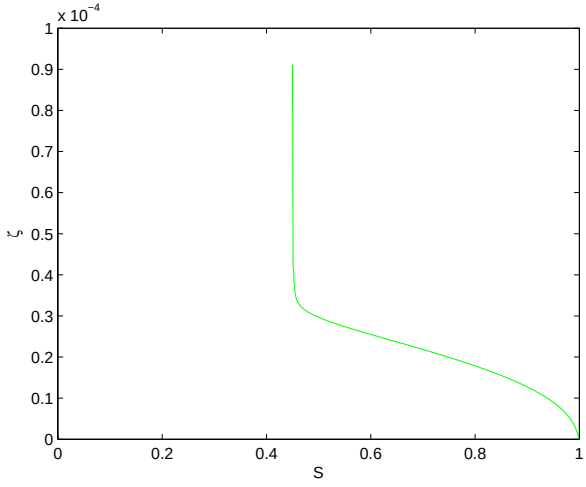

Figure 3.15: Travelling wave solution of (3.47) where $S_r = 0.45$ and $\delta = 10^{-4}$. Solutions of (3.47) apply only for $\zeta > 0$. $S \equiv 1$ for $\zeta \leq 0$.

Note that corresponding initial data for the convection-only model were

discussed in Subsection 2.2.2, Case 3 for that limiting model. In contrast to the present behaviour of a travelling wave, which approaches a shock as we take the limit $\delta \to 0$, in Chapter 2 we only found a rarefaction wave, not a shock, for the $\delta = 0$ problem. This difference of behaviour seems to result from having the diffusivity infinitely large in the saturated region (where $S = 1$), allowing any flux (positive or negative) in such a region.

The travelling wave solutions we have seen here, for the convection-diffusion model, tie in with the shock solutions for the convection model in Chapter 2. In particular, the shock speeds given by the general the Rankine-Hugoniot condition, (2.12), and its special or limiting cases are identical to the wave velocity found from condition (3.39), and its special or limiting cases. The wave velocity in (3.31) is the same shock speed as given in (2.15). Also, equation (3.45) agrees with shock speed that was determined in (2.17).
Due to the influence of gravity, the travelling wave solutions for the convection-diffusion model again move, in general, downwards as seen in the convection model. Following a similar argument as for the shock solutions, Case 3, in Chapter 2, we can determine the wave velocity more generally for the saturated region cases in the convection-diffusion model if there is a forcing pressure gradient imposed. Again, as we mentioned in Chapter 2, if we take an imposed pressure gradient in the saturated region is large and negative, the wave velocity becomes now positive as the moisture is sucked upwards, but this might not be very realistic. However, for Cases 1 and 7, it is possible to get upward motion simply by forcing the fluid up in the saturated region: a negative pressure gradient corresponding to positive pressure.

3.4 Self-Similar Solutions for the Diffusion Model Only

Recall that self-similar solutions to a nonlinear diffusion equation such as (3.1) take the form

$$S(t,z) = t^{\alpha}\Phi(\xi), \quad \text{where} \quad \xi = (z-z_0)t^{\beta} \text{ is the similarity variable.} \tag{3.50}$$

Then equation (3.1) with these new variables can be written as

$$\phi\left(\alpha\Phi + \beta\xi\frac{d\Phi}{d\xi}\right) = t^{2\beta+1}\frac{d}{d\xi}\left(\delta D\left(t^{\alpha}\Phi\right)\frac{d\Phi}{d\xi}\right). \tag{3.51}$$

The only possibility for equation (3.51) to be independent of t, given the function $D(\Phi)$, is to have $\alpha = 0$ and $\beta = -\frac{1}{2}$. Then (3.51) reduces to

$$\frac{d}{d\xi}\left(\delta D(\Phi)\frac{d\Phi}{d\xi}\right) + \frac{\phi\xi}{2}\frac{d\Phi}{d\xi} = 0, \tag{3.52}$$

with the similarity variable $\xi = (z - z_0)/\sqrt{t}$. This similarity variable, apparently first used by Boltzmann [10], transforms equations (3.2) and (3.3) to

$$\Phi = S_r, \quad \xi \to \infty \tag{3.53}$$

and

$$\Phi = S_l, \quad \xi \to -\infty \tag{3.54}$$

which imply

$$\frac{d\Phi}{d\xi} \to 0 \quad \text{for} \quad \xi \to \pm\infty. \tag{3.55}$$

$S(z,t) = \Phi(\frac{z}{t^{1/2}})$ represents the solution to the diffusion of a liquid in a porous medium without gravity between two asymptotic constant values, S_r at plus infinity and S_l at minus infinity. The limiting values can be anywhere in the range zero to one.

We can solve equation (3.52) numerically by using the Matlab bvp4c solver with the conditions (3.53) and (3.54) replaced with the boundary values S_r and S_l prescribed at some finite values of ξ. It is interesting to see the structures of the solutions when the two limiting values are small and large saturation. The results are shown in Figures 3.16, 3.17 and 3.18.

We consider now, alternatively, the boundary condition $S = S_l$ at $z = 0$ for $t \geq 0$ instead of the initial condition (3.9). For a problem in a half line, so that the problem is solved in $z > 0$ with prescribed data on $z = 0$, we can have

$$\Phi = S_l, \ \xi = 0, \tag{3.56}$$

instead of (3.54).

We now look at the local behaviour of equation (3.52), with condition (3.56) when $\Phi = 0$. Integrating (3.52) we obtain

$$D(\Phi)\frac{d\Phi}{d\xi} = c_0 - \frac{\phi}{2\delta}\int_0^\xi \xi \frac{d\Phi}{d\xi} d\xi = c_0 - \frac{\phi}{2\delta}\left(\xi\Phi - \int_0^\xi \Phi d\xi\right), \tag{3.57}$$

where c_0 is a constant of integration. For increasing solutions, say with $\Phi_r > \Phi_l \geq 0$, $\frac{d\Phi}{d\xi} > 0$ for $\xi > 0$, and we must have $c_0 > 0$.

For $S_l = 0$, taking $\xi \to 0^+$ gives $\Phi \to 0$ and then

$$\frac{d\Phi}{d\xi} \sim \frac{c_0}{D(\Phi)} \to \infty. \tag{3.58}$$

This also indicates that for Φ_l small, $\frac{d\Phi}{d\xi}$ should be large (although finite) at $\xi = 0$.
We can solve (3.52) numerically, to see the local behaviour, subject to (3.56). Numerical solutions are also shown in Figures 3.19, 3.20 and 3.21.

In the next two subsections, we study the local behaviour of equation (3.51) for $S = t^\alpha \Phi$ small (where the soil region is nearly dry) and for $S = t^\alpha \Phi$ close to 1 (where it is nearly saturated). We consider only the case when $\alpha = 0$ and $\beta = -\frac{1}{2}$ as obtained for the standard case. Other cases of α and β are possible for these two limiting cases but we leave these for future work.

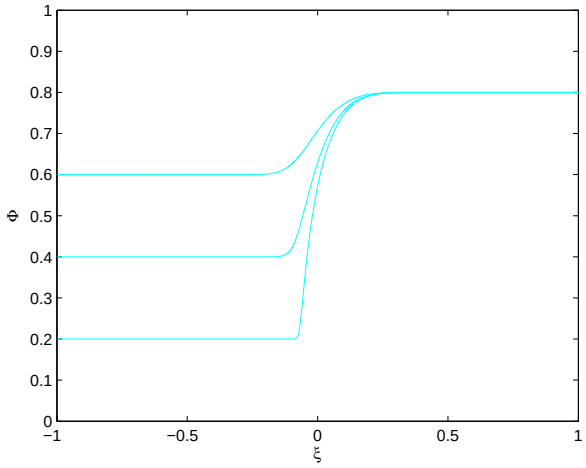

Figure 3.16: Self-similar solutions for the diffusion model (3.52). Here three different values of S_l=0.6, 0.4 and 0.2 are used with S_r=0.8. Note that the solutions get very steep and a corner forms as S_l decreases and whereas the solutions get smoother as S_l increases.

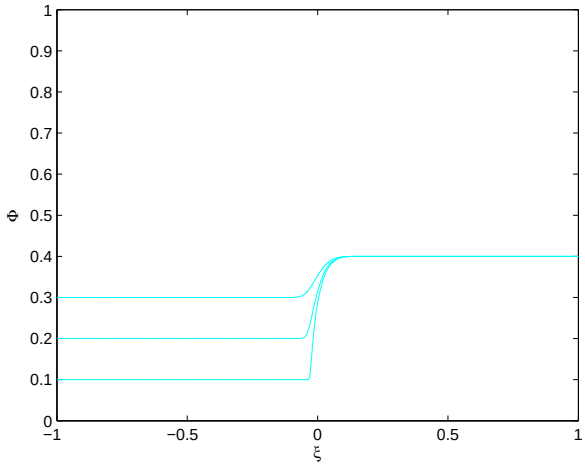

Figure 3.17: Self-similar solutions for (3.52), the diffusion model with low saturation, with (3.53) and (3.54). Here three different values of S_l=0.3, 0.2 and 0.1 are used with S_r=0.4. Note that the solutions get very steep and a corner forms as S_l decreases.

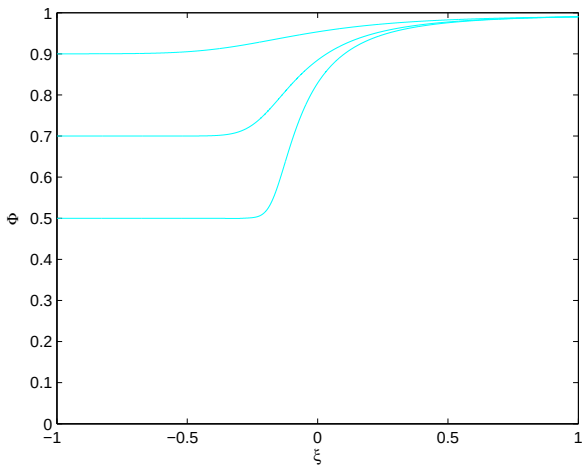

Figure 3.18: Self-similar solutions for (3.52), the diffusion model with high saturation, with (3.53) and (3.54). Here three different values of S_l=0.9, 0.7 and 0.5 are used with S_r=0.99. Both left and right limiting values for saturation are taken to be fairly large and we see that solutions seem to be very smooth, especially as S_l increases.

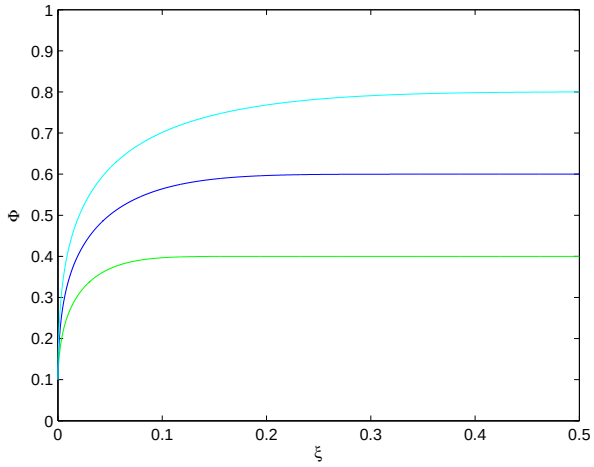

Figure 3.19: Self-similar solutions for the diffusion model. Here $S = S_l = 0.1$ at $\xi = 0$ and S_r=0.8, 0.6 and 0.4. The high slope on the left takes the form in equation (3.57). Note the high slope at $\xi = 0$ due to the small value of S_l.

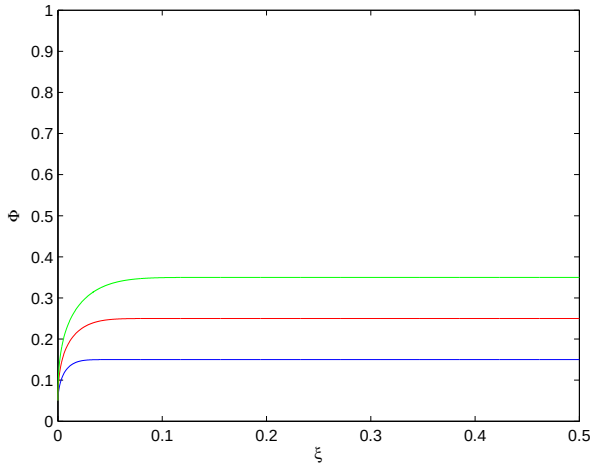

Figure 3.20: Self-similar solutions for (3.52) with low saturation subject to (3.53) and (3.56). Here $S = S_l = 0.05$ at $\xi = 0$ and S_r=0.35, 0.25 and 0.15. The limiting values for saturation on the right are taken to be fairly small. The high slope on the left takes the form in equation (3.57).

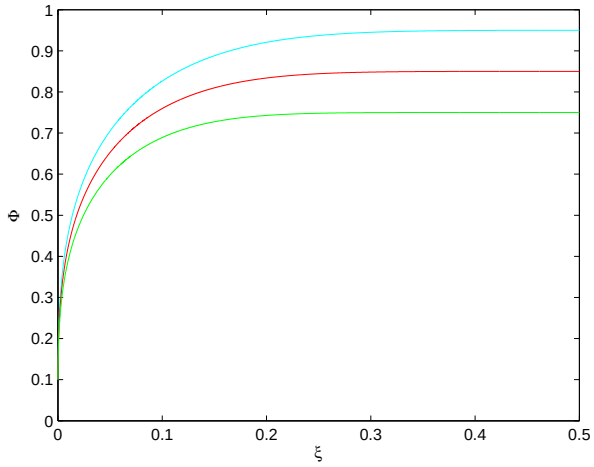

Figure 3.21: Self-similar solutions for (3.52) with high saturation subject to (3.53) and (3.56). Here $S = S_l = 0.1$ at $\xi = 0$ and S_r=0.95, 0.85 and 0.75. The limiting values for saturation on the right are taken to be fairly large. The high slope on the left takes the form in equation (3.57).

3.4.1 Limiting Case 1: Low Saturation

We look for a solution of equation (3.1) in self-similar form when S is small. Then by substituting the approximate form of $D(S)$ from (1.12) into equation (3.51), we obtain

$$\phi\left(\alpha\Phi + \beta\xi\frac{d\Phi}{d\xi}\right) = t^{(5/2)\alpha+2\beta+1}\frac{d}{d\xi}\left(1/4\delta\Phi^{5/2}\frac{d\Phi}{d\xi}\right). \tag{3.59}$$

One possibility for equation (3.59) to be independent of t is to have α =0 and $\beta = -\frac{1}{2}$, as before, then equation (3.59) becomes

$$\frac{d}{d\xi}\left(\delta\Phi^{5/2}\frac{d\Phi}{d\xi}\right) + \frac{\xi}{2}\frac{d\Phi}{d\xi} = 0. \tag{3.60}$$

Numerical solutions are shown in Figures 3.22 and 3.23 for (3.60) subject to the same conditions as in (3.53), (3.54) and (3.56). We again see that solutions get very steep as S_l decreases.

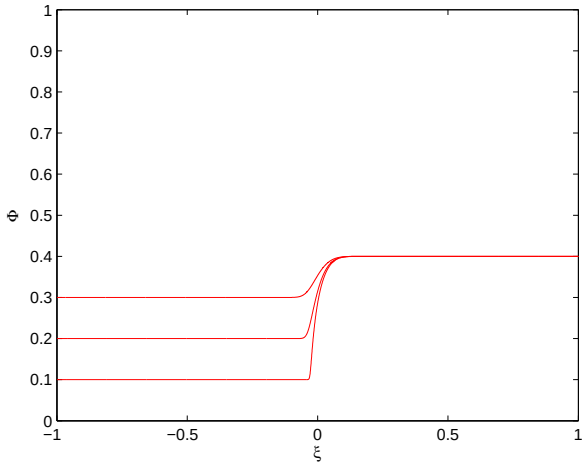

Figure 3.22: Self-similar solutions for (3.60), the diffusion model when S is small, subject to (3.53) and (3.54). Here three different values of $S = S_l$=0.3, 0.2 and 0.1 are used with S_r=0.4. The both limiting values for saturation are taken to be fairly small.

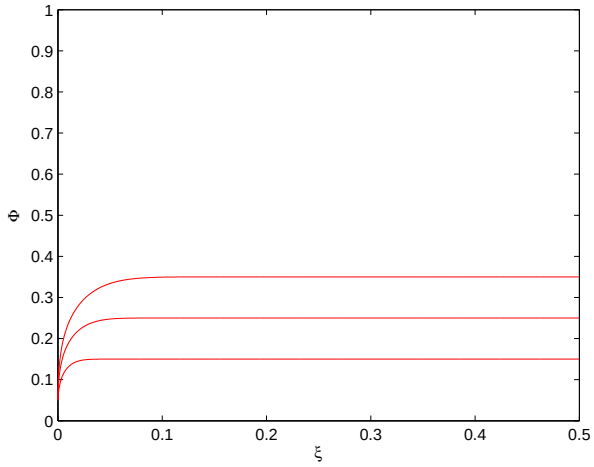

Figure 3.23: Self-similar solutions for (3.60), the diffusion model when S is small, subject to (3.53) and (3.56). Here $S = S_l = 0.05$ at $\xi = 0$ and S_r=0.35, 0.25 and 0.15. Solutions on the left take the form in equation (3.57). Solutions have large slope at $\xi = 0$, see (3.57).

Equation (3.60) can also be written as

$$\frac{d^2}{d\xi^2}\Phi^{7/2} + \frac{7\xi}{4\delta}\frac{d\Phi}{d\xi} = 0. \tag{3.61}$$

For simplicity, define $\Psi = \Phi^{7/2}$, hence equation (3.61) becomes

$$\frac{d^2}{d\xi^2}\Psi + \frac{\xi}{2\delta}\Psi^{-5/7}\frac{d\Psi}{d\xi} = 0. \tag{3.62}$$

We can simplify equation (3.62) by rescaling the variable $\xi = 2\delta\tilde{\xi}$ to remove the constants. Then we obtain

$$\frac{d^2\Psi}{d\tilde{\xi}^2} + \tilde{\xi}\Psi^{-5/7}\frac{d\Psi}{d\tilde{\xi}} = 0. \tag{3.63}$$

Looking at the terms in (3.63), the first scales as Ψ/ξ^2, while the second scales simply as $\Psi^{2/7}$. Balancing the two suggests a useful transformed variable might be

$$X = \tilde{\xi}^{-14/5}\Psi, \tag{3.64}$$

which gives $X > 0$ for any (non-zero) $\tilde{\xi}$ and $\Psi > 0$, then

$$\frac{d\Psi}{d\tilde{\xi}} = \tilde{\xi}^{14/5}\frac{dX}{d\tilde{\xi}} + \frac{14}{5}\tilde{\xi}^{9/5}X, \tag{3.65}$$

and

$$\frac{d^2\Psi}{d\tilde{\xi}^2} = \tilde{\xi}^{14/5}\frac{d^2X}{d\tilde{\xi}^2} + \frac{28}{5}\tilde{\xi}^{9/5}\frac{dX}{d\tilde{\xi}} + \frac{126}{25}\tilde{\xi}^{4/5}X. \tag{3.66}$$

Substituting (3.64), (3.65) and (3.66) into (3.63), we obtain

$$\tilde{\xi}^2\frac{d^2X}{d\tilde{\xi}^2} + \frac{28}{5}\tilde{\xi}\frac{dX}{d\tilde{\xi}} + \frac{126}{25}X + \tilde{\xi}X^{-5/7}\frac{dX}{d\tilde{\xi}} + \frac{14}{5}X^{2/7} = 0. \tag{3.67}$$

We can convert equation (3.67) to a simpler, autonomous, second order differential equation by using the transformation $\tilde{\xi} = e^s$:

$$\frac{d^2X}{ds^2} + \frac{23}{5}\frac{dX}{ds} + \frac{126}{25}X + X^{-5/7}\frac{dX}{ds} + \frac{14}{5}X^{2/7} = 0. \tag{3.68}$$

Equation (3.68) can be written as a first order system. Taking $u_1(s) = X(s)$ and $u_2(s) = X'(s)$, then we obtain

$$\begin{aligned} u_1'(s) &= u_2 \\ u_2'(s) &= -\frac{23}{5}u_2 - \frac{126}{25}u_1 - u_1^{-5/7}u_2 - \frac{14}{5}u_1^{2/7}. \end{aligned} \tag{3.69}$$

This system of differential equations has only one equilibrium point which is $(u_1^*, u_2^*) = ((-9/5)^{-7/5}, 0)$. This equilibrium point is not of physical relevance because it gives a negative solution. The u_1-nullcline ($u_1' = 0$) is given by the line $u_2 = 0$ (the u_1 axis) while the u_2-nullcline ($u_2' = 0$) is given by the function

$$u_2 = \frac{-14(9u_1^{5/7} + 5)}{5(23u_1^{5/7} + 5)}u_1.$$

On the u_2-nullcline, we have $u_2 \to 0$ as $u_1 \to 0$ and $u_2 \to \infty$ as $u_1 \to (-5/23)^{7/5}$. The Jacobian matrix for (3.69) is

$$J = \begin{bmatrix} 0 & 1 \\ -126/25 + 5/7u_1^{-12/7}u_2 - 4/5u_1^{-5/7} & -23/5 - u_1^{-5/7} \end{bmatrix},$$

and the linearization of this system near the equilibrium point $((-9/5)^{-7/5}, 0)$ gives

$$J_{((-9/5)^{-7/5},0)} = \begin{bmatrix} 0 & 1 \\ -18/5 & -14/5 \end{bmatrix}.$$

The corresponding eigenvalues are given by $5\lambda^2 + 14\lambda + 18 = 0$, so $\lambda_1 = 1/5(-7 + i\sqrt{41})$ and $\lambda_2 = 1/5(-7 - i\sqrt{41})$. Hence $((-9/5)^{-7/5}, 0)$ is a stable spiral. From the second equation in (3.69) we see that u_2' becomes large and positive as $u_1 \to 0^-$ while it becomes large and negative as $u_1 \to 0^+$. The phase plane of (3.69) is shown in Figure 3.24.

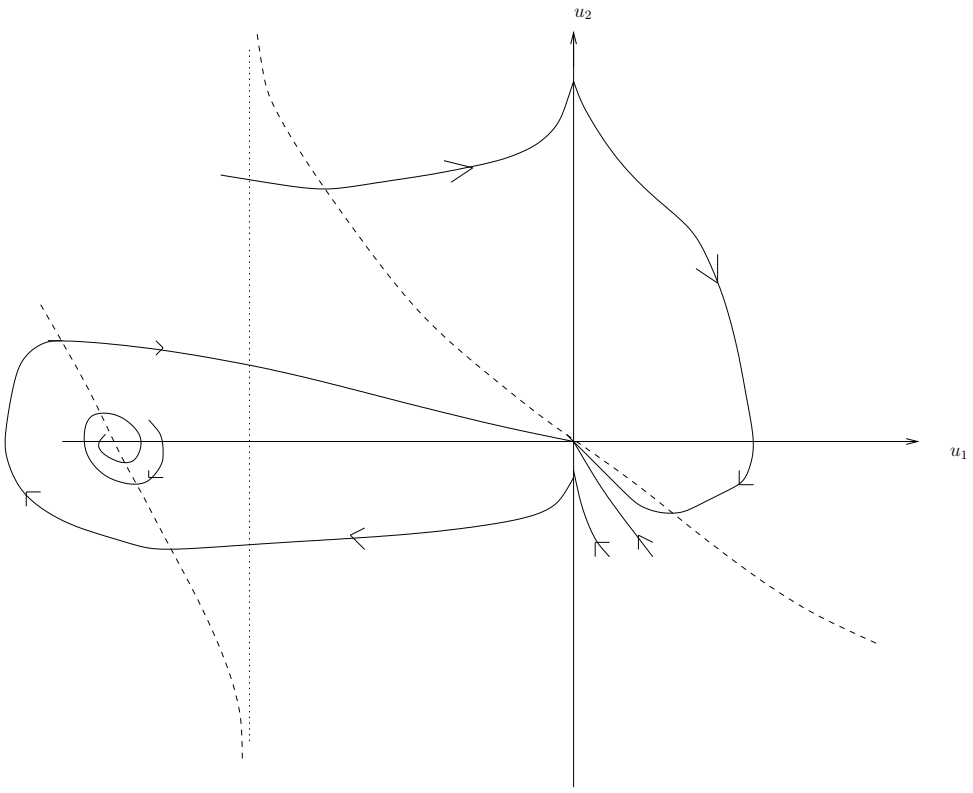

Figure 3.24: Phase plane of (3.69). The dashed line represents the u_2-nullcline. Trajectories have infinite slope on u_2 axis according to the second equation in (3.69). The sketched trajectories were checked by using numerical initial value problem solutions.

To study the solution behaviour of (3.69) near the point $(0, 0)$, we see that

from the second equation in (3.69) as u_1 and u_2 get close to $(0,0)$ the first and second terms become small and less important compared with the other terms, so system (3.69) reduces to

$$\begin{aligned} u_1'(s) &\sim u_2 \\ u_2'(s) &\sim -u_1^{-5/7}(\alpha_0 u_1 + u_2), \end{aligned} \tag{3.70}$$

where $\alpha_0 = 14/5$. Since we look for a local solution near $(0,0)$, we rescale $u_1 = \epsilon\tilde{u}_1$ and $u_2 = \epsilon\tilde{u}_2$, where $0 < \epsilon \ll 1$. Substituting these expressions into (3.70), we obtain

$$\begin{aligned} \tilde{u}_1'(s) &\sim \tilde{u}_2 \\ -\epsilon^{5/7}\tilde{u}_1^{5/7}\tilde{u}_2'(s) &\sim \alpha_0\tilde{u}_1 + \tilde{u}_2. \end{aligned} \tag{3.71}$$

From the second equation of (3.71) we can write

$$\tilde{u}_2 \sim -\alpha_0\tilde{u}_1 + \epsilon^{5/7}U, \tag{3.72}$$

where

$$U = -\tilde{u}_1^{5/7}\tilde{u}_2'(s), \tag{3.73}$$

and as $\epsilon \to 0$ the second term in (3.72) can be neglected so that $\tilde{u}_2 \sim -\alpha_0\tilde{u}_1$. Substituting this in the first equation of (3.71), we get $\tilde{u}_1'(s) \sim -\alpha_0\tilde{u}_1$ and solving for $\tilde{u}_1$, we obtain

$$\tilde{u}_1 \sim Ae^{-\alpha_0 s}, \tag{3.74}$$

where A is an arbitrary constant. Then

$$\tilde{u}_2(s) \sim -\alpha_0 Ae^{-\alpha_0 s} + \epsilon^{5/7}U. \tag{3.75}$$

By substituting (3.74) and (3.75) into (3.73), we obtain

$$U \sim -\alpha_0^2 A^{12/7}e^{-(12/7)\alpha_0 s}. \tag{3.76}$$

Clearly, $U \to 0$ as $s \to \infty$, then we see that (for this solution) from (3.74) and (3.75) $\tilde{u}_1 \to 0$ and $\tilde{u}_2 \to 0$ as $s \to \infty$.

Transforming from $\tilde{u}_1$ to S, we have from the basic form of the similarity solution when S is small, (3.50),

$$\begin{aligned} S(z,t) &= \Phi(\xi) = (1/(2\delta))^{4/5} X^{2/7} \xi^{4/5} \\ &= (A\epsilon)^{2/7} (1/(2\delta))^{4/5} (1/(2\delta))^{-4/5} \xi^{4/5} \xi^{-4/5} \\ &\sim (A\epsilon)^{2/7}. \end{aligned} \tag{3.77}$$

From (3.77) $S \to$ constant. This type of solution does not then satisfy our original assumptions, see (3.50), because we want $S \to 0$ as $\Phi \to 0$ (note $\alpha = 0$ in this case).

3.4.2 Limiting Case 2: High Saturation

We look now for a solution of equation (3.1) in a self-similar form with S near 1 in the form

$$S(t,z) = 1 - t^{\alpha}\Phi(\xi), \quad \xi = (z - z_0)t^{\beta}. \tag{3.78}$$

Substituting (3.78) into (3.1), we obtain

$$\phi\left(\alpha\Phi + \beta\xi\frac{d\Phi}{d\xi}\right) = t^{2\beta+1}\frac{d}{d\xi}\left(\delta D(1 - t^{\alpha}\Phi)\frac{d\Phi}{d\xi}\right). \tag{3.79}$$

By using the approximate form of $D(1-t^{\alpha}\Phi)$ for S near 1, see (1.18), equation (3.79) becomes

$$\phi\left(\alpha\Phi + \beta\xi\frac{d\Phi}{d\xi}\right) = t^{2\beta-1/2\alpha+1}\frac{d}{d\xi}\left(\frac{1}{2}\delta\Phi^{-1/2}\frac{d\Phi}{d\xi}\right). \tag{3.80}$$

To eliminate t in (3.80), again following the standard and low saturation cases we take $\alpha = 0$ and $\beta = -\frac{1}{2}$, then (3.80) reduces to

$$\frac{d}{d\xi}\left(\delta\Phi^{-1/2}\frac{d\Phi}{d\xi}\right) + \phi\xi\frac{d\Phi}{d\xi} = 0, \tag{3.81}$$

or

$$\frac{d^2}{d\xi^2}\Phi^{1/2} + \frac{\phi\xi}{2\delta}\frac{d\Phi}{d\xi} = 0. \tag{3.82}$$

For simplicity, define $\Psi = \Phi^{1/2}$, then $\frac{d\Phi}{d\xi} = 2\Psi\frac{d\Psi}{d\xi}$ and equation (3.82) becomes

$$\frac{d^2}{d\xi^2}\Psi + \frac{\phi\xi}{\delta}\Psi\frac{d\Psi}{d\xi} = 0. \tag{3.83}$$

Again we can use the bvp4c solver to solve equation (3.83) with the same artificial boundary conditions as earlier (see (3.53), (3.54) and (3.56)). The results are shown in Figures 3.25 and 3.26.

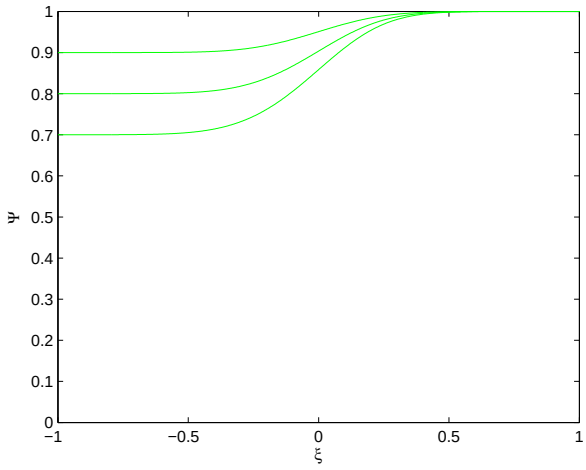

Figure 3.25: Self-similar solutions for (3.83), the diffusion model when S is close to 1, subject to (3.53) and (3.54). Here three different values of S_l=0.9, 0.8 and 0.7 are used with S_r=1. The limiting values for saturation are taken to be fairly large and we see that solutions seem to be very smooth, especially as S_l increases.

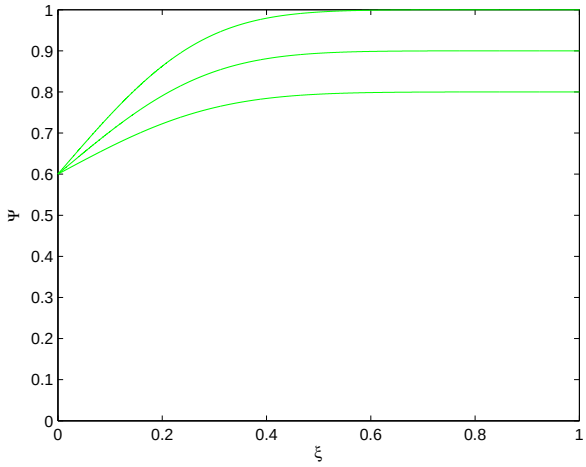

Figure 3.26: Self-similar solutions for (3.83), the diffusion model when S is close to 1, subject to (3.53) and (3.56). Here $\Psi(0) = 0.6$ and S_r=1, 0.9 and 0.8. The limiting values for saturation on the right are taken to be large.

Again as in the previous case, by changing the variable in equation (3.83) $\xi = (\delta/\phi)\tilde{\xi}$, we can get rid of the constants, and this time we obtain

$$\frac{d^2}{d\tilde{\xi}^2}\Psi + \tilde{\xi}\Psi\frac{d\Psi}{d\tilde{\xi}} = 0. \tag{3.84}$$

Equation (3.84) is still not easy to solve, it can be transformed in a manner similar to that in the previous case by introducing a new variable

$$X = \tilde{\xi}^2\Psi, \tag{3.85}$$

which makes X positive for any (non-zero) $\tilde{\xi}$ and $\Psi > 0$. Then

$$\frac{d\Psi}{d\tilde{\xi}} = \tilde{\xi}^{-2}\frac{dX}{d\tilde{\xi}} - 2\tilde{\xi}^{-3}X, \tag{3.86}$$

and

$$\frac{d^2\Psi}{d\tilde{\xi}^2} = \tilde{\xi}^{-2}\frac{d^2X}{d\tilde{\xi}^2} - 4\tilde{\xi}^{-3}\frac{dX}{d\tilde{\xi}} + 6\tilde{\xi}^{-4}X. \tag{3.87}$$

Plugging (3.85), (3.86) and (3.87) into (3.84), we obtain

$$\tilde{\xi}^2\frac{d^2X}{d\tilde{\xi}^2} - 4\tilde{\xi}\frac{dX}{d\tilde{\xi}} + 6X + X\left(\tilde{\xi}\frac{dX}{d\tilde{\xi}} - 2X\right) = 0. \tag{3.88}$$

As in the previous case this equation can be simplified by a change of independent variables $\tilde{\xi} = e^s$, then we get

$$\frac{d^2X}{ds^2} - 5\frac{dX}{ds} + 6X + X\left(\frac{dX}{ds} - 2X\right) = 0. \tag{3.89}$$

Equation (3.89) is now a second order autonomous ODE and hence we can write it as a first order by taking $u_1(s) = X(s)$ and $u_2(s) = X'(s)$, to get

$$\begin{aligned} u_1'(s) &= u_2 \\ u_2'(s) &= 5u_2 - 6u_1 - u_1u_2 + 2u_1^2. \end{aligned} \tag{3.90}$$

Clearly, this system of differential equations has two equilibrium points which are $(u_1^*, u_2^*) = (0, 0)$ and $(u_1^*, u_2^*) = (3, 0)$. The linear asymptotic stability of these equilibrium points is determined by the eigenvalues of the Jacobian matrix, which for (3.90) is

$$J = \begin{bmatrix} 0 & 1 \\ -6 - u_2 + 4u_1 & 5 - u_1 \end{bmatrix}.$$

Thus, it is straightforward to confirm that $(0, 0)$ is an unstable node, since the corresponding eigenvalues are $\lambda_1 = 3$ and $\lambda_2 = 2$ which are both positive. Similarly, $(3, 0)$ is a saddle node because the corresponding eigenvalues are $\lambda_1 = 1 + \sqrt{7} > 0$ and $\lambda_2 = 1 - \sqrt{7} < 0$. The u_1-nullcline ($u_1' = 0$) is given by the line $u_2 = 0$ (the u_1 axis) while the u_2-nullcline ($u_2' = 0$) is given by the function $u_2 = u_1(6 - 2u_1)/(5 - u_1)$. Note that the latter gives $u_2 \to -\infty$ as $u_1 \to 5_-$. The intersections of the nullclines give the above equilibrium points. We can now use phase plane techniques, plotting the trajectories in the (u_1, u_2)-plane, see Figure 3.27. Pplane is also used to plot several solutions of (3.90) in Figure 3.28.

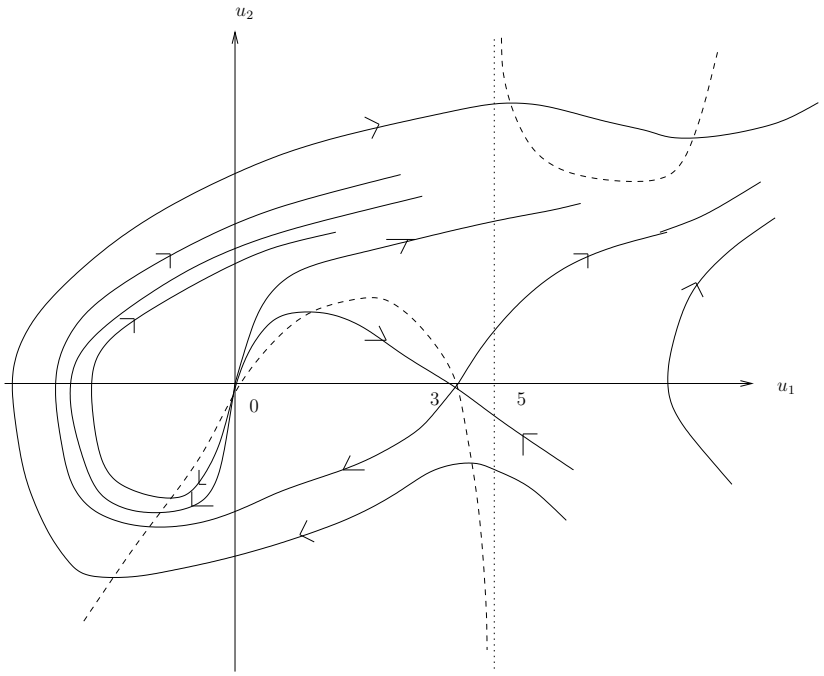

Figure 3.27: Phase plane for (3.90). The dashed line represents the u_2-nullcline.

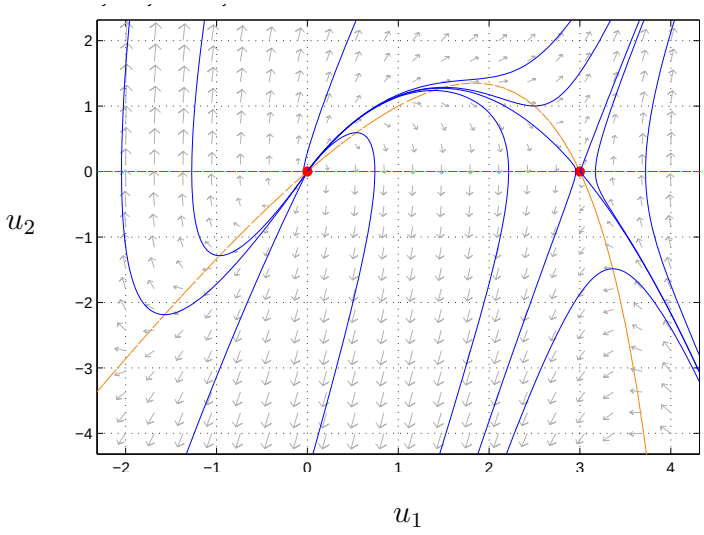

Figure 3.28: Pplane for (3.90). The two red dots are the equilibrium points while the two coloured curves (pink and orange) represent the nullclines.

Along the trajectories that cross the positive u_1 axis in Figure 3.27, u_1 must tend to some $u_1^0 > 0$ and then from the basic form of the similarity solution when S is close to 1, after transforming from u_1 to S, it follows that

$$\begin{aligned} S(z,t) &= 1 - \Phi(\xi) \\ &= 1 - \left(\frac{\delta^2 t u_1^0}{(\phi z)^2}\right)^2. \end{aligned}$$

We see that as $t \to 0$ or $z \to \infty$, $S \to 1$ and then this gives a nearly saturated region.

3.5 Self-Similar Solutions for the Convection-Diffusion Model

Let us consider self-similar solutions to the convection-diffusion equation (2.1) as in form (3.50). Then we can rewrite equation (2.1) in the new variables as

$$\phi\left(\alpha\Phi + \beta\xi\frac{d\Phi}{d\xi}\right) = t^{2\beta+1}\frac{d}{d\xi}\left(\delta D\left(t^\alpha\Phi\right)\frac{d\Phi}{d\xi} + t^{-(\alpha+\beta)}K\left(t^\alpha\Phi\right)\right). \tag{3.91}$$

Since equation (3.91) is dependent on t for any values of α and β, there is no similarity solutions with these two functions $D\left(t^\alpha\Phi\right)$ and $K\left(t^\alpha\Phi\right)$. We can, however, find self-similar solutions to equation (3.91) for the two limiting cases.

3.5.1 Limiting Case 1: Low Saturation

By using the approximate forms of $D(t^\alpha\Phi)$ and $K(t^\alpha\Phi)$ when $S = t^\alpha\Phi$ is small, as given by (1.12) and (1.13), equation (3.91) with the new functions then becomes

$$\alpha\Phi + \beta\xi\frac{d\Phi}{d\xi} = t^{2\beta+1}\frac{d}{d\xi}\left(\delta t^{5\alpha/2}\Phi^{5/2}\frac{d\Phi}{d\xi} + t^{-(\alpha+\beta)}t^{9\alpha/2}\Phi^{9/2}\right). \tag{3.92}$$

Equation (3.92) is independent on t if the exponents $\alpha = \beta = -\frac{2}{9}$. Since $\alpha < 0$ it follows from equation (3.50) that $S(z,t) = t^{-2/9}\Phi(\xi)$ and, for fixed ξ, the

solution decays with time. Equation (3.92) reduces to

$$\frac{d}{d\xi}\left(\delta\Phi^{5/2}\frac{d\Phi}{d\xi}+\Phi^{9/2}\right)+\frac{2}{9}\left(\Phi+\xi\frac{d\Phi}{d\xi}\right)=0, \tag{3.93}$$

which be written as

$$\frac{d}{d\xi}\left(\delta\Phi^{5/2}\frac{d\Phi}{d\xi}+\Phi^{9/2}\right)+\frac{2}{9}\frac{d}{d\xi}\left(\xi\Phi\right)=0. \tag{3.94}$$

Integrating both sides of (3.94) with respect to ξ, we get

$$\delta\Phi^{5/2}\frac{d\Phi}{d\xi}+\Phi^{9/2}+\frac{2}{9}\xi\Phi=C, \tag{3.95}$$

where C is a constant of integration. The behaviour of solutions to (3.95) depend on C. So we need to consider three main cases.

Case 1(i): $C=0$

To look for a simple solution, we first look at C=0. Then we have from equation (3.95) that $\Phi=0$ or

$$\delta\Phi^{3/2}\frac{d\Phi}{d\xi}+\Phi^{7/2}+\frac{2}{9}\xi=0. \tag{3.96}$$

For simplicity, define $\Psi=\Phi^{5/2}$, then $\frac{d\Psi}{d\xi}=\frac{5}{2}\Phi^{3/2}\frac{d\Phi}{d\xi}$. Hence equation (3.96) with this new variable is

$$\frac{d\Psi}{d\xi}+\frac{5}{2\delta}\left(\frac{2}{9}\xi+\Psi^{\frac{7}{5}}\right)=0. \tag{3.97}$$

This is a non-autonomous first order differential equation which cannot be solved in closed form. Equation (3.96) only holds where $\Psi>0$, as (3.95) is also achieved by having $\Psi=0$. We must then have

$$\frac{d\Psi}{d\xi}=\begin{cases}-\frac{5}{2\delta}(\frac{2}{9}\xi+\Psi^{\frac{7}{5}}) & \text{where } \Psi>0, \text{ say for } \xi_-<\xi<\xi_+,\\ 0 & \text{otherwise,}\end{cases} \tag{3.98}$$

with $\Psi(\xi_-)=\Psi(\xi_+)=0$. Here ξ_- and/or ξ_+ is possibly infinite. For $\xi<0$ and Ψ sufficiently small, we see from (3.98) that $\frac{d\Psi}{d\xi}>0$ and so that the solutions increase until they hit the nullcline $\xi=-(9/2)\Psi^{7/5}$. As $\xi\to 0^-$, $\frac{d\Psi}{d\xi}<0$ and so that the solutions decrease and cross the Ψ axis. They continue decreasing

for $\xi > 0$ until they hit the ξ axis according to $\Psi(\xi_+) = 0$. For $\xi > \xi_+$ and $\xi < \xi_-$ we see that from (3.98), solutions are zero. Also, for ξ small or Ψ large, equation (3.98) reduces to

$$\frac{d\Psi}{d\xi} = -\frac{5}{2\delta}\Psi^{\frac{7}{5}}. \tag{3.99}$$

Then solving (3.99) for Ψ, we obtain

$$\Psi = \frac{1}{((1/\delta)(\xi - \xi^*))^{\frac{5}{2}}}, \tag{3.100}$$

where ξ^* is an arbitrary constant. Clearly, from (3.100) solutions blow-up as $\xi \to \xi^*$. With the above information in hand, the phase plane for equation (3.98) can be constructed for ξ against Ψ, see Figure 3.29.

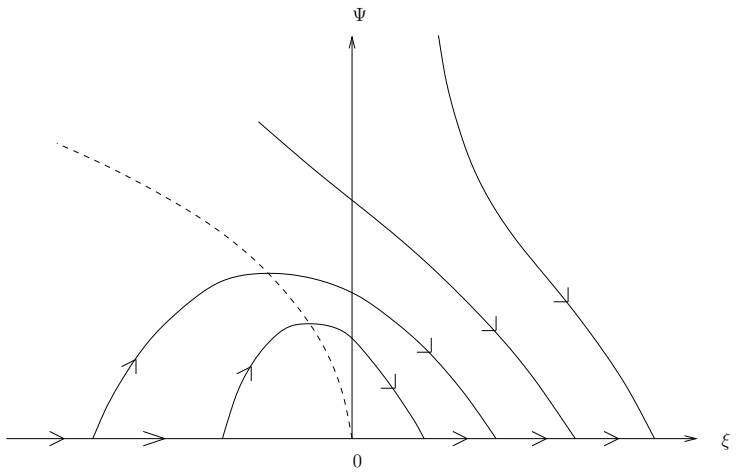

Figure 3.29: Phase plane for (3.98). The dashed line represents the nullcline of (3.98).

In Figure 3.29, there are some trajectories which cross the Ψ axis and then Ψ must tend to some $\Psi_1 > 0$ as $\xi = (z/t^{2/9}) \to 0^-$. From the basic form of the similarity solutions, see (3.50), we have that

$$S = t^\alpha \Phi(\xi) \sim t^\alpha \Psi_1 \to 0 \ \text{ as } t \to \infty, \tag{3.101}$$

which gives a nearly dry region in long time, but an unfortunately trivial so-

lution as there is no spatial dependence.

Equation (3.97) can also be written as

$$\delta\frac{d\Psi}{d\xi}+\frac{5}{2}\left(\frac{2}{9}\xi+\Psi^{\frac{7}{5}}\right)=0. \tag{3.102}$$

Since we have the small parameter δ multiplying the first derivative term, we can use asymptotic analysis to find approximate solutions. Assume now that the solution expanded in terms of δ takes the form

$$\Psi(\xi)=\Psi_0(\xi)+\delta\Psi_1(\xi)+\delta^2\Psi_2(\xi)+... \tag{3.103}$$

Substituting (3.103) into equation (3.102) gives

$$\delta\left(\frac{d\Psi_0}{d\xi}+\delta\frac{d\Psi_1}{d\xi}+...\right)+\frac{5}{2}\left(\frac{2}{9}\xi+\left(\Psi_0+\delta\Psi_1+\delta^2\Psi_2+...\right)^{7/5}\right)=0. \tag{3.104}$$

The terms independent of δ are

$$\frac{2}{9}\xi+\Psi_0^{7/5}=0 \tag{3.105}$$

and solving (3.105) for Ψ_0 gives

$$\Psi_0=\left(-\frac{2}{9}\xi\right)^{5/7}, \tag{3.106}$$

valid only for $\xi<0$. The asymptotic solution in (3.106) represents the null-cline, the dashed line that was shown in Figure 3.29. It follows from equation

(3.50) that

$$\begin{aligned} S(t,z) &= t^{-2/9}\Psi^{2/5}(\xi) \\ &\sim t^{-2/9}\Psi_0^{2/5}(\xi) \quad \text{from} \quad (3.103) \\ &\sim t^{-2/9}\left(-(2/9)\xi\right)^{2/7}, \quad \text{as in} \quad (3.106) \\ &\sim t^{-2/9}\left(-(2/9)\left(\frac{z-z_0}{t^{2/9}}\right)\right)^{2/7} \quad \text{from} \quad (3.50) \\ &\to 0 \quad \text{as} \quad t\to\infty. \end{aligned} \tag{3.107}$$

For fixed $z < z_0 = 0$ and taking $t \to \infty$, we have that $\xi = (z - z_0)t^{-2/9} \to 0^-$. Then we see that from (3.107) S becomes close to 0 as $\xi \to 0^-$ which gives a region which is nearly dry.

Case 1(ii): $C > 0$

For simplicity, we can change the variable Ψ in equation (3.95) to $\Psi = \Phi^{7/2}$, then $\frac{d\Psi}{d\xi} = \frac{7}{2}\Phi^{5/2}\frac{d\Phi}{d\xi}$. Hence equation (3.95) becomes

$$\delta\frac{d\Psi}{d\xi} + \frac{7}{2}\left(\frac{2}{9}\xi\Psi^{\frac{2}{7}} + \Psi^{\frac{9}{7}} - C\right) = 0. \tag{3.108}$$

We see, from (3.108) that, for $C > 0$ and Ψ sufficiently small, we have $\frac{d\Psi}{d\xi} > 0$ and so solutions increase until they hit the nullcline $\xi = \frac{9}{2}(C\Psi^{-\frac{2}{7}} - \Psi)$. Solutions above the nullcline decrease according to $\xi \sim \frac{9}{2}C\Psi^{-\frac{2}{7}}$ (since the second term in the nullcline becomes not important when Ψ small compared with the first term) i.e $\Psi \sim (9C/2\xi)^{7/2}$. For ξ not large and Ψ large, equation (3.108) reduces to

$$\frac{d\Psi}{d\xi} = -\frac{7}{2\delta}\Psi^{\frac{9}{7}}. \tag{3.109}$$

Solving (3.109) for Ψ, we obtain

$$\Psi = \frac{1}{((1/\delta)(\xi - \xi^*))^{\frac{7}{2}}}, \tag{3.110}$$

where ξ^* is an arbitrary constant. Clearly, solutions blow-up as $\xi \to \xi^*$. The phase plane is shown in Figure 3.30.

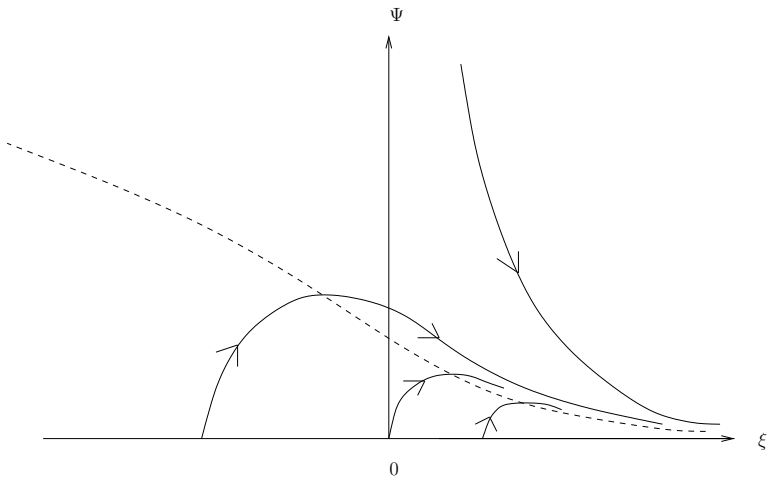

Figure 3.30: Phase plane for (3.108) with $\xi > 0$ and $C > 0$. The trajectories don't continue to the left on the ξ axis since (3.95) doesn't hold for $C > 0$ when $\Psi = \Phi = 0$. The dashed line represents the nullcline of (3.108).

Following a similar argument as in (3.101), we show that the region is a nearly dry in large time.
Asymptotic expansions can also be considered for (3.108) as was done for (3.102). Assuming a solution form as in (3.103) and substituting into (3.108), we obtain

$$\delta\left(\frac{d\Psi_0}{d\xi}+\delta\frac{d\Psi_1}{d\xi}+...\right)+\frac{7}{2}\left(\frac{2}{9}\xi\left(\Psi_0+\delta\Psi_1+...\right)^{\frac{2}{7}}+\left(\Psi_0+\delta\Psi_1+...\right)^{\frac{9}{7}}-C\right)=0. \tag{3.111}$$

As $\delta \to 0$, we are left with

$$\frac{2}{9}\xi\Psi_0^{2/7}+\Psi_0^{9/7}-C=0. \tag{3.112}$$

With Ψ_0 small, the second term on the left hand side of (3.112) becomes small compared with the other terms, and so it can neglected. Then solving (3.112) for Ψ_0, we obtain

$$\Psi_0=\left(\frac{9C}{2\xi}\right)^{7/2}. \tag{3.113}$$

It is clear that from (3.113),

$$\Psi_0 \to 0 \ \text{ as } \ \xi \to \infty. \tag{3.114}$$

We now study the solution of (3.108) for δ not being small. We first note (see the phase plane, Figure 3.30) that $\Psi \to 0^+$ as $\xi \to \infty$, so $\frac{d\Psi}{d\xi} \to 0$. Now we look for a solution in the form: $\Psi(\xi) = \Psi_0(\xi) + \Psi_1(\xi) + ...$. From our observation, the first and third terms in (3.108) become small and not important compared with the other terms. So, we are left with

$$\frac{2}{9}\xi\Psi_0^{2/7} \sim C, \tag{3.115}$$

and then

$$\Psi_0 \sim \left(\frac{9C}{2}\right)^{7/2} \xi^{-7/2}. \tag{3.116}$$

Equation (3.116) gives

$$\frac{d\Psi_0}{d\xi} = -a_0\xi^{-9/2} \text{ and } \Psi_0^{9/7} = b_0\xi^{-9/2}, \tag{3.117}$$

where $a_0 = (7/2)(9C/2)^{7/2}$ and $b_0 = (9C/2)^{9/2}$. Using (3.116) and (3.117), with the expansion, in (3.108), we obtain

$$-a_0\delta\xi^{-9/2} + \frac{7}{2}\left(\frac{2}{9}\xi(\Psi_0 + \Psi_1 + ...)^{2/7} + b_0\xi^{-9/2} - C\right) = 0. \tag{3.118}$$

After re-arranging, we find that

$$\frac{2}{9}\xi\Psi_0^{-5/7}\Psi_1 = (a_0\delta - (7/2)b_0)\xi^{-9/2}. \tag{3.119}$$

Solving for Ψ_1, we obtain

$$\Psi_1 = c_0\xi^{-8}, \tag{3.120}$$

where $c_0 = (9/2)(9C/2)^{5/2}(a_0\delta - (7/2)b_0)$. Clearly, from (3.120) we have that $\Psi_1 \to 0$ as $\xi \to \infty$ (and faster than Ψ_0).

From equation (3.50), it follows that such solutions give

$$\begin{aligned} S(t,z) &= t^{-2/9}\Psi^{2/7}(\xi) \\ &\sim t^{-2/9}\Psi_0^{2/7}(\xi) \quad \text{from} \quad (3.103) \\ &\sim t^{-2/9}\left(\frac{9C}{2\xi}\right), \quad \text{as in} \quad (3.113) \\ &\sim t^{-2/9}\left(\frac{9C}{2}\frac{t^{2/9}}{z-z_0}\right) \quad \text{from} \quad (3.50) \\ &\sim \frac{9C}{2(z-z_0)} \\ &\to 0 \qquad \text{as} \quad z-z_0 \to \infty. \end{aligned} \tag{3.121}$$

Again this gives a region is nearly dry. Note that to satisfy the original assumption of S being small, we see that from (3.121) this limiting solution only works for $z - z_0$ large. Unfortunately, it does not apply all the way down to $z = z_0$.

Case 1(iii): $C < 0$

Consider equation (3.108) but now with $C < 0$. A similar asymptotic argument as in Case 1(ii), see (3.113), indicates that

$$\Psi_0 \to 0 \ \text{ as } \ \xi \to -\infty, \tag{3.122}$$

and now it follows that for such solutions $S(z,t) \to 0$, as $z - z_0 \to -\infty$, see (3.121). As in the previous two cases, if Ψ gets large then the solution blows up as $\xi \to \xi^*$ for some finite ξ^*.
For $\xi < 0$ and Ψ small, we see that from (3.108), $\frac{d\Psi}{d\xi} > 0$ and so that solutions, inside the region of the nullcline, increase until they hit the nullcline, given by $\xi = \frac{9}{2}(C\Psi^{-\frac{2}{7}} - \Psi)$ where $C < 0$. After that solutions decrease until they hit the ξ axis. The phase plane is sketched in Figure 3.31.

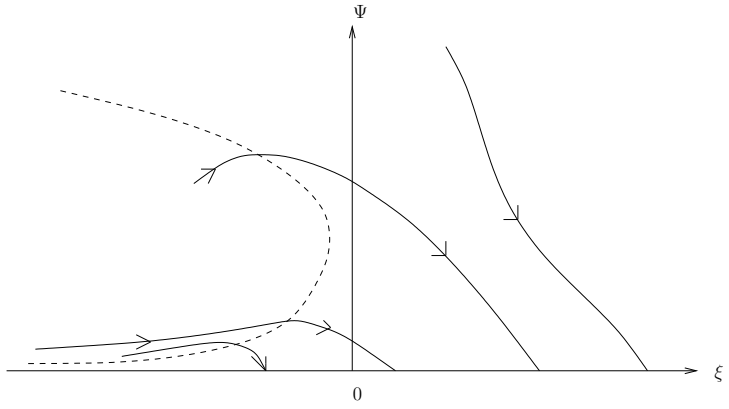

Figure 3.31: Phase plane for (3.108) with $\xi < 0$ and $C < 0$. The trajectories don't continue to the right on the ξ axis since (3.95) doesn't hold for $C < 0$ when $\Psi = \Phi = 0$. The dashed line represents the nullcline of (3.108).

3.5.2 Limiting Case 2: High Saturation

We now consider self-similar solutions to the convection-diffusion equation (2.1) when S is close to 1 as in form (3.78). Then equation (2.1) becomes

$$-\phi\left(\alpha\Phi + \beta\xi\frac{d\Phi}{d\xi}\right) = t^{2\beta+1}\frac{d}{d\xi}\left(-\delta D(1-t^{\alpha}\Phi)\frac{d\Phi}{d\xi} + t^{-(\alpha+\beta)}K(1-t^{\alpha}\Phi)\right). \tag{3.123}$$

Introducing the approximate forms of $D(1-t^{\alpha}\Phi)$ and $K(1-t^{\alpha}\Phi)$ when S is close to 1, see (1.18) and (1.19) respectively, we obtain

$$\phi\left(\alpha\Phi + \beta\xi\frac{d\Phi}{d\xi}\right) = t^{2\beta+1-\frac{\alpha}{2}}\frac{d}{d\xi}\left(\frac{1}{2}\delta\Phi^{-1/2}\frac{d\Phi}{d\xi}\right) + \sqrt{2}t^{\beta-\frac{\alpha}{2}+1}\Phi^{-1/2}\frac{d\Phi}{d\xi}. \tag{3.124}$$

This equation is independent on t if the exponents $\alpha = 2$ and $\beta = 0$, so that $\xi = z$, and (3.124) then reduces to

$$\frac{d}{d\xi}\left(\frac{1}{2}\delta\Phi^{-1/2}\frac{d\Phi}{d\xi}\right) + \sqrt{2}\Phi^{-1/2}\frac{d\Phi}{d\xi} - 2\phi\Phi = 0. \tag{3.125}$$

We write, for simplicity, $\Psi = \Phi^{1/2}$, then $\frac{d\Psi}{d\xi} = \frac{1}{2}\Phi^{-1/2}\frac{d\Phi}{d\xi}$, and substituting into equation (3.125) we end up with

$$\delta\frac{d^2\Psi}{d\xi^2} + 2\sqrt{2}\frac{d\Psi}{d\xi} - 2\phi\Psi^2 = 0. \tag{3.126}$$

Since there is a small parameter δ multiplying the highest derivative term, this can be regarded as is a singular perturbation problem. The procedure for doing singular perturbations requires finding outer and inner (or interior) solutions, then matching these two solutions.

Outer solution Let us first consider the outer region. We consider equation (3.126) with the physical parameter δ much smaller than one. We take a solution to be expanded in powers of δ as

$$\Psi(\xi) = \Psi_0(\xi) + \delta\Psi_1(\xi) + \delta^2\Psi_2(\xi) + \dots\ . \tag{3.127}$$

Substituting this into equation (3.126) gives

$$\delta\left(\frac{d^2\Psi_0}{d\xi^2} + \delta\frac{d^2\Psi_1}{d\xi^2} + \dots\right) + 2\sqrt{2}\left(\frac{d\Psi_0}{d\xi} + \delta\frac{d\Psi_1}{d\xi} + \dots\right) - 2\phi\left(\Psi_0 + \delta\Psi_1 + \dots\right)^2 = 0. \tag{3.128}$$

Proceeding in the usual manner yields the following equation

$$O(1) : 2\sqrt{2}\frac{d\Psi_0}{d\xi} - 2\phi\Psi_0^2 = 0.$$

Then the general solution for this equation takes this form

$$\Psi_0 = \frac{-1}{(\phi/\sqrt{2})\xi + c_0}, \tag{3.129}$$

where c_0 is an arbitrary constant. Without loss of generality, take $c_0 = 0$, then equation (3.129) gives a solution valid only for $\xi < 0$ since we require $\Psi_0 > 0$. Note that equation (3.129) agrees with solution (2.75) in Subsection 2.3.2. Equation (3.129) then becomes

$$\Psi_0 = \frac{-\sqrt{2}}{\phi\xi}. \tag{3.130}$$

Clearly, $\Psi_0 \to \infty$ as $\xi \to 0$ and decays to 0 as $\xi \to -\infty$. From equation (3.78), it follows that

$$\begin{aligned} S(t,z) &= 1 - t^2\Phi(\xi) \\ &\sim 1 - t^2\left(\frac{\sqrt{2}}{\phi(z-z_0)}\right)^2 \\ &\to 1 \quad \text{as} \quad t \to 0 \ \text{ or } \ z - z_0 \to -\infty. \end{aligned}$$

Rescale the independent variable We now look for a boundary or interior layer close to $\xi = \tilde{\xi} < 0$. Let

$$\xi - \tilde{\xi} = \epsilon(\delta)X,$$

where $\epsilon(\delta)$ is expected to be some power of δ. Using the new coordinate, equation (3.126) becomes

$$\frac{\delta}{\epsilon(\delta)^2}\frac{d^2\Psi_0}{dX^2} + \frac{2\sqrt{2}}{\epsilon(\delta)}\frac{d\Psi_0}{dX} - 2\phi\Psi_0^2 = 0. \tag{3.131}$$

In order to obtain a solution of (3.131), we require that at least two leading-order terms in (3.131) have the same order of magnitude. Hence, we need to consider three possible cases. Note that if we first assume that the second and third coefficients are the same order, this gives again the first term is smaller than other terms and hence this is the outer solution as seen before.
Assume the first and second coefficients dominate that of the third and are the same order,

$$\frac{\delta}{\epsilon(\delta)^2} \sim \frac{2\sqrt{2}}{\epsilon(\delta)},$$

then

$$\epsilon(\delta) = \delta.$$

Plugging this into equation (3.131), we get

$$\frac{1}{\delta}\frac{d^2\Psi_0}{dX^2} + \frac{2\sqrt{2}}{\delta}\frac{d\Psi_0}{dX} - 2\phi\Psi_0^2 = 0.$$

We see that the coefficients of the highest and first derivative are larger than the last term's coefficient, because $\frac{1}{\delta} > -2\phi$ as $\delta \to 0$, agreeing with our

supposition.
Assume the first and third coefficients are the same order,

$$\frac{\delta}{\epsilon(\delta)^2} \sim 1 \text{ with the second term much smaller.}$$

This gives

$$\epsilon(\delta) = \delta^{1/2},$$

which would give us the equation

$$\frac{d^2\Psi_0}{dX^2} + \frac{2\sqrt{2}}{\delta^{1/2}}\frac{d\Psi_0}{dX} - 2\phi\Psi_0^2 = 0.$$

Since the coefficient of the first derivative is much larger than the other two, this case is not possible. So from the second case the correct choice of the boundary layer, or interior layer, will be

$$\xi = \tilde{\xi} + \delta X,$$

and the equation is now

$$\frac{1}{\delta}\frac{d^2\Psi_0}{dX^2} + \frac{2\sqrt{2}}{\delta}\frac{d\Psi_0}{dX} - 2\phi\Psi_0^2 = 0. \tag{3.132}$$

We now seek an inner solution of the form

$$\Psi(X) = \Psi_0(X) + \delta\Psi_1(X) + \delta^2\Psi_2(X) + ...$$

Substituting this into equation (3.132) gives

$$\frac{1}{\delta}\left(\frac{d^2\Psi_0}{dX^2} + \delta\frac{d^2\Psi_1}{dX^2} + ...\right) + \frac{2\sqrt{2}}{\delta}\left(\frac{d\Psi_0}{dX} + \delta\frac{d\Psi_1}{dX} + ...\right) - 2\phi\left(\Psi_0 + \delta\Psi_1 + ...\right)^2 = 0.$$

Solving for Ψ_0 by balancing the terms in the equation by order of δ

$$O\left(\frac{1}{\delta}\right) : \frac{d^2\Psi_0}{dX^2} + 2\sqrt{2}\frac{d\Psi_0}{dX} = 0. \tag{3.133}$$

Integrating both sides of (3.133) gives

$$\frac{d\Psi_0}{dX} + 2\sqrt{2}\Psi_0 = A_0.$$

Hence the general solution is

$$\Psi_0 = \frac{1}{2\sqrt{2}}(A_0 - B_0 e^{-2\sqrt{2}X}),$$

with A_0 and B_0 constants. We notice that the constant A_0 can be determined by matching the solution whereas B_0 can not be determined (B_0 is equivalent to shift in $\tilde{\xi}$ of $O(\delta)$).

Matching the solutions To determine the unknowns in our outer and inner solutions we need to match the solutions. Matching requires that

$$\lim_{X\to\infty} \Psi_0(X) = \lim_{\xi\to\ \tilde{\xi}^+} \Psi_0(\xi),$$

so that

$$\frac{A_0}{2\sqrt{2}} = \frac{-\sqrt{2}}{\phi\tilde{\xi}}$$

so

$$A_0 = \frac{-4}{\phi\tilde{\xi}}.$$

Finally, the inner solution becomes

$$\Psi_0 = -\frac{1}{2\sqrt{2}}\left(\frac{4}{\phi\tilde{\xi}} + B_0 e^{-2\sqrt{2}X}\right),$$

or, with $X = \dfrac{\xi - \tilde{\xi}}{\delta}$,

$$\Psi_0 = -\frac{1}{2\sqrt{2}}\left(\frac{4}{\phi\tilde{\xi}} + B_0 e^{-2\sqrt{2}\dfrac{\xi-\tilde{\xi}}{\delta}}\right). \tag{3.134}$$

From (3.134), we see that as $(\xi - \tilde{\xi})/\delta \to \infty$, $\xi - \tilde{\xi}$ much larger than δ, the second term becomes small and can be neglected and then $\Psi_0 \to -4/(2\sqrt{2}\phi\tilde{\xi})$ which gives a positve constant since $\tilde{\xi} < 0$. As $(\xi - \tilde{\xi})/\delta \to -\infty$, Ψ_0 grows

with $B_0 < 0$ and decreases with $B_0 > 0$. The outer and inner solutions are plotted in Figure 3.32.

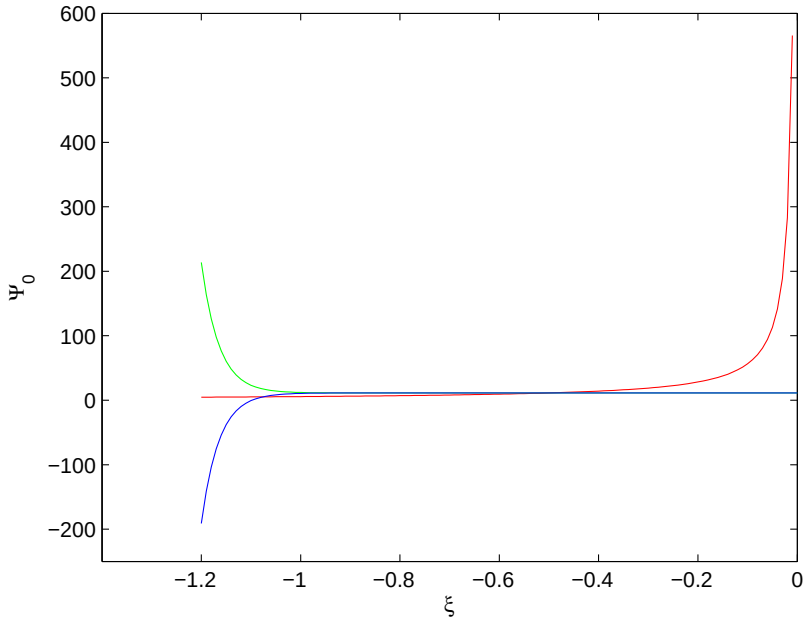

Figure 3.32: The outer solution to (3.126) shown by the red curve. The inner solution grows where $B_0 < 0$ and is shown by the green curve while it decreases where $B_0 > 0$ and is shown by the blue curve. Here we take $\tilde{\xi} = -1$, $B_0 = 1$ or -1, $\delta = 10^{-2}$ and $\phi = \dfrac{1}{4}$.

We can, alternatively, obtain qualitative information on the full equation (3.126) from a phase-plane analysis. For simplicity, we rescale the variables in equation (3.126) by using the following scalings:

$$\xi = A\chi, \quad \Psi = B\Theta, \tag{3.135}$$

where A and B are positive constants, to be determined. Substituting ξ and

Ψ into equation (3.126), we find that

$$\left(\frac{\delta B}{A^2}\right)\frac{d^2\Theta}{d\chi^2}+\left(\frac{2\sqrt{2}B}{A}\right)\frac{d\Theta}{d\chi}-2\phi B^2\Theta^2=0. \tag{3.136}$$

Multiplying both sides of (3.136) by $A^2/\delta B$, we obtain

$$\frac{d^2\Theta}{d\chi^2}+\left(\frac{2\sqrt{2}A}{\delta}\right)\frac{d\Theta}{d\chi}-\left(\frac{2\phi BA^2}{\delta}\right)\Theta^2=0. \tag{3.137}$$

Taking $A=\delta/2\sqrt{2}$ and $B=\delta/2\phi A^2$, equation (3.137) becomes

$$\frac{d^2\Theta}{d\chi^2}+\frac{d\Theta}{d\chi}-\Theta^2=0. \tag{3.138}$$

We suppose that the solution blows up at some point $\chi=\chi^*$. To study the asymptotic behaviour of (3.138) near the point χ^*, we first assume $\Theta\sim A(\chi^*-\chi)^{-\alpha}$, then $\Theta'\sim\alpha A(\chi^*-\chi)^{-\alpha-1}$ and $\Theta''\sim\alpha(\alpha+1)A(\chi^*-\chi)^{-\alpha-2}$ where the prime denotes the derivative with respect to χ. Substituting these expressions into (3.138), we get

$$\alpha(\alpha+1)A(\chi^*-\chi)^{-\alpha-2}\sim\alpha^2(\chi^*-\chi)^{-2\alpha}, \tag{3.139}$$

from which it follows that $\alpha=2$ and $A=6$. Then the asymptotic solution takes the form

$$\Theta\sim 6(\chi^*-\chi)^{-2}. \tag{3.140}$$

As (3.138) is a second-order ODE, we should expect a two-parameter family of solutions, while (3.140) only indicates the single parameter χ^*, the location of the blow-up point. In looking for the second parameter we seek the local form of the solution of a power series

$$\Theta\sim 6\tilde{\chi}^{-2}+a\tilde{\chi}^{-1}+b+c\tilde{\chi}+d\tilde{\chi}^2+e\tilde{\chi}^3+f\tilde{\chi}^4+... \tag{3.141}$$

Thus, equation (3.138) takes the form

$$36\tilde{\chi}^{-4} + 2a\tilde{\chi}^{-3} + 2d + ... - 12\tilde{\chi}^{-3} - a\tilde{\chi}^{-2} + c + 2d\tilde{\chi} + ... \sim$$

$$36\tilde{\chi}^{-4} + 12a\tilde{\chi}^{-3} + (12b + a^2)\tilde{\chi}^{-2} + (12c + 2ab)\tilde{\chi}^{-1} + (12d + 2ac + b^2) + ... = 0. \tag{3.142}$$

Comparing terms of the same order of $\tilde{\chi}$ we have

$$\begin{aligned}
\tilde{\chi}^{-3} &: -12 = 10a, \\
\tilde{\chi}^{-2} &: 12b = -a - a^2, \\
\tilde{\chi}^{-1} &: 12c = -2ab, \\
1 &: 10d = -2ac - b^2 + c, \\
\tilde{\chi} &: 6e + 2d = 12e + 2ad + 2bc, \\
\tilde{\chi}^2 &: 12f + 3e = 12f + 2ae + 2bd + c^2,
\end{aligned} \tag{3.143}$$

and then $a = \frac{-6}{5}, b = \frac{-1}{50}, c = \frac{-1}{250}, d = \frac{-7}{5000}$ and $e = \frac{-41}{50000}$. The coefficient of f is zero and (3.143) is impossible to satisfy. To avoid this, we can supplement the $f\tilde{\chi}^4$ term in (3.141) with a term $f^*\tilde{\chi}^4 \ln \tilde{\chi}$, then proceed in the usual manner. We obtain, in place of (3.143) (having cancelled the f terms)

$$\tilde{\chi}^2 \quad : \quad 12f^* \ln \tilde{\chi} + 7f^* + 3e = 12f^* \ln \tilde{\chi} + 2ae + 2bd + c^2, \tag{3.144}$$

and solving for f^*, we get $f^* = -3/50000$. Then the local asymptotic solution of the second parameter of equation (3.138) is:

$$\Theta \sim 6\tilde{\chi}^{-2} - \frac{6}{5}\tilde{\chi}^{-1} - \frac{1}{50} - \frac{1}{250}\tilde{\chi} - \frac{7}{5000}\tilde{\chi}^2 - \frac{41}{50000}\tilde{\chi}^3 - \frac{3}{50000}\tilde{\chi}^4 \ln \tilde{\chi} + f\tilde{\chi}^4..., \tag{3.145}$$

with the undetermined coefficient f giving us the missing parameter to describe the family of solutions.

To look for a decay solution of (3.138), we assume a solution takes the form $\Theta \sim A\chi^{-\alpha}$, then $\Theta' \sim -\alpha A\chi^{-\alpha-1}$ and $\Theta'' \sim \alpha(\alpha+1)A\chi^{-\alpha-2}$. Plugging these

expressions into (3.138), we get

$$-\alpha A\chi^{-\alpha-1} \sim A^2\chi^{-2\alpha}, \tag{3.146}$$

then we obtain $\alpha = 1$ and $A = -1$. Then

$$\Theta \sim -\frac{1}{\chi}, \tag{3.147}$$

and clearly $\Theta \to 0$ as $\chi \to \infty$.

We now determine the equilibrium point and study the stability of equation (3.138). Equation (3.138) is a second order autonomous ODE which we can write it as a first order system. Taking $u_1(\chi) = \Theta(\chi)$ and $u_2(\chi) = \Theta'(\chi)$, we have the system

$$\begin{aligned} u_1'(\chi) &= u_2 \\ u_2'(\chi) &= u_1^2 - u_2. \end{aligned} \tag{3.148}$$

This system of differential equations has only one equilibrium point which is $(u_1^*, u_2^*) = (0, 0)$. To study the stability of this equilibrium point we need to write this system in canonical form: write $w = u_1 + u_2$, then

$$\begin{aligned} w' &= u_1^2 = (w^2 - 2wu_2 + u_2^2) \\ u_2' &= -u_2 + (w^2 - 2wu_2 + u_2^2). \end{aligned} \tag{3.149}$$

This system, when linearized about the equilibrium $u_1^* = 0$, $u_2^* = 0$, has eigenvalues 0 and -1 and we cannot deduce the stability properties from this information. Centre manifold theory, [8], tells us that system has an invariant manifold $u_2 = h(w)$. We now compute the approximations to this invariant manifold.

Assume $u_2 = h(w) = aw^2 + bw^3 + cw^4 + O(w^5)$. Then

$$\begin{aligned} u_2' &= h'(w)w' \\ &= (2aw + 3bw^2 + 4cw^3 + O(w^4))(w^2 - 2w(aw^2 + bw^3 + ...)+ \\ &\quad (aw^2 + bw^3 + ...)^2) \\ &= 2aw^3 + O(w^4). \end{aligned}$$

From the second equation in (3.149), we have

$$\begin{aligned} u_2' &= -(aw^2 + bw^3 + cw^4 + Ow^5) + (w^2 - 2w(aw^2 + bw^3 + ...)+ \\ &\quad (aw^2 + bw^3 + ...)^2) \\ &= (-a + 1)w^2 + O(w^3). \end{aligned}$$

Comparing the two expressions we deduce that $a = 1$, and our centre manifold approximation is

$$u_2 = h(w) = w^2 + O(w^3).$$

The dynamics are then governed by the equation

$$w' = w^2 + O(w^3).$$

Hence the zero solution of (3.148) is unstable. To understand the behaviour of solutions to equation (3.148), we can use phase plane techniques, plotting the trajectories in the (u_1, u_2)-plane. Clearly, the u_1-nullcline ($u_1' = 0$) is given by the line $u_2 = 0$ while the u_2-nullcline ($u_2' = 0$) is given by $u_2 = u_1^2$. Note that the equilibrium point is given by the intersection of the nullclines. The form of the solution of equation (3.148) is then indicated by the phase plane sketched in Figure 3.33.

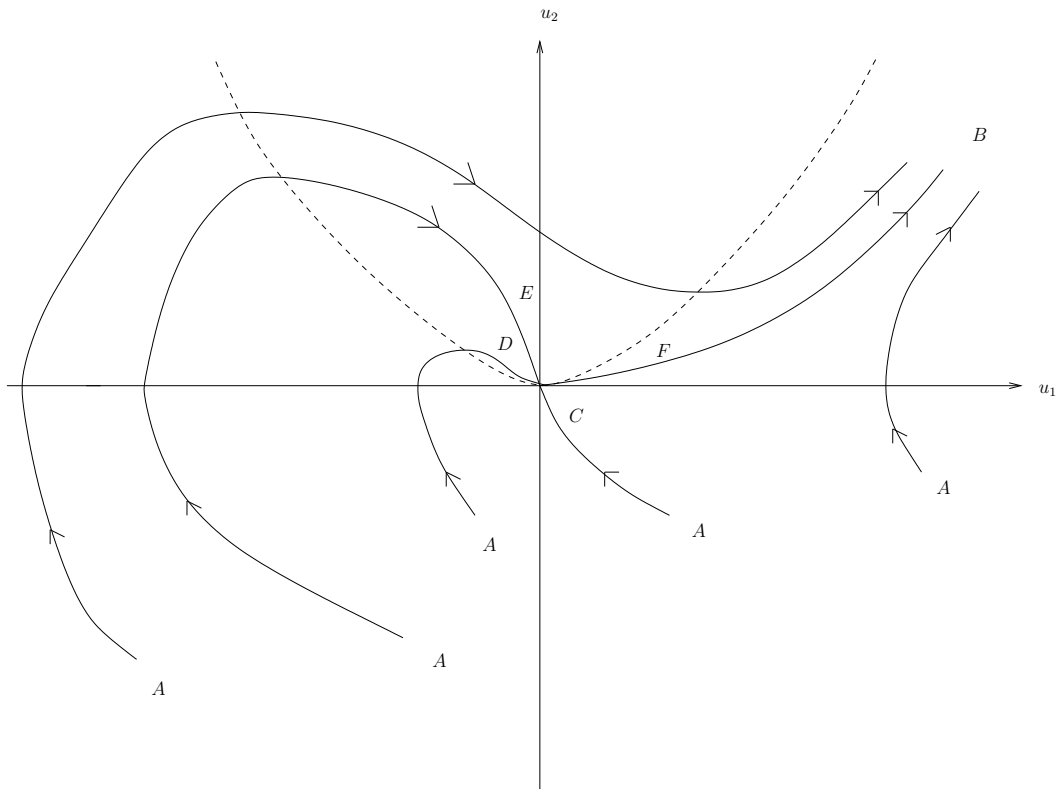

Figure 3.33: Phase plane for (3.148). The dotted line represents the nullcline $u_2 = u_1^2$.

We may consider the trajectories in Figure 3.33 as follows:
1) The trajectory $A - B$ on the right-hand side of the phase plane corresponds to the asymptotic solution as seen before in equation (3.140). This asymptotic solution has $\Theta = u_1 \to \infty$ as $\chi \to \chi^*$ for some finite χ^*. The blow-up behaviour happens at both B and A (for different χ^*). It also indicates what happens to the inner solution as seen in equation (3.134) with $B_0 < 0$ (green curve) in Figure 3.32.
2) The trajectory $A - C$ represents a decaying solution such as $u_1 \sim 1/\chi$ as $\chi \to \infty$.
3) The trajectory $F - B$ corresponds to the outer solution that was given in (3.130) which has $\Psi_0 = (4/(\phi\delta))u_1 \to \infty$ as $\xi = \delta/(2\sqrt{2})\chi \to \chi^*$ and $u_1 \to 0$ as $\chi \to -\infty$.
4) The trajectory $A - D$ represents a decaying solution such as $u_1 \sim -1/\chi$ as $\chi \to \infty$.

5) The trajectory $A - E$ indicates for a decaying solution such as $u_1 \sim ke^{-\chi}$ as $\chi \to \infty$ and where k is an arbitrary constant.
6) The trajectory on the left-hand side of the phase plane $A - B$ blows-up in the both sides of A and B. It corresponds to the inner solution as seen in equation (3.134) with $B_0 > 0$ (blue curve).
The phase plane analysis provides an indication as to how u_1 will change with respect to χ, see Figure 3.34.

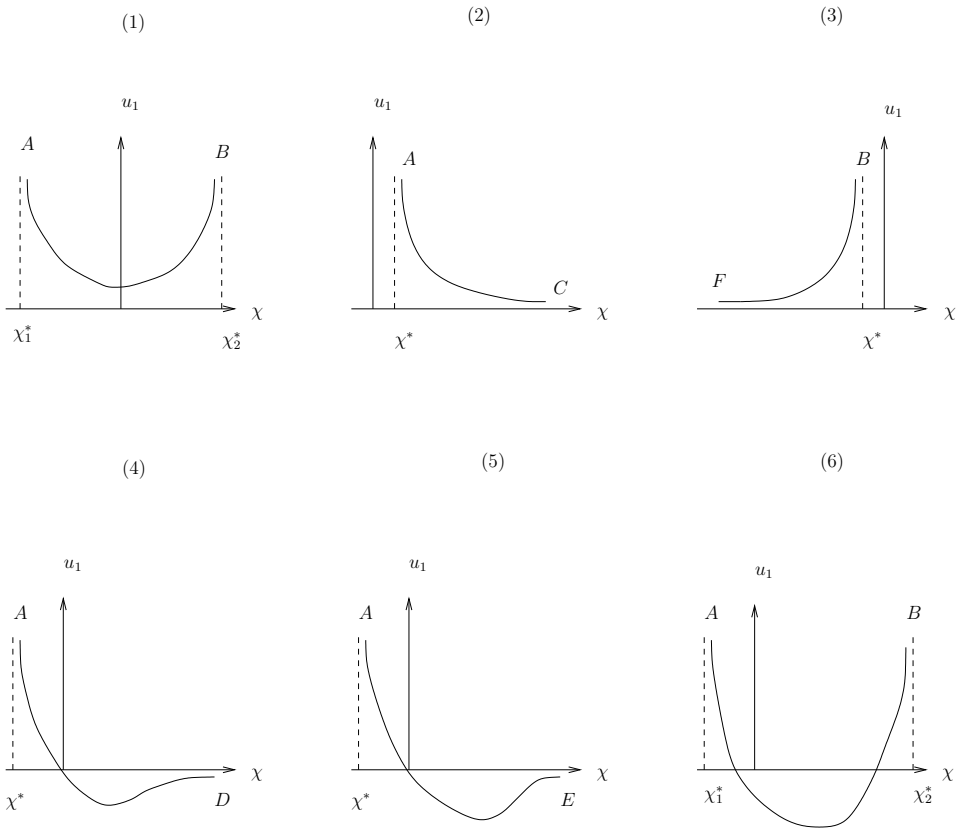

Figure 3.34: Various solutions for $\Theta = u_1$ against χ as determined from the trajectories in the previous phase-plane, Figure 3.33.

Figure 3.34 shows that:
(1) illustrates a $A - B$ trajectory as determined by the phase plane. We see that u_1 blows-up in the both directions at finite values $\chi = \chi_{1,2}^*$.
(2) illustrates a $A - C$ trajectory as determined in the phase plane. We see $u_1 \to 0^+$ as $\chi \to \infty$.

(3) illustrates a $F - B$ trajectory and we see $u_1 \to 0$ as $\chi \to -\infty$.
(4) illustrates a $A - D$ trajectory and we see that $u_1 \to 0$ as $\chi \to \infty$.
(5) illustrates a $A - E$ trajectory and again we have $u_1 \to 0$ as $\chi \to \infty$.
(6) illustrates a $A - B$ trajectory as determined in the phase plane, we see that u_1 blows-up in the both sides as $\chi \to \chi^*_{1,2}$.
The first three solutions apply for $u_1 > 0$, i.e $(1 - S)^{1/2} > 0$, but they suffer from blow-up. The last three solutions (4), (5) and (6) are not of physical relevance because each gives a solution which is somewhere negative.

Solutions of interest are the type indicated by trajectories shown in Figure 3.34, type 2 $A - C$, restricted to $\chi \geq 0 > \chi^*$ and type 3 $F - B$, restricted to $\chi \leq 0 < \chi^*$. Transforming now from u_1 to S, it then follows from, the basic form of similarity solution, (3.78) that

$$S = 1 - \left(\frac{4t}{\delta\phi}\right)^2 u_1^2 \left(\frac{\sqrt{2}z}{\delta}\right). \tag{3.150}$$

$u_1 \to 0$ as $\chi \to \infty$ or $\chi \to -\infty$, see Figure 3.34 (2) and (3), or as $t \to 0$, from (3.150) it gives a nearly saturated region. Note that these solutions work for $|z|$ large since $z = \xi = (\delta/2\sqrt{2})\chi$.

3.6 Numerical Results for Initial Value Problems

The aim of this section is to develop numerically an understanding of the relationship between the solution of convection-diffusion model, (2.1), and convection model, (2.2), and to see how the solution to equation (2.1) behaves as $\delta \to 0$.

Equation (2.1) is a parabolic PDE whereas equation (2.2) is a hyperbolic PDE. Therefore we must develop different numerical schemes for the two equations. These different schemes are both finite difference methods. In Chapter 2, we used a conservative upwind method for solving the nonlinear convection equation (2.2). In this chapter, we will discretize the nonlinear diffusion-convection equation (2.1) as shown in Subsection 3.6.1.

Equation (2.2) is derived from equation (2.1) when δ is small and S is smooth. If we have smooth initial data and very small δ, then the second order term in (2.1), $\frac{\partial}{\partial z}\left(\delta D\left(S\right)\frac{\partial S}{\partial z}\right)$, becomes very small and then can be neglected compared to other terms. The solutions to the two models therefore look nearly identical. In the event of a steepening solution, so that the solution to (2.2) forms a shock, the second-derivative term $\frac{\partial}{\partial z}\left(\delta D\left(S\right)\frac{\partial S}{\partial z}\right)$ grows, and becomes comparable with the others in equation (2.1), it serves to smooth the solution so that although it might become steep, a shock no longer appears.

3.6.1 Finite Difference Method for the Convection-Diffusion Model

In this section we use finite difference methods for the one dimensional nonlinear diffusion-convection model (2.1). In general, as obtaining a closed form solution is not possible for equation (2.1), we solve the problem by using a numerical method. In this technique, the approximations require that the model domain (space) and time be discretized. We first partition the intervals $[0, L]$ and $[0, T]$ into finite grids. We discretize by taking a mesh with a space step $\Delta z = 1/J$ where J is the total number of spatial nodes, so that $z_0 = 0, z_J = 1$ and a time step $\Delta t = 1/M$ where M is the number of time steps. Define the discrete mesh points (z_j, t_n) by

$$z_j = z_0 + j\Delta z \quad \text{for} \quad 0 \leq j \leq J,$$

$$t_{n+1} = t_n + n\Delta t \quad \text{for} \quad n \geq 0.$$

We wish to approximate the equation (2.1) at the mesh points so that

$$S(z_j, t_n) \simeq S_j^n,$$

where S_j^n is our numerical approximation. To solve (2.1), we use the forward differences for $\dfrac{\partial S}{\partial t}$. We have

$$\frac{\partial S}{\partial t} \simeq \frac{S_j^{n+1} - S_j^n}{\Delta t}, \tag{3.151}$$

at a grid point (j, n). Define

$$P = D(S)\frac{\partial S}{\partial z}. \tag{3.152}$$

Then the central finite difference approximation to the z derivative of (3.152) is

$$\frac{\partial P}{\partial z} \simeq \frac{P_{j+\frac{1}{2}} - P_{j-\frac{1}{2}}}{\Delta z} \tag{3.153}$$

at a grid point (j, n) and where

$$P_{j+\frac{1}{2}} = D\left(S_{j+\frac{1}{2}}\right)\frac{\partial S_{j+\frac{1}{2}}}{\partial z} \simeq D\left(\frac{S_{j+1} + S_j}{2}\right)\left(\frac{S_{j+1} - S_j}{\Delta z}\right) \tag{3.154}$$

and

$$P_{j-\frac{1}{2}} = D\left(S_{j-\frac{1}{2}}\right)\frac{\partial S_{j-\frac{1}{2}}}{\partial z} \simeq D\left(\frac{S_j + S_{j-1}}{2}\right)\left(\frac{S_j - S_{j-1}}{\Delta z}\right). \tag{3.155}$$

Using (3.154) and (3.155) in (3.153), we obtain

$$\frac{\partial P}{\partial z} \simeq \frac{1}{\Delta z}\left[D\left(\frac{S_{j+1} + S_j}{2}\right)\left(\frac{S_{j+1} - S_j}{\Delta z}\right) - D\left(\frac{S_j + S_{j-1}}{2}\right)\left(\frac{S_j - S_{j-1}}{\Delta z}\right)\right]. \tag{3.156}$$

Also, by using a central difference approximation to the z derivative of $\dfrac{\partial}{\partial z}\left(K(S)\right)$ in equation (2.1), we take

$$\frac{\partial K(S)}{\partial z} \simeq \frac{K(S_{j+1}^n) - K(S_{j-1}^n)}{2\Delta z} \tag{3.157}$$

at a grid point (j, n). Substituting (3.151), (3.156) and (3.157) into (2.1), we obtain

$$\begin{aligned}\phi\left(\frac{S_j^{n+1} - S_j^n}{\Delta t}\right) = \frac{\delta}{\Delta z^2}\Bigg[&D\left(\frac{S_{j+1} + S_j}{2}\right)(S_{j+1} - S_j) \\ &-D\left(\frac{S_j + S_{j-1}}{2}\right)(S_j - S_{j-1})\Bigg] \\ &+\frac{1}{2\Delta z}\left[K(S_{j+1}^n) - K(S_{j-1}^n)\right].\end{aligned}$$

Multiplying throughout by Δt, defining $r = \Delta t/\Delta z^2$ and $q = \Delta t/2\Delta z$, and re-arranging, we find that the approximate solution of (2.1) will satisfy

$$S_j^{n+1} = S_j^n + r\frac{\delta}{\phi}\left[D\left(\frac{S_{j+1}+S_j}{2}\right)(S_{j+1}-S_j)\right.$$
$$\left.-D\left(\frac{S_j+S_{j-1}}{2}\right)(S_j-S_{j-1})\right]$$
$$+\frac{q}{\phi}\left[K(S_{j+1}^n)-K(S_{j-1}^n)\right].$$

Figures 3.35 and 3.36 represent the numerical solutions for the convection model, (2.2), and the convection-diffusion model, (2.1), with initial condition (3.158) (see Example 1, Section 2.4) and zero-saturation boundary conditions. Note that a boundary layer forms for the convection-diffusion model at $z = 0$ when $t > 0.35$. In Figure 3.36, we choose one more value of small δ (black curve), and the time and space step sizes have been chosen to be smaller than those used in Figures 3.35.
The solutions of convection-diffusion equation, (2.1), produce what is effectively a shock, but smoothed. When we take δ small enough we see that numerical solutions to these two equations are very close together and they are essentially identical. The smoothing effect of the diffusion term is lost in the limit of $\delta \to 0$ giving a shock solutions, see Figures 3.37 and 3.38.

When we take δ small enough, we have to take the time step size to be very small to avoid stability problems which makes our numerics slow. For example, in Figure 3.38 we take small value of δ ($\delta = 5 \times 10^{-4}$) and hence we have to choose a very small time step ($\Delta t = 1/100000$ or smaller value) to get the code to work. For Figure 3.35, the minimum value of the space step which can be chosen is $\Delta z = 1/590$ when we choose $\Delta t = 1/10000$ otherwise the numerical solution becomes unstable.

The wave velocity of the numerical results was compared with theoretical value and they showed very good agreement. For example, the wave velocity in Figure 3.35 determined from the numerical simulation is $C_n = -4.18$ and agrees well with the theoretical value given by $C_t = -4.174$.

We impose no-flux boundary conditions at the end of interval in Figures 3.35-

3.38.

To complete our collection of numerical examples, following on from Examples 1 to 3 of Section 2.4 for the convection-only model, (2.2), we also solve, with this same numerical method, (2.1) with initial conditions (3.159) and (3.160), and still with constant-saturation boundary conditions. Note that as in Examples 1 to 3 of Section 3.6, the initial data is at least piecewise smooth, unlike the piecewise constant conditions of Subsection 2.2.3, but a shock develops for each case, see also Figures 3.39 and 3.40.

Example 1 Consider the convection model, (2.2), and the convection-diffusion model, (2.1), with initial condition

$$S(z,0) = S_* \sin(\pi z), \tag{3.158}$$

where $S_* = 0.8$ is the maximum saturation and the boundary conditions at the end of interval are $S(0,t) = S(1,t) = 0$. The initial condition and upper boundary condition are the same as those for the Example 1 used for the convection equation (see Chapter 2, Figure 2.36). We plot the solutions for different values of δ with small step size. The results are shown in Figures 3.35-3.38.

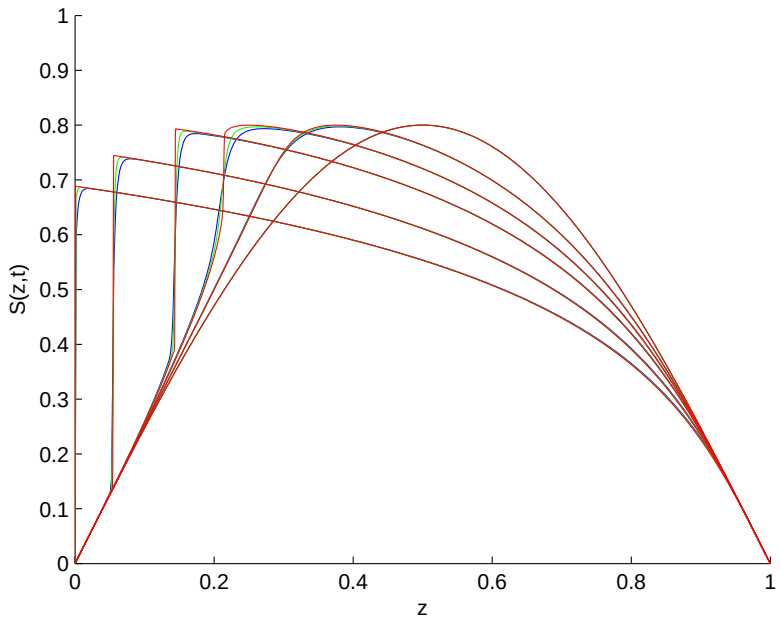

Figure 3.35: The numerical solutions to equations (2.2), in red, and (2.1) with (3.158) at times $t = 0$, 0.03, 0.06, 0.1, 0.2 and 0.35 (where the shock for the convection equation, (2.2), reaches $z = 0$) for different values of δ. Here, for (2.1), $\delta = 10^{-2}$ (blue curve) and $\delta = 5 \times 10^{-3}$ (green curve). Solution moves to the left corresponding to the negative speed. The values of the parameters used for the simulation are $\Delta t = 1/10000$ and $\Delta z = 1/590$.

.

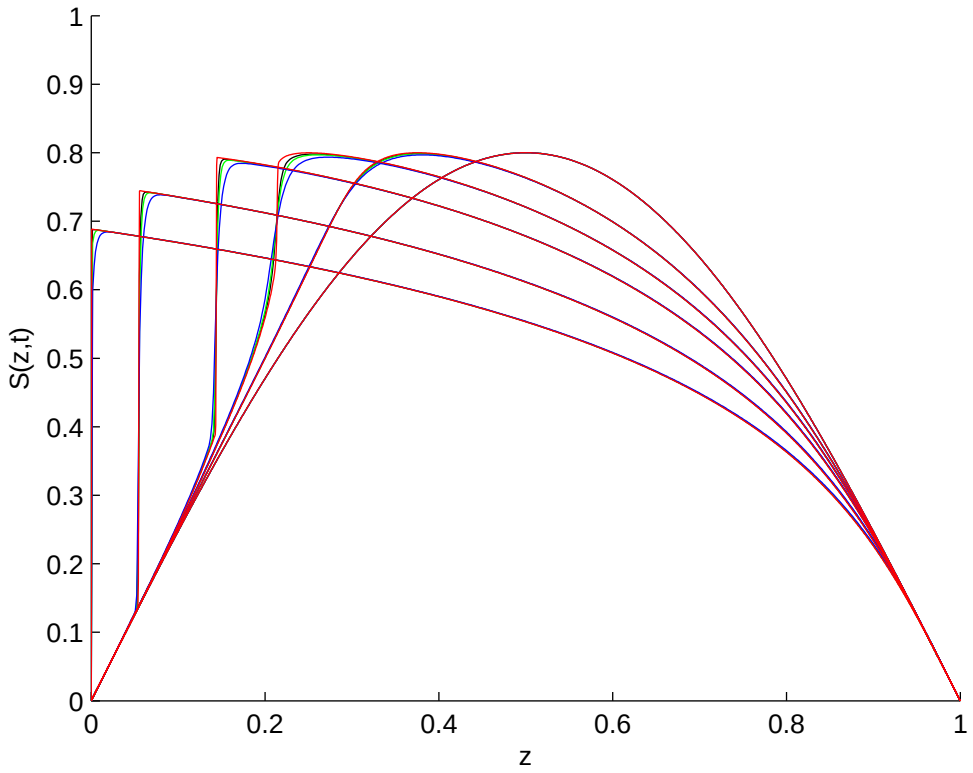

Figure 3.36: The numerical solutions to equations (2.2), in red, and (2.1) with (3.158) at times $t = 0$, 0.03, 0.06, 0.1, 0.2 and 0.35 (where the shock for the convection equation, (2.2), reaches $z = 0$) for different values of δ. Here, for (2.1), $\delta = 10^{-2}$ (blue curve), $\delta = 5 \times 10^{-3}$ (green curve) and $\delta = 3.3 \times 10^{-3}$ (black curve). Solution moves to the left corresponding to the negative speed. The values of the parameters used for the simulation are $\Delta t = 1/20000$ and $\Delta z = 1/700$. Note that here we take Δt and Δz slightly smaller than that used in Figure 3.35.

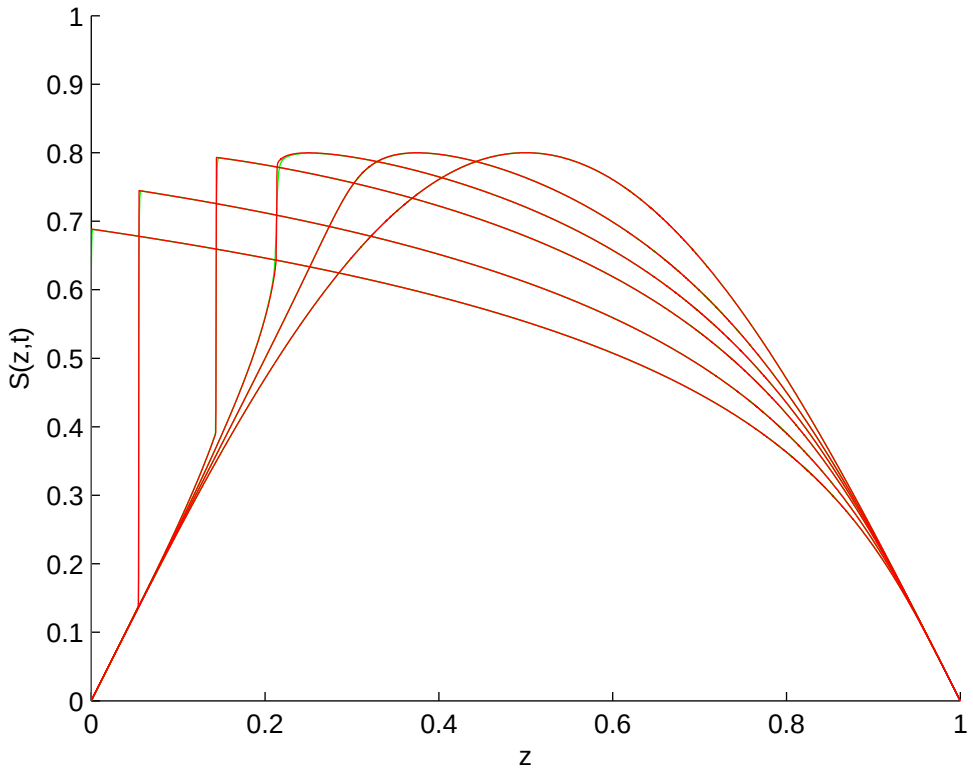

Figure 3.37: The numerical solutions to equations (2.2), in red, and (2.1), in green, with (3.158) at $t = 0$, 0.03, 0.06, 0.1, 0.2 and 0.35 (where the shock reaches $z = 0$). Here, for (2.1), $\delta = 10^{-3}$. Solution moves to the left corresponding to the negative speed. The values of the parameters used for the simulation are $\Delta t = 1/100000$ and $\Delta z = 1/5000$. Here the solution to equation (2.1) is very close to the solution of equation (2.2).

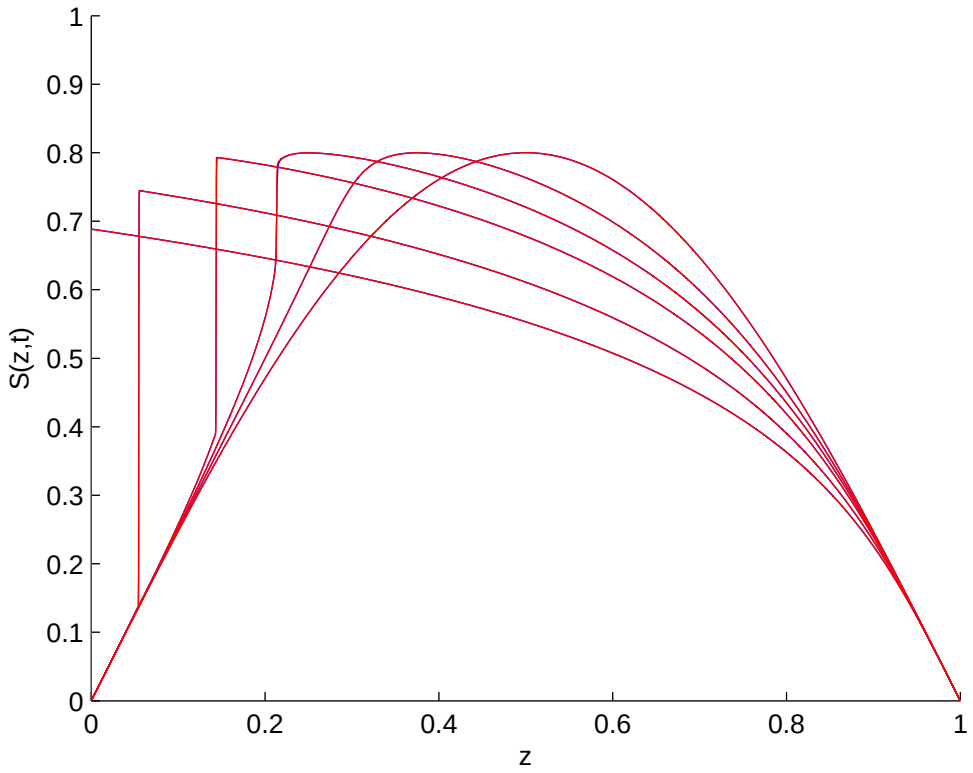

Figure 3.38: The numerical solutions to equations (2.2), in red, and (2.1), in blue, with (3.158) at $t = 0$, 0.03, 0.06, 0.1, 0.2 and 0.35 (where the shock reaches $z = 0$). Here, for (2.1), $\delta = 5 \times 10^{-4}$. Solution moves to the left corresponding to the negative speed. The values of the parameters used for the simulation are $\Delta t = 1/100000$ and $\Delta z = 1/5000$. Here, since δ has been taken to be very small, the shock looks very sharp at the time $t = 0.1$ and later. Solutions to both equations (2.2) and (2.1) look nearly identical.

Example 2 Consider the convection model, (2.2), and the convection-diffusion model, (2.1), with initial condition

$$S(z,0) = \begin{cases} 0.2 & z < 0.25 \\ 2.4z - 0.4 & 0.25 \leq z \leq 0.5 \\ 0.8 & z > 0.5, \end{cases} \tag{3.159}$$

and the boundary conditions $S(z_0, t) = 0.2$ and $S(z_J, t) = 0.8$ with $z_0 = 0.25$ and $z_J = 0.5$. The initial condition and upper boundary condition are the same as those for the Example 2 used for the convection equation (see Chapter 2, Figure 2.37). The results are shown in Figure 3.39.

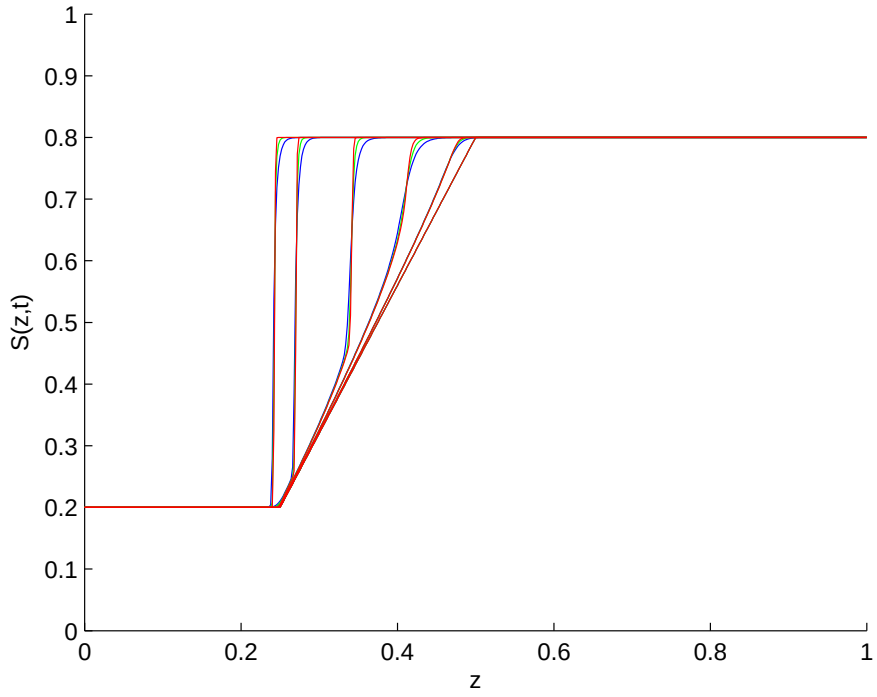

Figure 3.39: The numerical solutions to equations (2.2), in red, and (2.1) with (3.159) at times $t = 0,\ 5.5\times10^{-3},\ 0.02,\ 0.05,\ 0.11$ and 0.14 for different values of δ. Here, for (2.1), $\delta = 10^{-2}$ (blue curve) and $\delta = 5 \times 10^{-3}$ (green curve). Solution moves to the left corresponding to the negative speed. The values of the parameters used for the simulation are $\Delta t = 1/9000$ and $\Delta z = 1/500$.

Example 3 Consider the convection model, (2.2), and the convection-diffusion model, (2.1), with initial condition

$$S(z,0) = \begin{cases} 0 & z < 0.25 \\ 2z - 0.5 & 0.25 \leq z \leq 0.5 \\ 0.5 & z > 0.5, \end{cases} \tag{3.160}$$

and the boundary conditions $S(z_0, t) = 0$ and $S(z_J, t) = 0.5$ with $z_0 = 0.25$ and $z_J = 0.5$. The initial condition and upper boundary condition are the same as those for the Example 3 used for the convection equation (see Chapter 2, Figure 2.38). The results are shown in Figure 3.40.

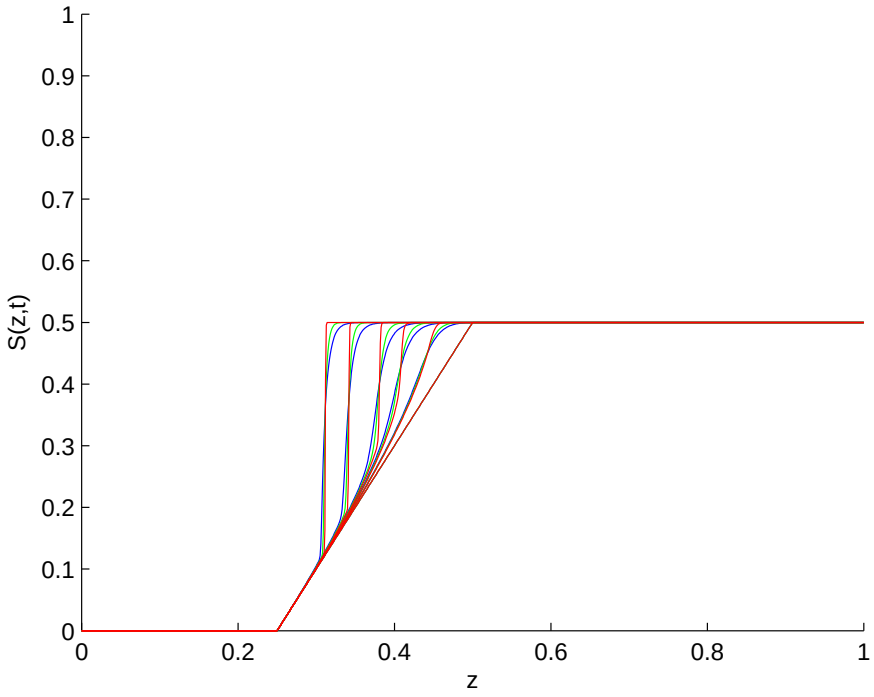

Figure 3.40: The numerical solutions to equations (2.2), in red, and (2.1) with (3.160) at times $t = 0,\ 0.1,\ 0.2,\ 0.3,\ 0.5$ and 0.7 for different values of δ. Here, for (2.1), $\delta = 10^{-2}$ (blue curve) and $\delta = 5 \times 10^{-3}$ (green curve). Solution moves to the left corresponding to the negative speed. The values of the parameters used for the simulation are $\Delta t = 1/10000$ and $\Delta z = 1/1000$.

3.7 Summary

We have shown that some progress can be made analytically and numerically for the nonlinear diffusion model and the convection-diffusion model. Travelling wave solutions for the nonlinear diffusion model were obtained in closed forms for the two limiting cases of low and high saturation (Subsection 3.2.1 and 3.2.2). Again travelling wave solutions for the convection-diffusion model were found in explicit forms for the same two limiting cases (Case 1 and Case 2 in Section 3.3). Also, we showed that several different cases of travelling wave solutions for the convection-diffusion model exist, according to whether the limiting saturations might be zero, one or in between. The travelling waves were front solutions.

Self-similar solutions exist for the diffusion model both for the full expression of $D(S)$ and for its limiting cases where $D(S)$ simplifies. However, for the convection-diffusion model self-similar solutions were found only for the limiting cases of low and high saturation, with simpler expressions for $D(S)$.

Additionally, numerical solutions were obtained for all different cases of TWS which confirmed the results of the analysis. A finite difference method was also used to solve the convection-diffusion model numerically. The numerical results, in general, show the effect of the diffusion term $\frac{\partial}{\partial z}\left(\delta D\left(S\right)\frac{\partial S}{\partial z}\right)$. In all the different initial value problems that were given in Examples 1, 2, and 3 (see equations (3.158), (3.159) and (3.160)), it was observed that the solutions produce something close to a shock after a time. As $\delta \to 0$, the solutions become sharper and approach the discontinuous solutions with true shocks. For small enough δ, solutions to the nonlinear convection-diffusion model look nearly identical to the solutions of convection model.

The analytical results of the nonlinear convection-diffusion model of Chapter 3 were compared with those results of convection-only model in Chapter 2. They showed a good qualitative agreement: with the possible exception of around shocks, the simpler convection-only model appears to give a good representation of the fuller convection-diffusion problem. The numerical results of the two models in Chapters 2 and 3 were also compared and the results, in general, were very close. The solution process of both numerical methods tend to be more stable and accurate.

Chapter 4

Full Model with Sink Term

4.1 Introduction

In this chapter, we study travelling wave solutions of the full model (1.9). Asymptotic solutions are found in closed forms for S small (a nearly dry region) and S close to 1 (a nearly saturated region). A phase plane analysis is used to study the behaviour of relevant nonlinear ODEs. The structure of the phase plane is of different type according to the value of wave velocity c. We show that a TWS exists. We have focused on local behaviour near a dry region and near a saturated region. By using the phase plane analysis for several values of the wave velocity c, we show that a TWS exists for the case when S is small. For the second case, when S close to 1, we used a simple scaling and we end up with the standard Airy equation. After that we show that a local TWS also exists for this case. Unfortunately, self-similar solutions were not found for the full model (1.9) not even for the two local cases (S is small and S close to 1). Self-similar solutions did exist for the diffusion-sink model (convection term dropped) with S close to 1 only. Also, self-similar solutions are found for the convection-sink model, again only near a saturated region. Finally, we used the method of characteristics to solve the convection model with sink term.

4.2 Travelling Wave Solutions for the Full Model

Recall that travelling wave solutions to the green roof model (1.9) take again the form $S(z,t) = S(\zeta)$ where $\zeta = z - ct$. Substituting this expression into (1.9) yields the ordinary differential equation

$$\frac{d}{d\zeta}\left(\delta D\left(S\right)\frac{dS}{d\zeta} + K\left(S\right)\right) + c\phi\frac{dS}{d\zeta} - R(S) = 0. \tag{4.1}$$

Writing $g(\zeta) = D(S)dS/d\zeta$, the ordinary differntial equation (4.1) can be written as a first order system

$$\begin{aligned}\frac{dS}{d\zeta} &= \frac{g}{D(S)}\\ \frac{dg}{d\zeta} &= \frac{1}{\delta}\left[\left(\frac{-g}{D(S)}\right)\left(K'(S) + c\phi\right) + R(S)\right],\end{aligned} \tag{4.2}$$

where $K'(S) = dK/dS$. We now look for an equilibrium point by setting $\dfrac{g}{D(S)} = 0$ in (4.2), then we have $R(S) = 0$ which gives $S = S_- = \epsilon/(\sqrt{1+\epsilon^2})$ where the value of ϵ is given in [18]. Thus, $(S_s, g_s) = (S_-, 0)$ is the only equilibrium point. The Jacobian matrix of the right-hand side of (4.2) near this equilibrium point is

$$J_{(S_-,0)} = \begin{bmatrix} 0 & 1/D(S_-) \\ \dfrac{1}{\delta}R'(S_-) & -\dfrac{1}{\delta}(K'(S_-) + c\phi)/D(S_-) \end{bmatrix},$$

where $R' = dR/dS$. Hence Det $J_{(S_-,0)} = -1/\delta(R'(S_-)/D(S_-)) < 0$ and
Tr $J_{(S_-,0)} = -1/\delta(c\phi/D(S_-))$, which depends on the value of c. Since Det $J < 0$, the equilibrium point $(S_-, 0)$ is a saddle node.
We can now use a phase plane analysis to study the behaviour of the nonlinear system (4.2).
The S-nullcline is given by the line $g = 0$ (the S axis) and $S = 1$ since $D(S) \to \infty$ at $S = 1$, then $g/D(S) = 0$. The g-nullcline is given by $g = D(S)R(S)/(K'(S) + c\phi)$. We have a finite value, say S_*, at which the g-nullcline has an asymptote ($g \to \pm\infty$ as $S \to S_*$ on nullcline).
The structure of the phase plane is of different types according to the value of the wave velocity c, with the phase plane taking different forms according

to whether: $S_* < 0$, $S_* = 0$, $0 < S_* < S_-$, $S_* = S_-$ and $S_* > S_-$. The wave velocity c can be written in term of the value S_* and so we get different forms of phase plane for different values of c. Let us now consider all the possible cases of c.
The wave moves up in the first case, with $c > 0$, while it moves down for the last three cases.

Case 1: $c > 0$

Using the approximate functions of $D(S)$, $K'(S)$ and $R(S)$ when S is close to 0, we have that the local behaviour of g-nullcline near $S = 0$ takes the form

$$g \sim \frac{\kappa S_- S^{5/2}}{4c\phi}, \tag{4.3}$$

where $\kappa = \eta/\epsilon$ is a positive constant. From (4.3) we see that g-nullcline $\to 0$ as $S \to 0^+$. Similarly, by using the approximate forms of $D(S)$, $K'(S)$ and $R(S)$ when S is close to 1, the local behaviour of the g-nullcline is

$$g \to \frac{\eta}{c\phi} \quad \text{as} \quad S \to 1, \tag{4.4}$$

so that on the nullcline g approaches a finite positive value as $S \to 1$.

We look now at the asymptotic behaviour of the system (4.2) (for $c \neq 0$) near $S = 0$ (a nearly dry region) and $S = 1$ (a nearly saturated region). To begin, we first use the approximate form of $D(S)$ when S is close to 0, from (1.12), into the first equation of (4.2), and we obtain

$$\frac{dS}{d\zeta} \sim 4gS^{-5/2}. \tag{4.5}$$

We assume that the function $g(\zeta)$ can be expanded in terms of δ in the form

$$g(\zeta) \sim g_0 + \delta g_1(\zeta) + \delta^2 g_2(\zeta) + ... \tag{4.6}$$

where g_0 is an arbitrary constant. Substituting (4.6) with δ is small into equation (4.5) gives

$$S^{5/2}\frac{dS}{d\zeta} \sim 4g_0. \tag{4.7}$$

Integrating (4.7), we obtain

$$S^{7/2} \sim 14 g_0 \zeta + \zeta_0, \tag{4.8}$$

where ζ_0 is a constant of integration. Without loss of generality, we can take $\zeta_0 = 0$. Then equation (4.8) gives a solution valid only for $g_0 > 0$ and $\zeta > 0$ or $g_0 < 0$ and $\zeta < 0$. Solving (4.8) for S, we obtain

$$S \sim (14 g_0 \zeta)^{2/7}. \tag{4.9}$$

For ζ small, the solution in (4.9) becomes close to zero which gives a region which is nearly dry. Now, using the approximate forms of $D(S)$, $K'(S)$ and $R(S)$ with S close to 0, from (1.12), (1.13) and (1.17) respectively, in the second equation of (4.2), we obtain

$$\begin{aligned} \frac{dg}{d\zeta} &\sim \frac{1}{\delta}\left[\left(\frac{-4g_0}{S^{5/2}}\right)\left((9/8)S^{7/2} + c\phi\right) - \frac{\eta s_-}{S}\right] && (4.10) \\ &\sim -\frac{1}{\delta}\left(\frac{4c\phi g_0}{S^{5/2}} + \frac{\eta s_-}{S}\right) \sim -\frac{1}{\delta}\left(\frac{4c\phi g_0 + \eta s_- S^{3/2}}{S^{5/2}}\right) \\ &\sim \frac{-4c\phi g_0}{\delta S^{5/2}} \quad \text{as} \quad S \to 0, && (4.11) \end{aligned}$$

where $s_- \sim \epsilon$. Substituting (4.9) into equation (4.11) and solving for g, we end up with

$$g \sim \left(\frac{-c\phi(14 g_0)^{2/7}}{\delta}\right)\zeta^{2/7} + g_0. \tag{4.12}$$

Using (4.9) in (4.12), we can write the function g in term of S as

$$g \sim \frac{-c\phi}{\delta} S + g_0. \tag{4.13}$$

From (4.9) and (4.13), solutions go into and come out of g axis at finite values of g. Also, solutions behave linearly. In this case when $c > 0$ we see from equation (4.13) that slope is negative near $S = 0$.

To study the asymptotic behaviour of the system (4.2) near $S = 1$, we use the approximate form of $D(S)$ when S is close to 1, from (1.18), in the first equation of (4.2), then again use an asymptotic expansion of $g(\zeta)$, from (4.6),

and solve for S to obtain

$$S \sim 1 - (1/2)g_0^2\zeta^2. \tag{4.14}$$

As $\zeta \to 0$, S becomes close to 1 which gives a region which is nearly saturated. Similarly, using the approximate forms of $D(S)$, $K'(S)$ and $R(S)$ when S is close to 1, from (1.18), (1.19) and (1.21), in the second equation of (4.2), we obtain

$$\begin{aligned}
\frac{dg}{d\zeta} &\sim \frac{1}{\delta}\left[-g_0\sqrt{2}(1-S)^{1/2}\left(\sqrt{2}(1-S)^{-1/2}+c\phi\right)+\eta\right] \\
&\sim \frac{1}{\delta}\left[-2g_0 - g_0\sqrt{2}(1-S)^{1/2}c\phi+\eta\right] \qquad (4.15) \\
&\sim \frac{1}{\delta}\left(-2g_0+\eta\right) \quad \text{as} \quad S \to 1. \qquad (4.16)
\end{aligned}$$

Then, solving (4.16) for g, we get

$$g \sim \frac{1}{\delta}\left(-2g_0+\eta\right)\zeta + g_0, \tag{4.17}$$

and from (4.14) g can be written in term of S

$$g \sim \frac{\sqrt{2}}{g_0\delta}\left(-2g_0+\eta\right)(1-S)^{1/2} + g_0. \tag{4.18}$$

Equation (4.18) indicates that the solutions go into and come out of the line $S = 1$ at finite values of g. The phase plane of (4.2) with $c > 0$ can be now constructed with the aid of the nullcline curve and the local behaviour of the g-nullcline given by (4.3) and (4.4), see Figure 4.1.

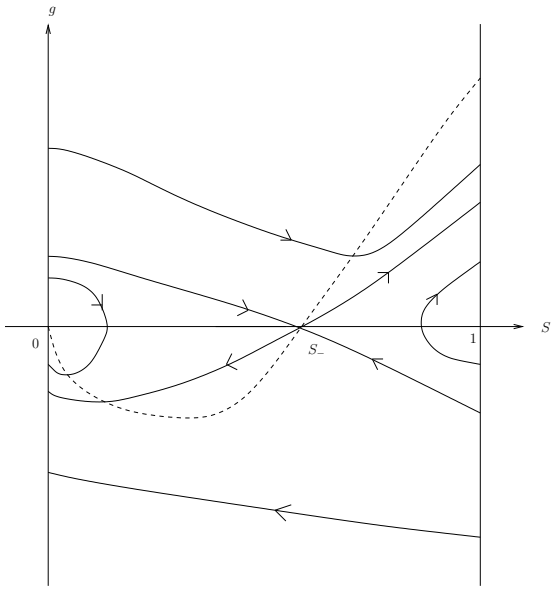

Figure 4.1: Phase plane for (4.2) with $c > 0$. The dashed line represents the nullcline of (4.2). The finite value, S_* at which the g-nullcline has an asymptote, lies in the left half plane and is not seen in this case. Solutions have negative slope at the g axis when S small according to (4.13). Note that from (4.18) the slopes of the curves sould be infinite at $S = 1$.

In the above figure, for $S < S_-$ there are two trajectories joining $S = 0$ and the equilibrium point $S = S_-$. These trajectories correspond to travelling wave solutions connecting two regions. These regions are a dry region ($S = 0$) above a partially saturated region ($S = S_-$) and a partially saturated region above a dry region. There are also two trajectories which link $S = S_-$ and $S = 1$. These trajectories represent travelling waves for a saturated region ($S = 1$) above a partially saturated region and a partially saturated region above a saturated region. Trajectories are also exist between $S = 0$ and $S = 1$ which represent travelling waves for a dry region above a saturated region and a saturated region above a dry region. The phase plane analysis provides an indication as to how S will change with respect to ζ. The corresponding travelling wave profiles are shown in Figure 4.2. The plant roots at low levels of saturation supply water to the soil (where the soil is fully dry). This behaviour could be physically unacceptable and conservation of mass is violated. These type of solutions are presented in Figure 4.2 cases (1), (2), (5) and (6). The plant

roots at high levels of saturation take up water from the soil (where the soil is fully saturted) and mass can be conserved as shown in Figure 4.2 cases (3), (4), (5) and (6).

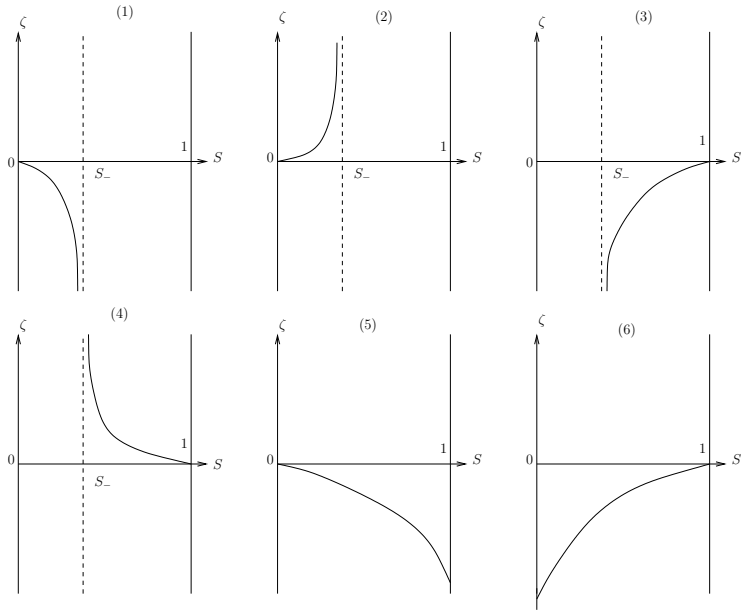

Figure 4.2: Travelling wave solutions for S against ζ as determined from the trajectories in the previous phase-plane, Figure 4.1.

In addition, there are trajectories connecting $S = 0$ to $S = 0$ (dry to dry) and others connecting $S = 1$ to $S = 1$ (saturated to saturated). The former indicate a partially saturated region moving up between two dry regions (see left-hand plot of Figure 4.3). This unphysical case has water being supplied to the soil by the roots in the moist region and conservation of mass is violated at its end points. The second class of travelling wave has a partially saturated region moving up between two fully saturated regions (see right-hand sketch of Figure 4.3) and is more physical. Water is taken up by plant roots everywhere. Mass can be conserved due to the ability for saturated regions to sustain arbitrary flux.

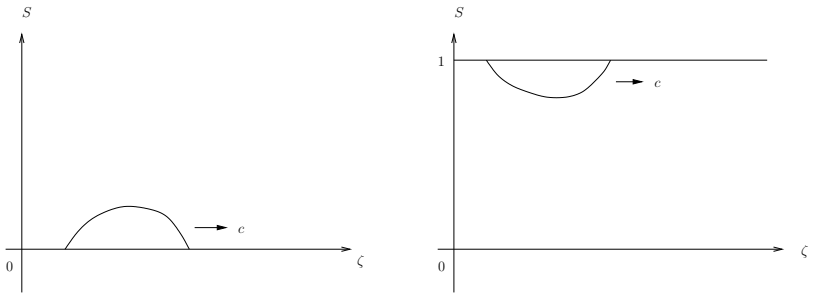

Figure 4.3: Local solutions near $S = 0$ (on the left) and near $S = 1$ (on the right) with $c > 0$. In the left picture, a wet region moves up in otherwise dry soil. In the right sketch there is space (vapour or air) in the pores within the bounded region, moving up between two saturated regions.

Case 2: $c = 0$

For (4.2) when $c = 0$, the S-nullcline is again given by the line $g = 0$ and $S = 1$ while the g-nullcline is given by $g = D(S)R(S)/K'(S)$. As in the previous case, using the approximate forms of $D(S)$, $K'(S)$ and $R(S)$ near 0, the local behaviour of the g-nullcline takes the form

$$g = \frac{-2\eta s_-}{9S^2}, \tag{4.19}$$

and, clearly, this gives that the g-nullcline $\to -\infty$ as $S \to 0_+$. Similarly, the local behaviour of the g-nullcline near 1 takes the form

$$g \sim \eta \quad \text{as} \quad S \to 1. \tag{4.20}$$

We look now at the local behaviour of the system (4.2) (when $c = 0$) for a nearly dry region and for a nearly saturated region. Using a similar argument to that in Case 1, taking $c = 0$ in (4.10) we obtain

$$\frac{dg}{d\zeta} \sim -\frac{1}{\delta}\frac{\eta s_-}{S} \quad \text{as} \quad S \to 0. \tag{4.21}$$

Again substituting (4.9) into equation (4.21) and solving for g, we obtain

$$g \sim -\frac{7}{5\delta}\eta s_{-}\left(14g_0\right)^{-2/7}\zeta^{5/7} + g_0, \tag{4.22}$$

where g_c is an arbitrary constant. Using (4.9) in (4.22), we have

$$g \sim -\frac{\eta s_{-}}{10\delta g_0}S^{5/2} + g_0. \tag{4.23}$$

From (4.9) and (4.23), solutions go into and come out of g axis at finite values of g. Also, they are horizontal at the g axis.
The local behaviour of the system (4.2) (when $c = 0$) near $S = 1$, can be obtained by taking $c = 0$ in (4.15) which gives the same solutions that got in equation (4.18). The phase plane of (4.2) when $c = 0$ is sketched in Figure 4.4.

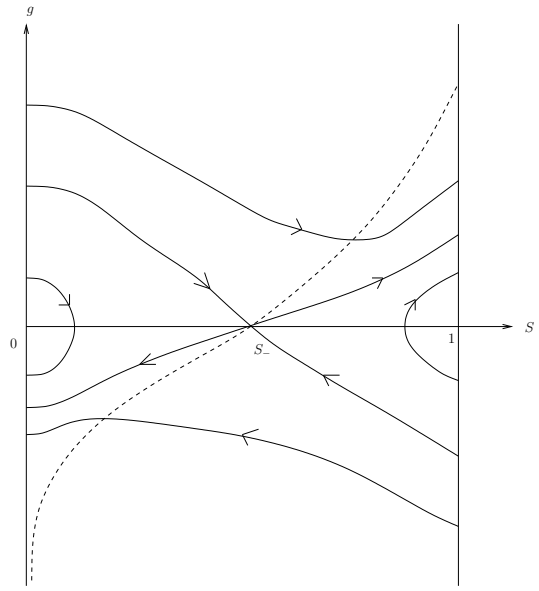

Figure 4.4: Phase plane of (4.2) with $c = 0$. Travelling waves exist from $S = 0$ to $S = S_-$. Travelling waves also exist from $S = S_-$ to $S = 1$. Travelling waves are also possible from $S = 0$ to $S = 1$. Local solutions exist near $S = 0$ and near $S = 1$. The dashed line represents the nullcline solution of (4.2) with $c = 0$. The finite value, S_* at which the g-nullcline has an asymptote, lies at $S = 0$. Solutions are horizontal at the g axis when S is small according to (4.23). Note that from (4.18) the slopes of the curves sould be infinite at $S = 1$.

The local behaviour of the solution of (4.2) near $S = 0$ and near $S = 1$ and the general form of the phase plane for the remaining three cases can again be obtained as for Case 1. We get same sorts of travelling waves as shown in Figures 4.5, 4.6 and 4.7. Note that for Case 4 on substituting the value of wave velocity $c = -K'(S_*)/\phi$ in the second equation of (4.2), the g-nullcline now can be written as $S = S_* = S_-$ or $g = D(S)R(S)/(K'(S) - K'(S_*)) > 0$, as shown in Figure 4.6.

Case 3: $-K'(S_*)/\phi < c < 0$

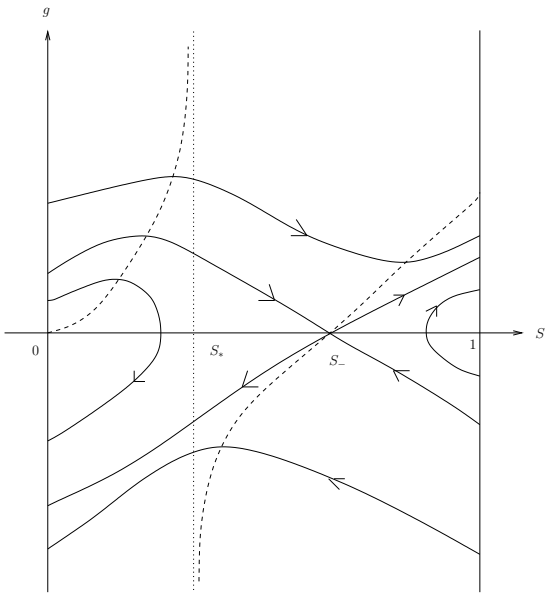

Figure 4.5: Phase plane for (4.2) with $-K'(S_*)/\phi < c < 0$. Travelling wave solutions are possible between $S = 0$ and $S = S_-$ and also link $S = S_-$ and $S = 1$. Travelling waves are possible between $S = 0$ and $S = 1$. Local solutions exist near $S = 0$ and near $S = 1$. Solutions have positive slope at the g axis when S is small according to (4.13). The dashed line represents the nullcline of (4.2). The finite value, S_* at which the g-nullcline has an asymptote, lies to the left of S_-. Note that from (4.18) the slopes of the curves sould be infinite at $S = 1$.

Case 4: $c = -K'(S_*)/\phi$

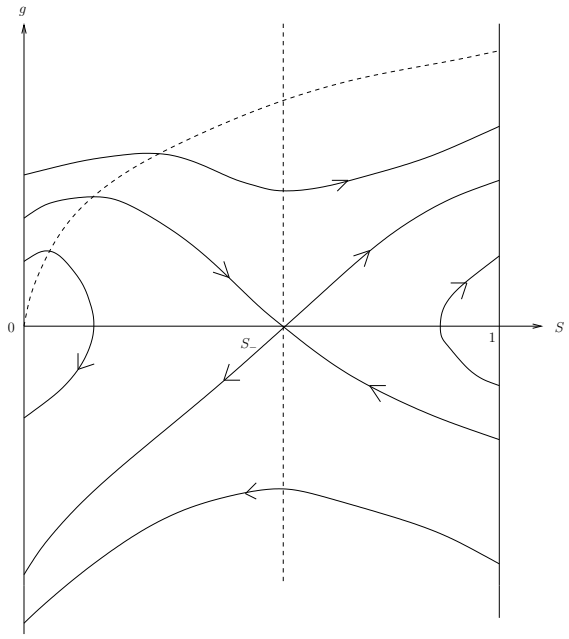

Figure 4.6: Phase plane for (4.2) with $c = -K'(S_*)/\phi$. Travelling wave solutions exist between $S = 0$ and $S = S_-$ and also between $S = S_-$ and $S = 1$. Travelling waves are possible between $S = 0$ and $S = 1$. Local solutions exist near $S = 0$ and near $S = 1$. Solutions have positive slope at the g axis when S is small according to (4.13). The dashed line represents the nullcline of (4.2). Note that from (4.18) the slopes of the curves sould be infinite at $S = 1$.

Case 5: $c < -K'(S_*)/\phi$

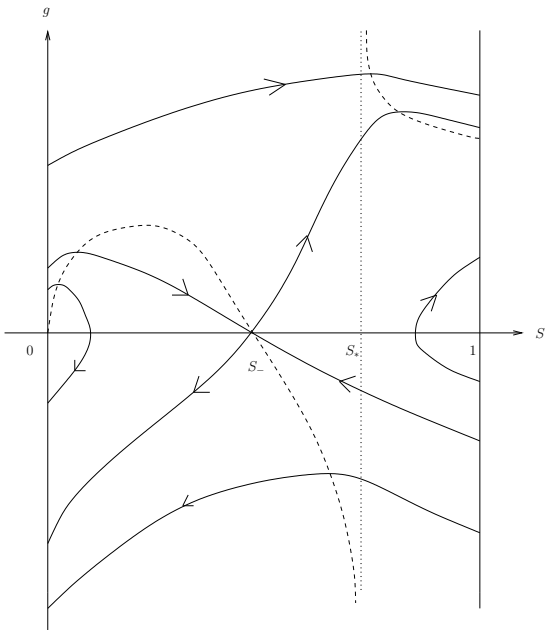

Figure 4.7: Phase plane for (4.2) with $c < -K'(S_*)/\phi$. Travelling wave solutions exist between $S = 0$ and $S = S_-$ and also between $S = S_-$ and $S = 1$. Travelling waves link $S = 0$ and $S = 1$. Local solutions exist near $S = 0$ and near $S = 1$. Solutions have positive slope at the g axis when S is small according to (4.13). The dashed line represents the nullcline of (4.2). The finite value, S_* at which the g-nullcline has an asymptote, lies to the right of S_-. Note that from (4.18) the slopes of the curves sould be infinite at $S = 1$.

In the next two sections, we discuss the local asymptotic behaviour in equation (4.1) for S small (where the soil region is nearly dry) and for S close to 1 (where it is nearly saturated).

4.2.1 Case 1: Low Saturation

We use the approximate forms of $D(S)$, $K(S)$ and $R(S)$ when S is small as got from (1.12), (1.13) and (1.16) respectively. Substituting these into equation

(4.1), we obtain

$$\frac{d}{d\zeta}\left(\delta\frac{1}{4}S^{5/2}\frac{dS}{d\zeta}\right)+\left(\frac{9}{8}S^{7/2}+c\phi\right)\frac{dS}{d\zeta}-\kappa\left(S-s_{-}\right)=0.$$

For simplicity, define $\Psi = S^{7/2}$, then $\dfrac{d\Psi}{d\zeta} = \dfrac{7}{2}S^{5/2}\dfrac{dS}{d\zeta}$. Hence the above equation becomes

$$\frac{\delta}{14}\frac{d^2\Psi}{d\zeta^2}+\left(\frac{9}{8}\Psi+c\phi\right)\frac{2}{7}\Psi^{-5/7}\frac{d\Psi}{d\zeta}-\kappa(\Psi^{2/7}-s_{-})=0. \tag{4.24}$$

We can write equation (4.24) as a first order system. Taking $u_1(\zeta) = \Psi(\zeta)$ and $u_2(\zeta) = \Psi'(\zeta)$, we have the system

$$\begin{aligned} u_1'(\zeta) &= u_2 \\ u_2'(\zeta) &= -\frac{2}{7}\left(\frac{9}{8}u_1+c\phi\right)u_1^{-5/7}u_2+\kappa(u_1^{2/7}-s_{-}), \end{aligned} \tag{4.25}$$

where the prime denotes the derivative with respect to ζ. It is easy to see that we have only one equilibrium point in this nonlinear system, namely $(u_1^s, u_2^s) = (s_-^{7/2}, 0)$. At this equilibrium point $S = u_1^{2/7} = s_-$ and no water enters or leaves roots.

At a general point (u_1, u_2) the Jacobian matrix of the linearized system is given by

$$J=\begin{bmatrix} 0 & 1 \\ -\left(\dfrac{9}{98}u_1^{-5/7}u_2-c\phi\dfrac{10}{49}u_2u_1^{-12/7}\right)+\dfrac{2}{7}\kappa u_1^{-5/7} & -\dfrac{2}{7}\left(\dfrac{9}{8}u_1+c\phi\right)u_1^{-5/7} \end{bmatrix}.$$

At $(u_1^s, u_2^s) = (s_-^{7/2}, 0)$, this becomes

$$J_{(s_-^{7/2},0)}=\begin{bmatrix} 0 & 1 \\ \dfrac{2}{7}\kappa s_-^{-5/2} & -\dfrac{2}{7}(\dfrac{9}{8}s_-^{7/2}+c\phi)s_-^{-5/2} \end{bmatrix}$$

$$=\begin{bmatrix} 0 & 1 \\ a_0 & -b_0 \end{bmatrix},$$

where $a_0 = (2/7)\kappa s_-^{-5/2} > 0$ and $b_0 = (2/7)((9/8)s_-^{7/2} + c\phi)s_-^{-5/2}$. Thus, Det $J_{(s_-^{7/2},0)} = -a_0 < 0$ and Tr $J_{(s_-^{7/2},0)} = -b_0$. This shows that the equilibrium point $(s_-^{7/2}, 0)$ is a saddle node because Det $J < 0$. The u_1-nullcline is given by the line $u_2 = 0$ (the u_1 axis) while the u_2-nullcline is $u_2 = 7u_1^{5/7}\kappa(u_1^{2/7} - s_-)/2((9/8)u_1 + c\phi)$. We see that on the u_2-nullcline, $u_2 \to 0$ as $u_1 \to 0$. The u_2-nullcline has asymptotes $u_2 \to \pm\infty$ as $u_1 \to u_1^*$ where u_1^* is some finite value. The phase plane analysis is used to study (4.25) for several values of the wave velocity c which we come to below. The phase plane takes different forms according to whether: $u_1^* < 0$, $u_1^* = 0$, $0 < u_1^* < u_1^s$, $u_1^* = u_1^s$ and $u_1^* > u_1^s$, where u_1^s is the equilibrium point.

Case 1: $c > 0$

Using a similar argument to that in the standard case, we can find the asymptotic behaviour of the system (4.25) near $u_1 = 0$. Assume now $u_1 \ll 1$ and $|u_2| \ll 1$, then the system (4.25) reduces to

$$\begin{aligned} u_1'(\zeta) &= u_2 \\ u_2'(\zeta) &= -\frac{2}{7}c\phi u_1^{-5/7}u_2 - \kappa s_-. \end{aligned} \tag{4.26}$$

Assume that u_2 has a finite value i.e $u_2 \sim u_0$, from the first equation in (4.26), we have

$$u_1 \sim u_0(\zeta + \zeta_0), \tag{4.27}$$

where ζ_0 is a constant of integration. Substituting (4.27) in the second equation of (4.26) (assuming that $u_1^{5/7} \ll |u_2|$), we obtain

$$u_2'(\zeta) \sim -\frac{2}{7}c\phi u_0^{2/7}(\zeta + \zeta_0)^{-5/7}. \tag{4.28}$$

Solving (4.28) for u_2, we obtain

$$u_2(\zeta) \sim u_0 - c\phi u_0^{2/7}(\zeta + \zeta_0)^{2/7}. \tag{4.29}$$

Substituting (4.27) into (4.29), we obtain

$$u_2 \sim u_0 - c\phi u_1^{2/7}. \tag{4.30}$$

Clearly, equations (4.27) and (4.30) indicate that the solutions go into and come out of u_2 axis at finite values of u_2. Equation (4.30) gives a negative slope if $u_0 < c\phi u_1^{2/7}$ where $c > 0$. The phase plane of (4.25) with $c > 0$ can be drawn with the aid of the nullcline curves, see Figure 4.8.

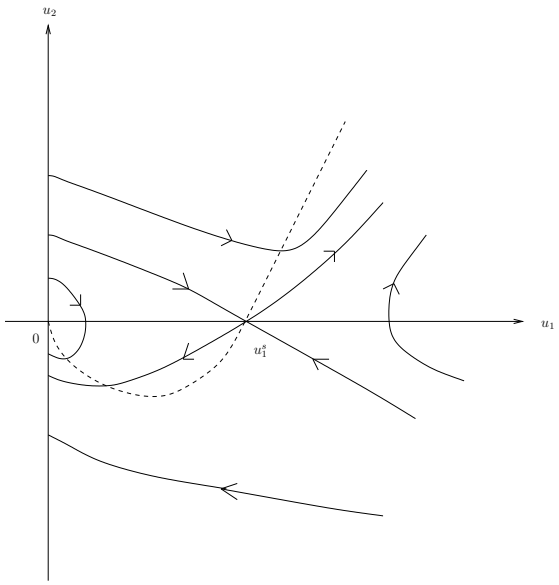

Figure 4.8: Phase plane for (4.25) with $c > 0$. The finite value, u_1^*, lies in the left half plane and is not seen in this case. The dashed line represents the nullcline of (4.25). Solutions at the u_2 axis have negative slope according to (4.30).

Figure 4.8 shows two trajectories joining the saddle point $u_1 = u_1^s$ and $u_1 = 0$. These trajectories correspond to travelling waves from $u_1 = 0$ to $u_1 = u_1^s$ and from $u_1 = u_1^s$ to $u_1 = 0$. They connect two regions which are a dry region above a partially saturated region and a partially saturated region above a dry region. Also, local travelling waves exist near $u_1 = 0$. The travelling waves for this limiting case agree with the travelling waves that are found in Figure 4.1 which join the equilibrium point, $S = S_-$, and $S = 0$.

Case 2: $c = 0$

From (4.25) with $c = 0$ we have

$$\begin{aligned} u_1'(\zeta) &= u_2 \\ u_2'(\zeta) &= -\frac{9}{28}u_1^{2/7}u_2 + \kappa(u_1^{2/7} - s_-). \end{aligned} \tag{4.31}$$

The u_1-nullcline is $u_2 = 0$ while the u_2-nullcline is given by $u_2 = 28\kappa(u_1^{2/7} - s_-)/(9u_1^{2/7})$. Note that on the u_2-nullcline we see that $u_2 \to -\infty$ as $u_1 \to 0$ and also $u_2 = 0$ at $u_1 = s_-^{7/2}$. To see the local behaviour near $u_1 = 0$, we take $c = 0$ in (4.28), to get $u_2'(\zeta) = 0$, zero slope on u_2 axis, which gives $u_2=$ constant. Then from (4.27) solutions go into and come out of u_2 axis at finite values of u_2, see Figure 4.9.

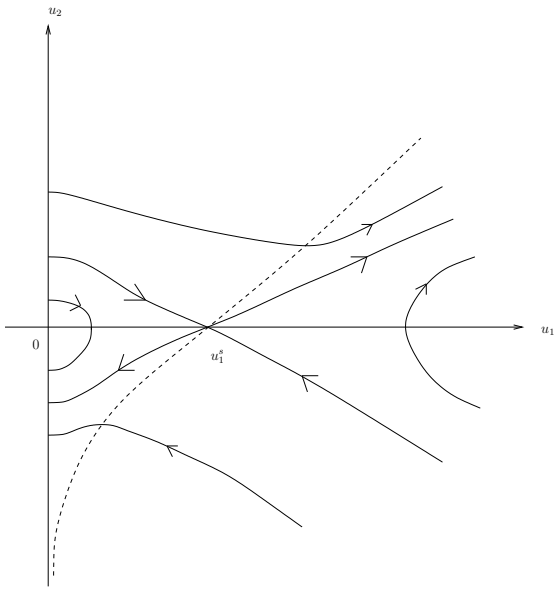

Figure 4.9: Phase plane for (4.31). Solutions exist between $u_1 = 0$ and $u_1 = u_1^s$. The finite value, u_1^*, lies on $u_1 = 0$. Note that solutions are horizontal at the u_2 axis when u_1 small. The dashed line represents the nullcline of (4.31). The travelling waves for this limiting case agree with the travelling waves that are shown in Figure 4.4.

Like Case 2, for Cases 3, 4 and 5, the local behaviour of (4.25) near $u_1 = 0$ and the general form of the solution can again be obtained as for Case 1. The types of the travelling waves are again the same as in Case 1. The results are shown in Figures 4.10, 4.11 and 4.12. The u_2-nullcline for Case 4 is given by $u_1 = u_1^* = u_1^s$ or
$u_2 = 28u_1^{5/7}\kappa(u_1^{2/7} - s_-)/9(u_1 - u_1^s)$ as shown in Figure 4.11.

Case 3: $-9u_1^*/8\phi < c < 0$

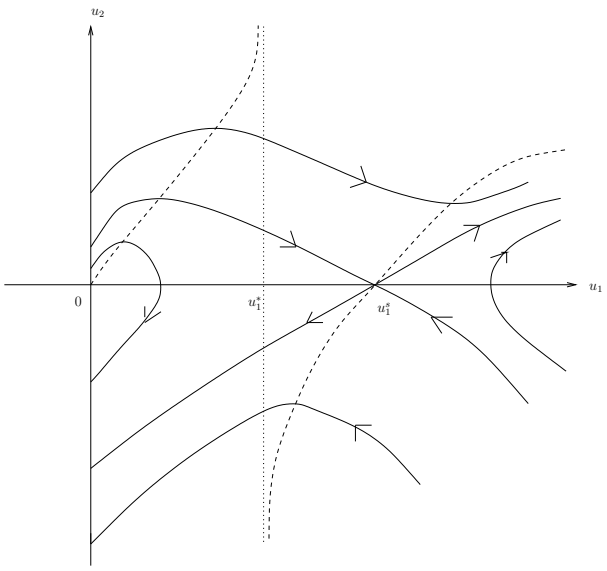

Figure 4.10: Phase plane for (4.25) with $-9u_1^*/8\phi < c < 0$. Travelling waves exist from $u_1 = 0$ to $u_1 = u_1^s$ and from $u_1 = u_1^s$ to $u_1 = 0$. Also, local travelling waves exist near $u_1 = 0$. Solutions at the u_2 axis have positive slope according to (4.30). The finite value, u_1^*, is positive but lies to the left of the equilibrium point u_1^s. The dashed line represents the nullcline of (4.25). The travelling waves for this limiting case agree with the travelling waves that are shown in Figure 4.5.

Case 4: $c = -9u_1^*/8\phi$

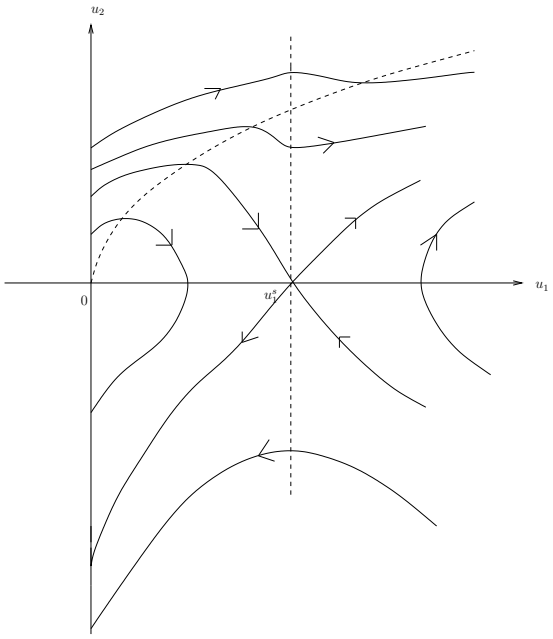

Figure 4.11: Phase plane for (4.25) with $c = -9u_1^*/8\phi$. Travelling waves exist from $u_1 = 0$ to $u_1 = u_1^s$ and from $u_1 = u_1^s$ to $u_1 = 0$. Local travelling waves exist near $u_1 = 0$. Solutions at the u_2 axis have positive slope according to (4.30). The finite value $u_1^* = u_1^s$. The dashed line represents the nullcline of (4.25). The travelling waves for this limiting case agree with the travelling waves that are shown in Figure 4.6.

Case 5: $c < -9u_1^*/8\phi$

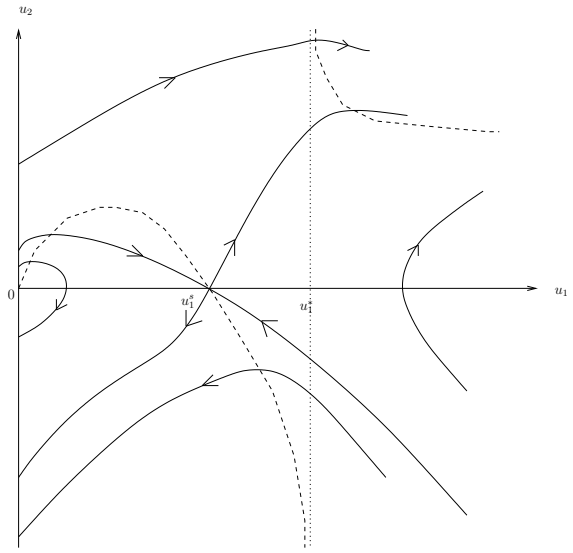

Figure 4.12: Phase plane for (4.25) with $c < -9u_1^*/8\phi$. Travelling waves exist from $u_1 = 0$ to $u_1 = u_1^s$ and from $u_1 = u_1^s$ to $u_1 = 0$. Local travelling waves exist near $u_1 = 0$. Solutions at the u_2 axis have positive slope according to (4.30). The finite value, u_1^*, lies in the right equilibrium point u_1^s. The dashed line represents the nullcline of (4.25). The travelling waves for this limiting case agree with the travelling waves that are shown in Figure 4.7.

Comparing all these cases for the limiting case with those done for the standard case, we see that the phase plane analysis for all these cases show the same qualitative behaviour. The limiting cases reproduce the left-hand portions of the phase planes for the fuller model.

4.2.2 Case 2: High Saturation

Introducing the approximate forms of $D(S)$, $K(S)$ and $R(S)$ with S close to 1, from (1.18), (1.20) and (1.21) respectively, into equation (4.1), we obtain

$$\frac{d}{d\zeta}\left(\frac{\delta}{\sqrt{2}\sqrt{1-S}}\frac{dS}{d\zeta}\right) + c\phi\frac{dS}{d\zeta} - \eta = 0.$$

For simplicity, define $\Psi = \sqrt{1-S}$, then $\dfrac{d\Psi}{d\zeta} = -\dfrac{1/2}{\sqrt{1-S}}\dfrac{dS}{d\zeta}$. Hence the above equation reduces to

$$\sqrt{2}\delta\frac{d^2\Psi}{d\zeta^2} + 2c\phi\Psi\frac{d\Psi}{d\zeta} + \eta = 0. \tag{4.32}$$

Equation (4.32) can be written as a first order system. Taking $u_1(\zeta) = \Psi(\zeta)$ and $u_2(\zeta) = \Psi'(\zeta)$, we obtain

$$\begin{aligned} u_1'(\zeta) &= u_2 \\ u_2'(\zeta) &= -\frac{1}{\sqrt{2}\delta}\left(2c\phi u_1 u_2 + \eta\right). \end{aligned} \tag{4.33}$$

Clearly, the u_1-nullcline is $u_2 = 0$ while the u_2-nullcline is given by $u_2 = -\eta/(2c\phi u_1)$ and then the u_2-nullcline $\to \pm\infty$ as $u_1 \to 0$. Also, the u_2-nullcline $\to 0$ as $u_1 \to \pm\infty$. Phase planes of (4.33) are sketched in Figures 4.13 and 4.14 for different values of the wave velocity c. Note that physically, we are only concerned with $u_1 \geq 0$ ($u_1 = \Psi = \sqrt{1-S}$) and $u_1 < 0$ is only included for mathematical completeness. When $c = 0$, we can easily solve (4.33) for u_1 to obtain $u_1 = (-\eta/(2\sqrt{2}\delta))\zeta^2 + c_1\zeta + c_0$ where c_1 and c_0 are arbitrary constants. For simplicity, take $c_1 = c_0 = 0$, we have $u_1 \to 0$ as $\zeta \to 0^-$. This just gives the local form of the steady solution near a saturated region.

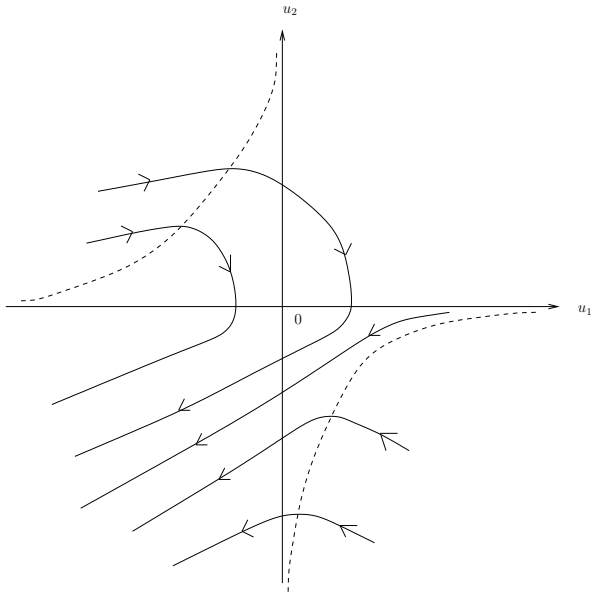

Figure 4.13: Phase plane for (4.33) with $c > 0$. The dashed line represents the nullcline of (4.33).

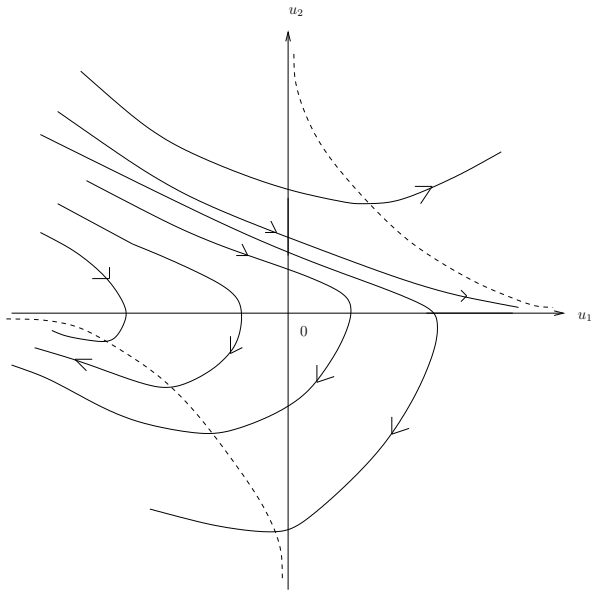

Figure 4.14: Phase plane for (4.33) with $c < 0$. The dashed line represents the nullcline of (4.33).

In Figure 4.13 the trajectories cross the u_2 axis at finite values of u_2. On the u_2 axis we have $u_1 = \Psi = 0$. From our definition we write $S = 1 - \Psi^2$ and then $S = 1$ on the u_2 axis which gives a saturated region. A similar argument applies for Figure 4.14.
Integrating now both sides of (4.32) we find that

$$\sqrt{2}\delta\frac{d\Psi}{d\zeta} + c\phi\Psi^2 + (\eta\zeta - c_0) = 0, \tag{4.34}$$

where c_0 is a constant of integration which we can take to be zero, without loss of generality. Equation (4.34) is a Ricatti equation and it can be turned into the Airy equation (see [3]) with the transformation

$$\Psi = \frac{P'}{r_0 P}, \tag{4.35}$$

where $r_0 = c\phi$. Substituting (4.35) into (4.34), we obtain

$$P'' + r_0\eta\zeta P = 0,$$

where the prime denotes the derivative with respect to ζ. For simplicity this equation becomes

$$P'' + r_1\zeta P = 0, \tag{4.36}$$

where $r_1 = r_0\eta$. To get rid of r_1, consider now the scaling of variable

$$\zeta = \alpha\tilde{\zeta},$$

with the scaling factor α still undetermined. Substitution of this transformation into equation (4.36) leads to

$$\frac{1}{\alpha^2}P'' + r_1\alpha\tilde{\zeta}P = 0,$$

where the derivative is now respect to $\tilde{\zeta}$. Multiplying by the factor α^2 and choosing $\alpha = -r_1^{-1/3}$ we obtain the reduced equation

$$P'' - \tilde{\zeta}P = 0. \tag{4.37}$$

This is the standard Airy equation. There are two linearly independent solu-

tions of the above equation denoted by $A_i(\tilde{\zeta})$ and $B_i(\tilde{\zeta})$. The behaviour of the both solutions is oscillatory as $\tilde{\zeta} \to -\infty$. $A_i(\tilde{\zeta})$ decays exponentially as $\tilde{\zeta} \to \infty$ while $B_i(\tilde{\zeta})$ grows exponentially fast as $\tilde{\zeta} \to \infty$, for more details see [5]. The asymptotic behaviour of the solutions for large values of $\tilde{\zeta}$ takes the forms

$$A_i(\tilde{\zeta}) \sim \frac{1}{2\sqrt{\pi}} \tilde{\zeta}^{-1/4} e^{-(2/3)\tilde{\zeta}^{3/2}} \quad \text{as} \quad \tilde{\zeta} \to \infty,$$

$$B_i(\tilde{\zeta}) \sim \frac{1}{\sqrt{\pi}} \tilde{\zeta}^{-1/4} e^{(2/3)\tilde{\zeta}^{3/2}} \quad \text{as} \quad \tilde{\zeta} \to \infty.$$

Then the general solution for equation (4.37) can be written as

$$P \sim (-r_1^{1/3}\zeta)^{-1/4} \left(C_1 e^{-(2/3)(-r_1^{1/3}\zeta)^{3/2}} + C_2 e^{(2/3)(-r_1^{1/3}\zeta)^{3/2}} \right) \quad \text{for} \quad \zeta \to -\infty,$$

where C_1 and C_2 constants. Then from equation (4.35) we find that

$$\Psi \sim \frac{1}{r_0} (-r_1^{1/3}\zeta)^{1/2} r_1^{1/3} \left(\frac{C_1 e^{-(2/3)(-r_1^{1/3}\zeta)^{3/2}} - C_2 e^{(2/3)(-r_1^{1/3}\zeta)^{3/2}}}{C_1 e^{-(2/3)(-r_1^{1/3}\zeta)^{3/2}} + C_2 e^{(2/3)(-r_1^{1/3}\zeta)^{3/2}}} \right).$$

For $C_2 \neq 0$, we have

$$\Psi \sim -\frac{1}{r_0} r_1^{1/2} (-\zeta)^{1/2} \quad \text{as} \quad \zeta \to -\infty.$$

For $C_1 \neq 0 = C_2$, we left with

$$\Psi \sim \frac{1}{r_0} r_1^{1/2} (-\zeta)^{1/2} \quad \text{as} \quad \zeta \to -\infty. \tag{4.38}$$

Unfortunately, this type of solution does not make sense in this limit. It fails to satisfy the original assumption, $S = 1 - \Psi^2$ with $\Psi \to 0$.
Such solutions in Figures 4.13 and 4.14 that cross the u_2 axis at finite values of u_2 are in a good agreement with the asymptotic solutions that are shown in the standard case when S is close to 1.

4.3 Self-Similar Solutions for the Diffusion-Sink Model

We begin again by introducing the similarity variables in the form

$$S(t,z) = t^{\alpha}\Phi(\xi), \quad \text{where} \quad \xi = (z-z_0)t^{\beta} \text{ is the similarity variable.} \tag{4.39}$$

Then equation (1.9) with the convective term absent takes the form

$$\phi\left(\alpha\Phi + \beta\xi\frac{d\Phi}{d\xi}\right) = t^{2\beta+1}\frac{d}{d\xi}\left(\delta D\left(t^{\alpha}\Phi\right)\frac{d\Phi}{d\xi}\right) - t^{1-\alpha}R(t^{\alpha}\Phi). \tag{4.40}$$

There is no similarity solution to equation (4.40) for any values of α and β with these two functions $D\left(t^{\alpha}\Phi\right)$ and $R\left(t^{\alpha}\Phi\right)$ because it is always dependent on t.
To look for a similarity solutions when $S = t^{\alpha}\Phi$ is small, we use the approximate forms of $D(t^{\alpha}\Phi)$ and $R(t^{\alpha}\Phi)$ from (1.12) and (1.16). Then equation (4.40) with the new functions becomes

$$\alpha\left(\Phi + \beta\xi\frac{d\Phi}{d\xi}\right) = t^{2\beta+1}\frac{d}{d\xi}\left(\delta t^{5\alpha/2}\Phi^{5/2}\frac{d\Phi}{d\xi}\right) - t^{1-\alpha}\kappa(t^{\alpha}\Phi - S_{-}), \tag{4.41}$$

and again equation (4.41) is still dependent on t, so there is still no similarity solution in this limiting case. The only way to find a self-similar solution is the limiting case when S is close to 1.

4.3.1 High Saturation

Recall that the variables for S close to 1 take the form

$$S(t,z) = 1 - t^{\alpha}\Phi(\xi), \quad \xi = (z-z_0)t^{\beta}. \tag{4.42}$$

Then equation (1.9) without the convective term becomes

$$-\phi\left(\alpha\Phi + \beta\xi\frac{d\Phi}{d\xi}\right) = -t^{2\beta+1}\frac{d}{d\xi}\left(\delta D\left(1-t^{\alpha}\Phi\right)\frac{d\Phi}{d\xi}\right) - t^{1-\alpha}R(1-t^{\alpha}\Phi).$$

Using the approximate forms of $D(1-t^{\alpha}\Phi)$ and $R(1-t^{\alpha}\Phi)$ near 1 from (1.18) and (1.21), this gives

$$\phi\left(\alpha\Phi+\beta\xi\frac{d\Phi}{d\xi}\right)=t^{2\beta+1-1/2\alpha}\frac{d}{d\xi}\left(\frac{1}{2}\delta\Phi^{-1/2}\frac{d\Phi}{d\xi}\right)+t^{1-\alpha}\eta. \tag{4.43}$$

To eliminate t in (4.43) we must have $\alpha=1$ and $\beta=-\frac{1}{4}$, then equation (4.43) reduces to

$$\delta\frac{d}{d\xi}\left(\frac{1}{2}\Phi^{-1/2}\frac{d\Phi}{d\xi}\right)-\phi\left(\Phi-\frac{1}{4}\xi\frac{d\Phi}{d\xi}\right)+\eta=0.$$

For simplicity, take $\Psi=\Phi^{1/2}$, then we end up with

$$\delta\frac{d^2}{d\xi^2}\Psi-\phi\left(\Psi^2-\frac{1}{2}\xi\Psi\frac{d\Psi}{d\xi}\right)+\eta=0. \tag{4.44}$$

In equation (4.44), let $u_1(\xi)=\Psi(\xi)$ and $u_2(\xi)=\Psi'(\xi)$. We obtain the system

$$\begin{aligned} u_1'(\xi) &= u_2(\xi) \\ u_2'(\xi) &= \frac{1}{\delta}\left(\phi(u_1^2-\frac{1}{2}\xi u_1u_2)-\eta\right). \end{aligned}$$

The system of differential equations has only one equilibrium point which is $\left(\sqrt{\frac{\eta}{\phi}},0\right)$. At this point we have from the basic form of the similarity solution, see (4.42),

$$\begin{aligned} S &= 1-tu_1^2 \\ &= 1-t(\eta/\phi), \end{aligned} \tag{4.45}$$

which gives a region which is nearly saturated with t small. From (4.45), we have

$$\frac{\partial S}{\partial t}=-\frac{\eta}{\phi}. \tag{4.46}$$

The saturation decreases at rate η/ϕ as the plant roots remove water from the region at rate η.

The Jacobian matrix of this system can be written as

$$J = \begin{bmatrix} 0 & 1 \\ \frac{1}{\delta}\left(\phi(2u_1 - \frac{1}{2}\xi u_2)\right) & \frac{1}{\delta}\left(-\frac{1}{2}\phi\xi u_1\right) \end{bmatrix}$$

which near the equilibrium point above gives

$$J_{(\sqrt{\eta/\phi},0)} = \begin{bmatrix} 0 & 1 \\ 2A_0 & -\frac{1}{2}\xi A_0 \end{bmatrix}$$

where $A_0 = \frac{\phi}{\delta}\sqrt{\frac{\eta}{\phi}}$. The linearised system near the equilibrium is then

$$\begin{aligned} v' &= v_2 \\ v_2' &= 2A_0 v - \frac{1}{2}\xi A_0 v_2, \end{aligned} \tag{4.47}$$

where $v = u_1 - \sqrt{\frac{\eta}{\phi}}$ and $v_2 = u_2$. Alternatively, the system (4.47) can be written as a second order equation

$$v'' + \frac{1}{2}A_0\xi v' - 2A_0 v = 0. \tag{4.48}$$

For simplicity, we can use the following scaling for ξ:

$$\xi = \frac{2}{A_0}\tilde{\xi}.$$

By substituting the above into equation (4.48) we obtain

$$v'' + \tilde{\xi}v' - 4v = 0. \tag{4.49}$$

Now, we can use a power series solution to solve this type of differential equation. So assume there is a solution of the form

$$v = \sum_{n=0}^{\infty} c_n \tilde{\xi}^n. \tag{4.50}$$

Then

$$v' = \sum_{n=1}^{\infty} n c_n \tilde{\xi}^{n-1}, \tag{4.51}$$

and

$$v'' = \sum_{n=2}^{\infty} n(n-1) c_n \tilde{\xi}^{n-2}. \tag{4.52}$$

Substituting (4.50), (4.51) and (4.52) into the differential equation (4.49), we get

$$\sum_{n=0}^{\infty}(n+2)(n+1)c_{n+2}\tilde{\xi}^n + \tilde{\xi}\sum_{n=1}^{\infty} n c_n \tilde{\xi}^{n-1} - \sum_{n=0}^{\infty} 4c_n\tilde{\xi}^n = 0$$

$$\sum_{n=0}^{\infty}(n+2)(n+1)c_{n+2}\tilde{\xi}^n + \sum_{n=1}^{\infty} n c_n \tilde{\xi}^{n} - \sum_{n=0}^{\infty} 4c_n\tilde{\xi}^n = 0$$

$$(2c_2 - 4c_0) + \sum_{n=1}^{\infty}[(n+2)(n+1)c_{n+2} + (n-4)c_n]\tilde{\xi}^n = 0.$$

Setting the coefficients equal to 0,

$$n = 0 \quad : \quad 2c_2 - 4c_0 = 0$$

$$n > 0 \quad : \quad (n+2)(n+1)c_{n+2} + (n-4)c_n = 0,$$

and solving gives

$$n = 0 \quad : \quad c_2 = 2c_0$$

$$n > 0 \quad : \quad c_{n+2} = \frac{(4-n)c_n}{(n+1)(n+2)}.$$

For even n $(n = 2k, k = 1, 2, 3, ...)$ we have

$$c_2 = 2c_0,\ c_4 = (1/3)c_0,\ c_6 = 0,\ c_8 = 0,\ c_{10} = 0, ...$$

Then for a simple solution we have

$$v_1(\tilde{\xi}) = 1 + 2\tilde{\xi}^2 + \frac{1}{3}\tilde{\xi}^4.$$

For a general solution we can then try

$$v = v_1 w. \tag{4.53}$$

This gives

$$v' = (4\tilde{\xi} + (4/3)\tilde{\xi}^3)w + (1 + 2\tilde{\xi}^2 + (1/3)\tilde{\xi}^4)w'$$

and

$$v'' = (4 + 4\tilde{\xi}^2)w + (8\tilde{\xi} + 8/3\tilde{\xi}^3)w' + (1 + 2\tilde{\xi}^2 + 1/3\tilde{\xi}^4)w'' \tag{4.54}$$

Substituting these expressions into (4.49), and after re-arranging, we find that

$$\frac{w''}{w'} = -\left(\tilde{\xi} + \frac{2(4\tilde{\xi} + (4/3)\tilde{\xi}^3)}{1 + 2\tilde{\xi}^2 + (1/3)\tilde{\xi}^4}\right). \tag{4.55}$$

Then integrating both sides we obtain

$$w' = C_0 e^{-\frac{\tilde{\xi}^2}{2}} \left(1 + 2\tilde{\xi}^2 + (1/3)\tilde{\xi}^4\right)^{-2}, \tag{4.56}$$

where C_0 is a constant of integration. Integrating again

$$w = C_0 \int_{\tilde{\xi}}^{\infty} e^{-\frac{\tilde{\xi}^2}{2}} \left(1 + 2\tilde{\xi}^2 + (1/3)\tilde{\xi}^4\right)^{-2} d\tilde{\xi} + C_1, \tag{4.57}$$

where C_1 is another constant of integration. From (4.53), we have

$$v = \left(1 + 2\tilde{\xi}^2 + (1/3)\tilde{\xi}^4\right)\left[C_0 \int_{\tilde{\xi}}^{\infty} e^{-\frac{\tilde{\xi}^2}{2}} \left(1 + 2\tilde{\xi}^2 + (1/3)\tilde{\xi}^4\right)^{-2} d\tilde{\xi} + C_1\right]. \tag{4.58}$$

For $C_1 \neq 0$, from (4.58) we see that the integral term decays exponentially fast to 0 as $\tilde{\xi} \to \infty$ and then we left with

$$v \sim \frac{C_1}{3}\tilde{\xi}^4 \quad \text{as} \quad \tilde{\xi} \to \infty. \tag{4.59}$$

Transforming now from v to S, it then follows from (4.42) that

$$S = 1 - t\left(k\left((A_0/2)\left(\frac{z - z_0}{t^{1/4}}\right)\right)^4 + \sqrt{\frac{\eta}{\phi}}\right)^2. \tag{4.60}$$

Unfortunately, the second term in (4.60) becomes large as $t \to 0$ ($\tilde{\xi} \to \infty$) which we do not want.
We must then have $C_1 = 0$, then it is clear from (4.58) that the solution v decays exponentially fast to 0 as $\tilde{\xi} \to \infty$. From (4.42), we can write the solution S in terms of v:

$$S = 1 - t\left(v + \sqrt{\frac{\eta}{\phi}}\right)^2, \tag{4.61}$$

then it follows that

$$S \sim 1 - t\frac{\eta}{\phi} \quad \text{for} \quad t \to 0. \tag{4.62}$$

For $z > z_0$, $\tilde{\xi} \to \infty$ as $t \to 0$, equation (4.62) with t small gives a region which is nearly saturated. The saturation in this region decreases at rate η/ϕ and the plant roots remove moisture at rate η. Note that for $C_0 = C_1 = 0$ in (4.58), we have $v = 0$ which again gives us equation (4.62).

4.4 Self-Similar Solutions for the Convection-Sink Model

Consider now the equation (1.9) in the absence of the diffusion term and by introducing the similarity variables from equation (4.39), we get

$$\phi\left(\alpha\Phi + \beta\xi\frac{d\Phi}{d\xi}\right) = t^{2\beta+1}\frac{d}{d\xi}\left(K(t^\alpha\Phi)\right) - t^{1-\alpha}R(t^\alpha\Phi). \tag{4.63}$$

Since equation (4.63) depends on t for any values of α and β there are no similarity solutions. For the local case when S is small, using the approximate functions of $K(t^\alpha\Phi)$ and $R(t^\alpha\Phi)$, from (1.13) and (1.16), in (4.63), we obtain

$$\phi\left(\alpha\Phi + \beta\xi\frac{d\Phi}{d\xi}\right) = \phi t^{2\beta+1+(9/2)\alpha}\frac{d}{d\xi}\left(\Phi^{9/2}\right) - \kappa(t\Phi - s_- t^{1-\alpha}). \tag{4.64}$$

Again equation (4.64) is still dependent on t and so similarity solutions do not exit for small $S = t^\alpha\Phi$. The only way in which such a can solution apply is for local behaviour when S is close to 1, which we come to now.

4.4.1 High Saturation

Introducing now the similarity variables as in (4.42) into eqaution (1.9) without the diffusion term, we obtain

$$-\phi\left(\alpha\Phi+\beta\xi\frac{d\Phi}{d\xi}\right)=t^{2\beta+1}\frac{d}{d\xi}\left(K(1-t^{\alpha}\Phi)\right)-t^{1-\alpha}R(1-t^{\alpha}\Phi). \tag{4.65}$$

By using the approximate functions $K(1-t^{\alpha}\Phi)$ and $R(1-t^{\alpha}\Phi)$ when S is close to 1, from (1.19) and (1.21) respectively, equation (4.65) then becomes

$$\phi\left(\alpha\Phi+\beta\xi\frac{d\Phi}{d\xi}\right)=\sqrt{2}t^{\beta-\alpha/2+1}\Phi^{-1/2}\frac{d\Phi}{d\xi}+t^{1-\alpha}\eta. \tag{4.66}$$

Equation (4.66) is independent on t if the exponents $\alpha=1$ and $\beta=-\dfrac{1}{2}$ and it then reduces to

$$\phi\left(\Phi-\frac{1}{2}\xi\frac{d\Phi}{d\xi}\right)=\sqrt{2}\Phi^{-1/2}\frac{d\Phi}{d\xi}+\eta. \tag{4.67}$$

Solving (4.67) for $\frac{d\Phi}{d\xi}$ gives

$$\frac{d\Phi}{d\xi}=\frac{\phi\Phi-\eta}{(1/2\phi)\xi+\sqrt{2}\Phi^{-1/2}}. \tag{4.68}$$

There is only one equilibrium solution which is $\Phi=\eta/\phi$, obtained by setting the right hand side of the equation (4.68) equal to zero. From the basic form of the similarity solution, (4.42), we have

$$S=1-t\frac{\eta}{\phi}. \tag{4.69}$$

As $t\to 0$, the solution on equilibrium approches 1 and then gives a nearly saturated region. The saturation decreases at rate η/ϕ as the moisture is taken up by plant roots at rate η. The nullcline of (4.68) is

$$\xi=\frac{-2\sqrt{2}}{\phi}\left(\frac{1}{\sqrt{\Phi}}\right), \tag{4.70}$$

and we see from (4.70) that on the nullcline $\xi\to-\infty$ as $\Phi\to 0^{+}$ and $\xi\to 0$ as $\Phi\to\infty$. A phase plane is shown in Figure 4.15.

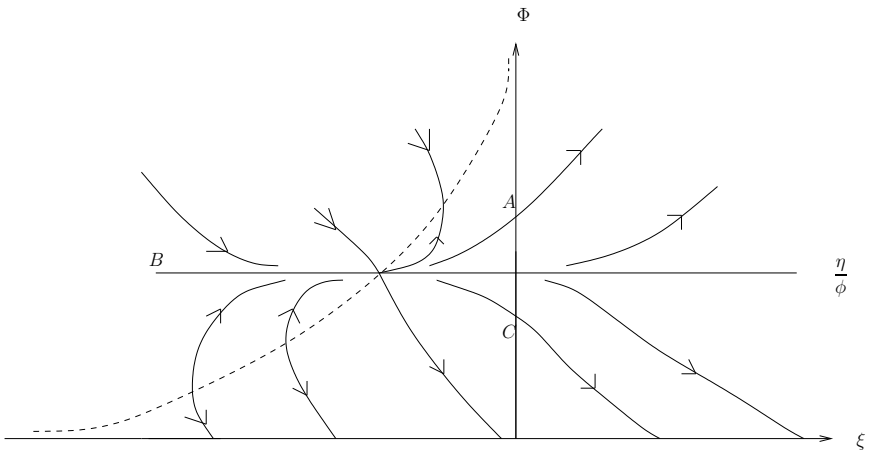

Figure 4.15: Phase plane for (4.68). The dashed line represents the nullcline.

In Figure 4.15, for $\xi < 0$ and with $\Phi > \xi^{-2}$, solutions tend to the equilibrium point or decrease towards the nullcline. With $\Phi < \xi^{-2}$ the solutions fall to 0 where $0 < \Phi < \eta/\phi$. Other such solutions grow where $\Phi > \eta/\phi$ and can cross the Φ axis, say at Φ_0. For $\xi > 0$ and $\Phi > \eta/\phi$, we see that from (4.68) $\frac{d\Phi}{d\xi} > 0$ and then Φ is increasing as $\xi \to \infty$. For $\xi > 0$ and $\Phi < \eta/\phi$, the solutions fall to 0 at finite values of ξ.
For such solutions as $B - A$ and $B - C$ where $\xi < 0$, we have that for $z < z_0$ and $t \to 0$, $\xi \to -\infty$ and the solutions are given again by equation (4.69) which gives a nearly saturated region. These two solutions for S in term of $t\Phi$, $S = 1 - t\Phi(\xi)$, are shown in Figure 4.16.

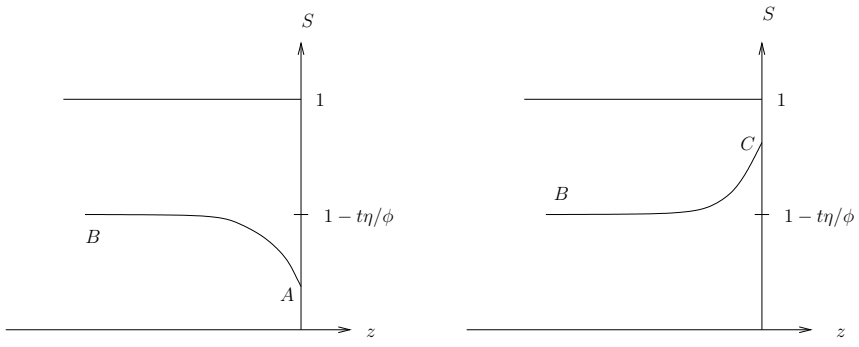

Figure 4.16: Left: Φ increases, and hence $S = 1 - t\Phi$ decreases, following $B - A$ in Figure 4.15. Right: Φ decreases, and hence $S = 1 - t\Phi$ increases, following $C - A$ in Figure 4.15.

4.4.2 Method of Characteristics for the Convection-Sink Model

In Chapter 2, we discussed the method of characteristics with initial condition (2.4) for the nonlinear convection model (2.2). In this section we reintroduced the sink term $R(S)$ to (2.2), then we have

$$\phi \frac{\partial S}{\partial t} - \frac{\partial}{\partial z} K(S) = -R(S), \tag{4.71}$$

where R is a nonlinear sink term depending on S alone and which satisfies $R(S_-) = 0$ for $S_- = \dfrac{\epsilon}{\sqrt{1+\epsilon^2}}$. Consider now the method of characteristics for (4.71) subject to step-function initial data (2.4). We can then reduce our partial differential equation (4.71) to a system of ordinary differential equations

$$\frac{dt}{ds} = \phi, \quad \frac{dz}{ds} = -c(S), \quad \frac{dS}{ds} = -R(S), \tag{4.72}$$

where $c(S)$ is the wave velocity which is given by $c(S) = -(1/\phi)(d/dS)(K(S))$. Since the right-hand side of (4.71) becomes large and positive, see the approximate form for the sink term when S close to 0 that is shown in Section 1.1, we consider here only the region where $S_- \leq S \leq 1$. Again the form of solution for our special initial data, (2.4), depends on the relation between S_l and S_r where $S_- \leq S_l \leq 1$, $S_- \leq S_r \leq 1$ are both constant. Following a similar

argument to that in Subsections 2.2.2 and 2.2.3, we can find several cases of rarefaction waves and shock solutions. Most of these cases have been done but not included in the thesis, it still need more work with numerical solutions in each case. Solving now (4.72), we obtain

$$t = \phi \int_S^{S_0} \frac{1}{R(S)} dS, \quad z = -\int_S^{S_0} c(S) dS, \tag{4.73}$$

where $S_- \leq S_r < S_0 < S_l \leq 1$ for the rarefaction waves or
$S_- \leq S_l < S_0 < S_r \leq 1$ for the shock cases. For the convection model (2.2), the characteristics are straight lines (seen from (2.5)). Here, in the convection-sink model, (4.71), the characteristics are curves according to (4.73) since S in (4.72) is not constant along the characteristic. Note that in the region where $S = S_-$, the characteristics for (4.71) are now straight lines because the right-hand side is zero.

Travelling wave solutions of the full green roof model, (1.9), exist for several cases according to the wave velocity c. We found approximate forms of asymptotic solutions for the two limiting cases (Section 4.2). We showed that travelling wave solutions exist locally. Local solutions for low and high saturation fit in with the standard case. Self-similar solutions exist for the diffusion-sink model with high saturation case only. Also, self-similar solutions were found for the convection-sink model, again for the high saturation case only. Solutions to the nonlinear convection model with sink term can be found in an integral form by using the method of characteristics.

Chapter 5

Conclusions and Future Work

5.1 Conclusions

In this thesis, we have studied a green roof model. We first, in Chapter 2, considered a convection model in the absence of diffusion and sink terms. Next, in Chapter 3, we reintroduced the diffusion term and discussed a convection-diffusion model, without the sink term. Finally, in Chapter 4, we considered the green roof model where all the terms are present. Much of the work in this thesis concerned travelling wave solutions and self-similar solutions. Particularly, the two limiting cases near a dry region and near a saturated region.

For the convection model we showed that rarefaction waves and shock solutions exist for several cases. Also, self-similar solutions were found. In particular, local behaviour near a dry region and near a saturated region were found in closed forms. The conservative upwind method was used to obtain a numerical scheme for solving the convection model.

For the nonlinear diffusion model, travelling wave solutions and self-similar solutions exist. Also, they were found locally. For the convection-diffusion model we showed that travelling wave solutions exist for several cases according to whether the limiting saturations might be zero, one or in between. Travelling wave solutions for the two limiting cases were found in explicit forms. Also, self-similar solutions were only found for the two limiting cases of the convection-diffusion model. Numerical solutions were obtained for the convection-diffusion model by using a finite difference method.

For the full green roof model, we showed that travelling wave solutions exist for several cases according to the wave velocity c. We also showed that travelling wave solutions exist for the two limiting cases of low and high saturation. Self-similar solutions were not found. Also, self-similar solutions were not found even for the two limiting cases. Self-similar solutions for the diffusion-sink model and the convection-sink model were only found for a region which is nearly saturated. In addition to that, we reintroduced the sink term to the convection model, to get a convection-sink model, in Chapter 4 and we showed that rarefaction waves and shock solutions also exist for several cases similar to those found in Chapter 2.

When accounting for the uptake of water by plant roots at low levels of saturation, we have generally approximated the take-up law (1.14) by a linear function, both of which change sign at saturation level $S = S_-$, i.e roots supply water to the soil for $S < S_-$. Ideally, we would work with the fuller model (1.14) rather than the linear approximation, however, there is reason to suspect that even (1.14) needs modification. Not only does it become negative for $S < S_-$, in dry soil roots act as a water source, but this rate becomes, according to (1.14), infinitely large as $S \to 0$. In addition, experimental results are needed to find parameter values that were given in the green roof model. In particular, L, K_0 and D_0 play important roles for determining the value of δ.

The analytical results of the nonlinear convection-diffusion model and convection model showed a finite speed. They showed a very good agreement with numerical results. These results give a good indications of how fast water gets through a soil layer. The water moves down corresponding to a negative speed which moves in the direction of gravity.

5.2 Future Work

It would be interesting to consider the self-similar solutions of the two limiting cases for the diffusion model for other possible cases of different values of α and β in (3.59) and (3.80). The results may be compared with that values of α and β that we already used.
Travelling wave solutions for the diffusion-sink model, in the absence of the convection term, can be studied along with their limiting cases as we have done for the full green roof model.

In order to study the stability of the travelling wave solutions, we need to linearize the partial differential equation about the wave. The spectrum of the differential operator should provide about the stability of the wave with respect to the the nonlinear partial differential equation.

Perturbation methods can be used to find approximate solutions to some ODEs that were derived from the full model, for example see (4.24), (4.34) and (4.44). They can provide solutions that give a good fit with the analytic and numeric results that we found for these equations.
It would also be interesting to investigate the steady-state solutions for some models such as a diffusion model or convection-diffusion model and try to compare that with other solutions we got.
Numerical solutions can be used for solving some ODEs that were derived from the full model such as equations (4.2) and (4.25).

We have some travelling wave and self-similar results for the green roof model and that was only for one space dimension. With more time we may extend our study to two dimensions. The mathematical analysis for the resulting equation is more complicated and so we leave it for future work.

Bibliography

[1] C. C. Adley, M. Cooker, G. L. Fay, I. Hewitt, A. A. Lacey, N. Mellgren, M. Robinson, and M. Vynnycky. A mathematical model of the rainwater flows in a green roof. *Mathematics in industry case studies*, in press, 2014.

[2] W. F. Ames. *Numerical methods for partial differential equations*. Computer Science and Scientific Computing. Academic Press, Inc., Boston, MA, third edition, 1992.

[3] G. I. Barenblatt. *Scaling, self-similarity, and intermediate asymptotics*, volume 14 of *Cambridge Texts in Applied Mathematics*. Cambridge University Press, Cambridge, 1996.

[4] G. I. Barenblatt and Ya B. Zeldovitch. Self-similar solutions as intermediate asymptotics. *Annual reviews of fluid mechanics*, 4:285–312, 1972.

[5] J. Bear. *Dynamics of fluids in porous media*. American Elsevier. New York, 1972.

[6] R. L. Burden and J. D. Faires. *Numerical analysis*. Prindle, Weber & Schmidt, Boston, Mass., 1978.

[7] J. G. Caputo and Y. A. Stepanyants. Front solutions of Richards' equation. *Transp. Porous Media*, 74(1):1–20, 2008.

[8] J. Carr. *Applications of centre manifold theory*, volume 35 of *Applied Mathematical Sciences*. Springer-Verlag, New York, 1981.

[9] E. Cumberbatch and A. Fitt. *Mathematical modeling*. Cambridge university press, Cambridge, 2001.

[10] W. Eckhaus. *Matched asymptotic expansions and singular perturbations*. North-Holland Publishing Co., Amsterdam, 1973.

[11] W. Eckhaus. *Asymptotic analysis of singular perturbations*, volume 9 of *Studies in Mathematics and its Applications*. North-Holland Publishing Co., Amsterdam, 1979.

[12] D. M. Etter and D. C. Kuncicky. *Introduction to MATLAB*. Prentice Hall. USA, 2011.

[13] N. D. Fowkes and J. J. Mahony. *An introduction to mathematical modelling*. John Wiley & Sons Ltd., Chichester, 1994.

[14] A. C. Fowler. *Mathematical models in the applied sciences*. Cambridge Texts in Applied Mathematics. Cambridge University Press, Cambridge, 1997.

[15] A. Georgescu. *Asymptotic treatment of differential equations*, volume 9 of *Applied Mathematics and Mathematical Computation*. Chapman & Hall, London, 1995.

[16] B. H. Gilding and R. Kersner. *Travelling waves in nonlinear diffusion-convection reaction*. Progress in Nonlinear Differential Equations and their Applications, 60. Birkhäuser Verlag, Basel, 2004.

[17] M. Guedda. Self-similar solutions to a convection-diffusion processes. *Electron. J. Qual. Theory Differ. Equ.*, (electronic), 1-18, 2000.

[18] I. Hewitt, A. A. Lacey, N. Mellgren, M. Vynnycky, M. Robinson, and M. Cooker. Designing a green roof for Ireland. *MIIS Eprints Archive report*, 2009.

[19] D. J. Higham and N. J. Higham. *MATLAB guide*. Society for industrial and applied mathematics (SIAM), Philadelphia, PA, second edition, 2005.

[20] E. J. Hinch. *Perturbation methods*. Cambridge Texts in Applied Mathematics. Cambridge University Press, Cambridge, 1991.

[21] S. Howison. *Practical applied mathematics*. Cambridge Texts in Applied Mathematics. Cambridge University Press, Cambridge, 2005.

[22] L. Kosareo and R. Ries. Comparative environmental life cycle assessment of green roofs. *Building and environment*, 42(7): 2606-2613, 2007.

[23] M. Köhler. Long-term vegetation research on two extensive green roofs in Berlin. *Urban Habitats*, 4(1): 3-25, 2006.

[24] A. A. Lacey and A. K. Alzahrani. Local self-similar solutions for a green roof model. (in preparation), 2014.

[25] A. A. Lacey and A. K. Alzahrani. Local travelling wave solutions for a green roof model. (in preparation), 2014.

[26] A. A. Lacey, J. R. Ockendon, and A. B. Tayler. "Waiting-time" solutions of a nonlinear diffusion equation. *SIAM J. Appl. Math.*, 42(6):1252–1264, 1982.

[27] R. J. LeVeque. *Numerical methods for conservation laws*. Lectures in Mathematics ETH Zürich. Birkhäuser Verlag, Basel, 1990.

[28] R. J. Leveque. *Nonlinear conservation laws and finite volume methods for astrophysical fluid flow*. Springer Berlin Heidelberg, Berlin, 1-159, 1998.

[29] J. D. Logan. *An introduction to nonlinear partial differential equations*. Pure and Applied Mathematics (Hoboken). Wiley-Interscience [John Wiley & Sons], Hoboken, NJ, second edition, 2008.

[30] C. Lustri. Continuum modelling of traffic flow. Web discussion page, 2010.

[31] J. D. Murray. *Mathematical biology*, volume 19 of *Biomathematics*. Springer-Verlag, Berlin, second edition, 1993.

[32] A. H. Nayfeh. *Perturbation methods*. Wiley Classics Library. New York, 2000.

[33] C. Obertscheider. *Burgers' Equation*. Preprint, 2001.

[34] J. Ockendon, S. Howison, A. Lacey, and A. Movchan. *Applied partial differential equations*. Oxford University Press, Oxford, revised edition, 2003.

[35] P. J. Olver. *Introduction to partial differential equations*. Undergraduate Texts in Mathematics. Springer, 2014.

[36] J. R. Philip. *Theory of infiltration*. In Advances in Hydroscience, Academic Press, N.Y., 215-296, 1969.

[37] L. A. Richards. Capillary conduction of liquids through porous mediums. *Physics*, 1, 318-333, 1931.

[38] T. Roose and A. C. Fowler. A mathematical model for water and nutrient uptake by plant root systems. *J. Theoret. Biol.*, 228(2):173–184, 2004.

[39] T. Roose and A. C. Fowler. A model for water uptake by plant roots. *J. Theoret. Biol.*, 228(2):155–171, 2004.

[40] P. L. Sachdev. *Nonlinear diffusive waves*. Cambridge University Press, Cambridge, 1987.

[41] F. Sanchez-Garduno, P. K. Maini, and E. Kappos. A review of travelling wave solutions of one-dimensional reaction-diffusion equations with non-linear diffusion term. *Forma*, 11(1), 45-59, 1997.

[42] R. A. Satnoianu, P. K. Maini, F. S. Garduno, and J. P. Armitage. Travelling waves in a nonlinear degenerate diffusion model for bacterial pattern formation. *Discrete Contin. Dyn. Syst. Ser. B*, 1(3):339–362, 2001.

[43] S. Schecter. Traveling-wave solutions of convection-diffusion systems by center manifold reduction. *Mathematics department, North Carolina State University, Raleigh, USA*, 1998.

[44] E. Smith, R. J. Smettem, P. Broadbridge, and D. A. Woolhiser. *Infiltration Theory for Hydrologic Applications*. American Geophysical Union, 15, pp. 1-212, 2002.

[45] G. D. Smith. *Numerical solution of partial differential equations*. Oxford Applied Mathematics and Computing Science Series. The Clarendon Press Oxford University Press, New York, third edition, 1985.

[46] J. Smoller. *Shock waves and reaction-diffusion equations*, volume 258 of *Grundlehren der Mathematischen Wissenschaften*. Springer-Verlag, New York, second edition, 1994.

[47] John C. Strikwerda. *Finite difference schemes and partial differential equations*. Wadsworth & Brooks/Cole Advanced Books & Software, Pacific Grove, CA, 1989.

[48] A. Tveito and R. Winther. *Introduction to partial differential equations: a computational approach*. Vol. 29, Springer, 2005.

[49] M. T. Van Genuchten. A closed-form equation for predicting the hydraulic conductivity of unsaturated soils. *Soil Sci. Soc. Am. J.*, 44(5): 892-898, 1980.

[50] J. L. Vázquez. The porous medium equation. New contractivity results. In *Elliptic and parabolic problems*, volume 63 of *Progr. Nonlinear Differential Equations Appl.*, pages 433–451. Birkhäuser, Basel, 2005.

[51] J. L. Vázquez. *The porous medium equation*. Oxford Mathematical Monographs. The Clarendon Press Oxford University Press, Oxford, 2007.

[52] Aizik I. Volpert, Vitaly A. Volpert, and Vladimir A. Volpert. *Traveling wave solutions of parabolic systems*, volume 140 of *Translations of Mathematical Monographs*. American Mathematical Society, Providence, RI, 1994. Translated from the Russian manuscript by James F. Heyda.

[53] C. G. Wark and W. W. Wark. Green roof specifications and standards. *The Construction Editor*, 56(8), 2003.

[54] G. B. Whitham. *Linear and nonlinear waves*. Pure and Applied Mathematics (New York). John Wiley & Sons Inc., New York, 1999.

[55] T. P. Witelski. Perturbation analysis for wetting fronts in Richards' equation. *Trans. in Por. Med.*, 27(2): 121-134, 1997.